Development of Selective Phosphatidylinositol 5-Phosphate 4-Kinase γ (PI5P4Kγ) Inhibitors with a Non-ATP-competitive, Allosteric Binding Mode

Helen K. Boffey,[1‡] Timothy P. C. Rooney,[1‡] Henriette M. G. Willems,[1‡] Simon Edwards,[1‡] Christopher Green,[2] Tina Howard,[3] Derek Ogg,[3] Tamara Romero,[1] Duncan E. Scott,[1] David Winpenny,[1] James Duce,[1] John Skidmore,[1] Jonathan H. Clarke[1] and Stephen P. Andrews[1]*

Addresses

[1]Jonathan Clarke, Helen Boffey, Simon Edwards, Tamara Romero, Timothy Rooney, Duncan Scott, Henriette Willems, David Winpenny, James Duce, John Skidmore and Stephen P Andrews: The ALBORADA Drug Discovery Institute, University of Cambridge, Island Research Building, Cambridge Biomedical Campus, Hills Road, Cambridge, CB2 0AH, United Kingdom

[2]Christopher Green: UK Dementia Research Institute, University of Cambridge, Island Research Building, Cambridge Biomedical Campus, Hills Road, Cambridge, CB2 0AH, United Kingdom

[3]Tina Howard, Derek Ogg: Peak Proteins, Alderley Park, Macclesfield, Cheshire, SK10 4TG, United Kingdom

Corresponding Author

*E-mail: spa26@cam.ac.uk

[‡]These authors contributed equally.

Abstract

Phosphatidylinositol 5-phosphate 4-kinases (PI5P4Ks) are emerging as attractive therapeutic targets in diseases such as cancer, immunological disorders and neurodegeneration, owing to their central role in regulating cell signalling pathways that are either dysfunctional or can be modulated to promote cell survival. Different modes of binding may enhance inhibitor selectivity and reduce off-target effects in cells. Here we describe efforts to improve the physicochemical properties of the selective PI5P4Kγ inhibitor, NIH-12848 (**1**). These improvements enabled demonstration that this chemotype engages PI5P4Kγ in intact cells and that compounds from this series do not inhibit PI5P4Kα or PI5P4Kβ. Furthermore, the first X-ray structure of PI5P4Kγ bound to an inhibitor has been determined with this chemotype, confirming an allosteric binding mode. An exemplar from this chemical series adopted two distinct modes of inhibition, including through binding to a putative lipid interaction site which is 18 Å from the ATP pocket.

Introduction

A large, heterogeneous group of kinase and phosphatase enzymes is responsible for the inter-conversion of different phosphoinositide lipids present in cells, and these are involved in nearly all aspects of cell physiology[1]. Lipid mediators have key functions in membrane trafficking, channel regulation, cell proliferation and cell stress/death responses and hence are well documented in diseases such as cancer, developmental disorders (including channelopathies and ciliopathy syndromes), bacterial and viral infections (including Hepatitis C and coronavirus), and neurodegeneration[2–5].

One class of these enzymes, the phosphatidylinositol 5-phosphate 4-kinases (PI5P4Ks), is functionally expressed in mammals to regulate cellular levels of their substrate, PI5P, or generate specific pools of PI(4,5)P_2 product[1,6,7]. The α, β and γ PI5P4K isoforms have been associated with a wide range of physiological roles including insulin signalling, receptor recycling, gene regulation and cell stress responses[8–11]. This has led to specific implications for PI5P4Ks in disease, especially in cancer where all three isoforms have been found to be upregulated[12–14]. Studies with knockout mice have also shown that PI5P4Kβ deletion leads to an insulin sensitivity phenotype[15], and that deletion of PI5P4Kγ results in immune hyperactivity indicative of autoimmune disease[16]. Interestingly, this latter observation was mediated through target of rapamycin (mTOR) complex regulation, which has also been associated with PI5P4K activity[17,18].

The role of the PI5P4Ks in response to cell starvation, a process that leads to negative regulation of mTORC1 activity to initiate autophagy, has also been documented[19–22]. The regulation of mTORC1 by PI5P4Kγ results in basal activation of the complex whereas reduced PI5P4Kγ activity in starvation conditions initiates autophagy[19]. Al-Ramahi and co-workers were able to show physiological relevance to neurodegenerative disease using pharmacological inhibition to reduce levels of mutant huntingtin protein in fibroblasts from Huntington disease patients and aggregated protein in a neuronal model, and that this effect was coincident with increased autophagic flux and specific to the PI5P4Kγ isoform[23]. PI5P4Kγ is therefore a target for small molecule inhibition in the context of neurodegenerative diseases.

The role of PI5P4Kγ in disease makes it a potentially important therapeutic target, however development has been hampered by the lack of potent and specific inhibitors. Furthermore, in contrast to the protein kinase family which has a relatively well-conserved active site[24], the more diverse lipid kinase family has less structural similarity,[2,25,26] hindering rational structure-based design. Despite the lack of structural similarity between lipid and protein kinases, a comprehensive study of the selectivity profiles of protein kinase inhibitors previously showed that some exhibit weak activity towards the lipid PI5P 4-kinases,[27] whilst other publications have shown that some protein

kinase inhibitors display activity against PI5P4Kγ, e.g. tyrphostin[28] and palbociclib[29] (see supporting information Table S1 for more details from our own screening of selected PI5P4Kγ inhibitors). Most significantly, NIH-12848 (**1**)[30] and NCT-504 (**2**)[23] have been disclosed as selective PI5P4Kγ inhibitors (Figure 1). Compound **1** was reported to have an IC_{50} of 2-3 μM in a radiometric ^{32}P-ATP/PI5P incorporation assay (see supporting information Table S2). Compound **2** was identified following a high-throughput screen and, when tested against a panel of 442 kinases, was found to have activity against only PI5P4Kγ (IC_{50} = 16 μM in a ^{32}P-ATP/PI5P incorporation assay). In 2020, pan PI5P4K inhibitors were reported, including covalent inhibitors THZ-P1-2 (**3**) and 'compound 30' (**4**),[31,32] as well as non-covalent 'compound 13' (**5**)[33] (Figure 1 and Table S1). Compound **4** displayed an IC_{50} of 1.3 μM against PI5P4Kα in a bioluminescent assay and 9.9 μM against PI5P4Kβ in a fluorescence polarisation assay but inhibited PI5P4Kγ by only 22% when tested in a KINOMEscan assay at 1 μM. In the same assays, compound **3** showed similar activity against PI5P4Kα and β but a more significant PI5P4Kγ inhibition of 91% and a PI5P4Kγ K_D of 4.8 nM[34]. Compound **5** has demonstrated similar levels activity in these PI5P4Kα and β assays (IC_{50} = 2.0 and 22 μM, respectively) as well as 100% inhibition of PI5P4Kγ in the KINOMEscan assay when tested at 1 μM and a PI5P4Kγ K_D of 3.4 nM[34].

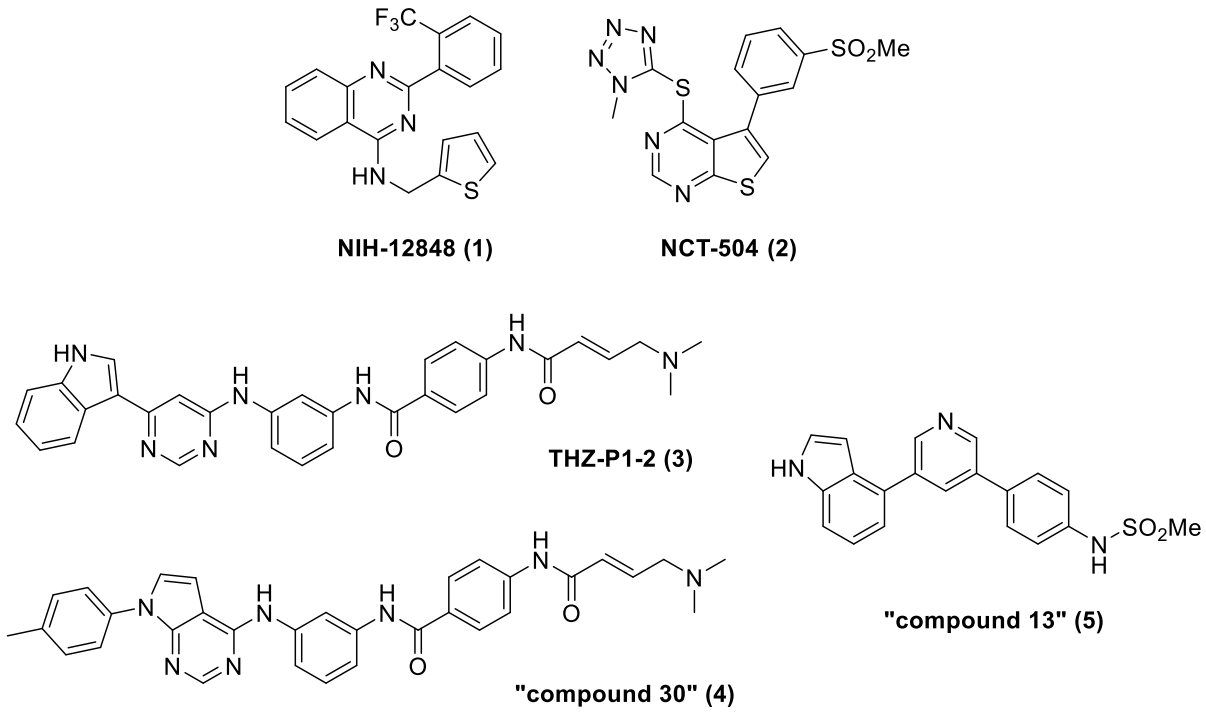

Figure 1. Structures of PI5P4Kγ inhibitors.

Herein we describe efforts to improve physicochemical properties of **1** to identify useful tool molecules. Compound **1** is an attractive starting point as it is inherently PI5P4K sub-type selective, yet there is scope for development as it is a lipophilic molecule (clogP 6.5) with poor solubility (<5 μM). Furthermore, **1** has been proposed to interact with an alternative region of the PI5P4Kγ catalytic site, potentially acting as a competitor for the PI5P substrate rather than for ATP binding[30] offering a unique opportunity to study lipid kinase structural biology.

Results

The optimisation campaign began with simple modifications of the parent molecule **1**, either through purchasing or synthesizing close analogues with subtle changes to the trifluoromethylphenyl group or thiophene (Table 1). To enable direct comparisons, Promega's ADP-Glo reporter assay was developed using a mutant form of the kinase. PI5P4Kγ-WT (wild type) has particularly low enzymatic activity, which is not trivial to measure. Conversion of the PI5P4Kγ catalytic site to the corresponding PI5P4Kα G loop sequence has been shown to increase kinase functional activity[25] and enabled the development of an inhibition assay with a usable window. The mutations (insertion of three amino acids (QAR) at 139 plus an additional 11 amino acid mutations; S132L, E133P, S134N, E135D, G136S, D141G, G142A, E156T, N198G, E199G and D200E) correspond to the PI5P4Kα residues and the resulting PI5P4Kγ construct containing these has been referred to as PI5P4Kγ+[25]. To mitigate concerns about being misled by the use of the PI5P4Kγ+ construct and the possible introduction of PI5P4Kα activity into the molecules, our screening cascade included measurement of ADP-Glo activity at PI5P4Kα-WT (as well as PI5P4Kβ-WT to fully understand emerging selectivity profiles). Moreover, cellular target engagement was periodically determined for exemplars; this determined compound binding to overexpressed PI5P4Kγ-WT in HEK293 cells through changes in target-protein thermal stability, monitored using DiscoverX's INCell Pulse assay. Further, we established a cell-free thermal shift assay with PI5P4Kγ-WT and determined that this chemical series showed a good correlation for measured ΔT_m with PI5P4Kγ-WT and the ADP-Glo pIC_{50} with PI5P4Kγ+ (see supporting information Figure S1 and Table S3). In general, for this chemical series we observed a good correlation between PI5P4Kγ+ and PI5P4Kγ-WT binding and undetectable levels of PI5P4Kα and PI5P4Kβ inhibition.

Structural information for each of the PI5P4K isoforms was publicly available at the start of this program in the form of X-ray crystal structures deposited in the Protein Data Bank, but there were no published structures with drug-like ligands bound. The only crystal structure of PI5P4Kγ publicly available at that time (pdb: 2GK9) does

not have a ligand bound, but crystal structures of PI5P4Kβ bound to nucleotides[35] enabled us to pinpoint the ATP-binding pocket for PI5P4Kγ. However, **1** could not be docked into this pocket in a convincing binding pose, a finding that is consistent with Clarke *et al.*'s evidence from HDX mass spectrometry[30] that this ligand does not bind in the ATP-binding pocket. No other binding pocket for **1** could be identified in the 2GK9 structure so we proceeded with our attempts to optimize **1** through classical medicinal chemistry approaches, without structural guidance.

During initial SAR scoping with PI5P4Kγ+, a brief scan of a variety of small substituents with different electronic properties at position R^1 did not reveal any advantages (e.g. **6**–**9** Table 1) and replacement of the thiophene with other ring systems showed a preference for aromatic rings with a heteroatom at the ortho position (compare **10**–**14**, Table 1). Extending the R^2 methylene linker to ethylene was not tolerated (**15**), nor was *N*-methylation (data not shown). On balance, from this initial set of thiophene replacements, pyridine **14** was preferred as it showed a reduced lipophilicity compared to **1** (clogP 5.5), and a modest improvement in solubility to 9 μM, which resulted in a significant improvement in measured Caco-2 permeability from 6.4 to 85 × 10^{-6} cm/s (Table 2). In the thermal shift assay with PI5P4Kγ-WT protein, **14** showed a ΔT_m of 6.3 °C vs 4.7 °C for **1** and ΔT_m <1 °C against both PI5P4Kα and PI5P4Kβ (Table S4).

Table 1. SAR and physicochemical properties for variation of R^1 and R^2.

	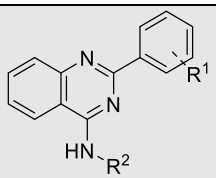		inhibition of PI5P4K[a]				ΔT_m/ °C[b]	Physicochemical properties	
Compound	R^1	R^2	PI5P4Kα pIC_{50}	PI5P4Kβ pIC_{50}	PI5P4Kγ+ pIC_{50}	PI5P4Kγ + LE	PI5P4Kγ WT	MW	clogP
1	2-CF_3	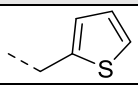	<4.3	<4.6	6.1	0.32	4.7	385	6.5
6	H	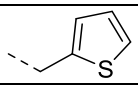	<4.3	<4.6	<4.3		-1.1	317	5.6
7	2-CH_3	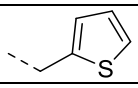	<4.3	<4.6	<4.5		2.7	331	6.1
8	2-OCH_3	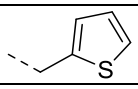	<4.6	<4.6	<4.3		0.1	347	5.4
9	4-Cl	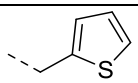	<4.3	ND	<4.3		-1.6	352	6.2
10	2-CF_3	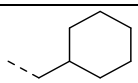	<4.3	<4.6	<4.3		-0.8	385	6.9
11	2-CF_3	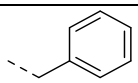	<4.3	<4.6	5.2	0.26	4.6	379	6.6

12	2-CF_3	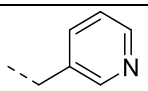	<4.3	ND	<4.3		1.4	380	5.3
13	2-CF_3	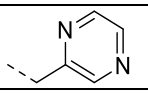	<4.3	ND	5.5	0.27	6.1	381	4.3
14	2-CF_3	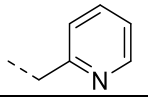	<4.3	<4.6	5.5	0.27	6.3	380	5.5
15	2-CF_3	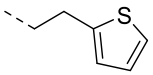	<4.3	ND	<4.3		-1.4	399	6.8
16	2-CF_3-4-F	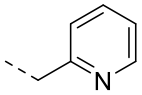	<4.3	ND	6.0	0.29	ND	398	5.7
17	2-CF_3-5-F	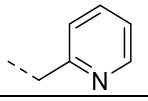	<4.3	ND	5.4	0.26	ND	398	5.7
18	3-CF_3	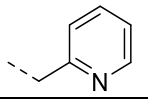	<4.3	ND	<4.3		1.3	380	5.5
19	4-CF_3	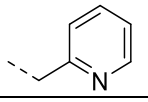	<4.3	ND	<4.3		1.7	380	5.5
20	3-OMe	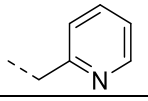	<4.3	ND	5.1	0.27	5.1	342	4.4
21	4-OMe	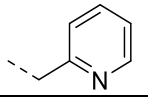	<4.3	ND	5.1	0.27	5.1	342	4.4
22	2-$CH(CH_3)_2$	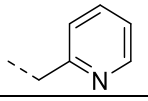	<4.3	<4.6	6.5	0.34	7.8	354	5.9
23	2-*c*Pr	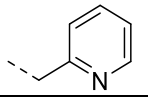	<4.3	ND	5.6	0.29	ND	352	5.4
24	2-CH_2CH_3	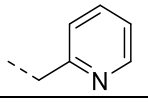	<4.3	ND	5.3	0.29	4.9	340	5.5
25	2-Ph	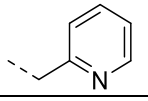	<4.3	ND	5.0	0.24	4.4	388	6.3
26	2-CN	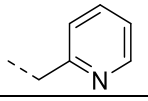	<4.3	ND	<4.3		2.9	337	4.5
27	2-NMe_2	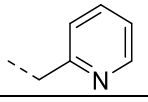	<4.3	ND	<4.3		2.7	355	4.8
28	2-$CH(CH_3)_2$	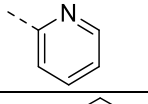	<4.3	ND	<4.6		ND	340	6.3
29	2-$CH(CH_3)_2$	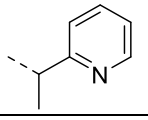	<4.3	<4.6	4.4	0.22	0.2	368	6.4
30	2-$CH(CH_3)_2$	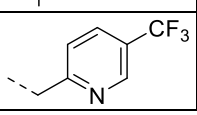	<4.3	ND	<4.3		ND	422	6.7

31	2-$CH(CH_3)_2$	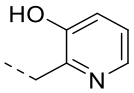	5.8	ND	6.2	0.31	7.0	370	5.6

[a] determined by ADP-Glo; [b]thermal shift determined with WT protein, see supporting information for further details

A further iteration of R^1 modification was then conducted using the 2-pyridyl analogue **14** as a template. Addition of a fluoro substituent was beneficial for potency at position 4 but not 5 (**16** and **17**). Movement of the trifluoromethyl group from the 2-postion to either 3- or 4-position of the phenyl ring was not tolerated (**18** and **19**, respectively), whereas 3- or 4-methoxy was tolerated to some degree (**20** and **21**, respectively). Small lipophilic substituents gave the greatest PI5P4Kγ+ inhibition when used at position 2, with *i*-Pr>c-Pr>Et>Ph (**22**, **23**, **24** and **25**, respectively). Indeed **22** was one of the most ligand efficient (LE) analogues identified during this campaign (LE = 0.34) and showed sub-micromolar activity in the cellular target engagement assay with PI5P4Kγ-WT (Table 3). However, although significantly improved over **1**, compound **22** still has a high lipophilicity (clogP = 5.9) which appears to limit its aqueous solubility and microsomal stability (Table 2). Polar groups at position 2 helped to reduce clogP but were detrimental to potency in the primary assay, including electron withdrawing groups (**26**) and electron donating groups (**27**).

Table 2. In vitro ADMET and physicochemical properties of selected examples.

Compound	TPSA	clogP	MW	HLM $t_{1/2}$ (mins)[a]	mPPB (%)[b]	P_{app} A->B (10^{-6} cm/s)[c]	ER[c]	Solubility (μM)	mchrom $LogD_{7.4}$[d]
1	38	6.5	385	21	>99	6.4	0.9	<5	6.3
14	51	5.5	380	31	>99	85	0.4	9	4.9
22	51	5.9	354	37	>99	91	0.3	<5	5.7
35	51	4.6	344	41	97	106	0.5	113	4.2
38	64	4.7	381	100	99	146	0.5	6	3.2
40	56	5.2	357	47	99	122	0.4	7	4.5

[a]Human liver microsomal hepatic stability. [b]mouse plasma protein binding. [c]Caco-2 cell permeability, A->B = apical-to-basolateral, ER = efflux ratio. [d]Determined by HPLC method.

Having identified 2-*iso*propylphenyl as the preferred substituent at position 2 of the quinazoline for potency gains, we next looked at adding further substituents to the 2-pyridyl ring and modifying the quinazoline core. Deletion or branching of the methylene linker (**28** and **29** respectively) was not tolerated, nor was the addition of a 5-trifluoromethyl substituent (**30**). Addition of a 3-hydroxy group (**31**) was also well tolerated. This modification introduced some inhibition of PI5P4Kα, as well as some polarity which may be of use for further development, but these aspects were not pursued.

The quinazoline core presented a number of opportunities for investigation, including adding substituents, introducing heteroatoms to modulate logP and protein contacts, and modifying the ring geometries (Table 3). We generated a series of analogues of **22** to explore this aspect of the SAR. A bromo substituent at position 6 of the quinazoline (**32**) gave a small increase in potency at the cost of significantly increased MW and clogP, whereas an amino group at the same position (**33**) maintained activity with a smaller MW penalty and a positive impact on clogP.

Table 3. SAR and physicochemical properties for variation of the core.

	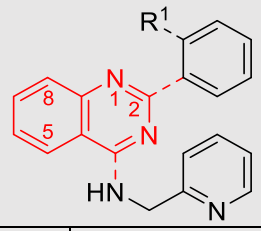		inhibition of PI5P4K[a]				Target engage-ment[b]	Physico-chemical properties	
Compound	R^1	Core	PI5P4Kα pIC_{50}	PI5P4Kβ pIC_{50}	PI5P4Kγ+ pIC_{50}	PI5P4Kγ + LE	PI5P4Kγ WT pIC_{50}	MW	clogP
22	$CH(CH_3)_2$	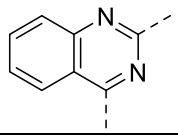	<4.3	<4.6	6.5	0.34	6.2	354	5.9
32	$CH(CH_3)_2$	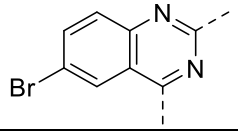	<4.3	ND	6.7	0.33	ND	433	6.6
33	$CH(CH_3)_2$	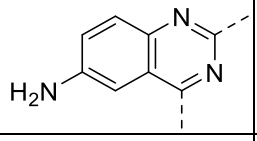	<4.3	ND	6.5	0.32	ND	369	5.1
34	$CH(CH_3)_2$	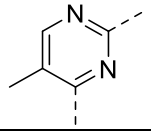	<4.7	<4.6	5.4	0.31	5.4	318	5.0
35	CF_3	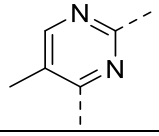	<4.3	<4.6	5.0	0.28	ND	344	4.6

36	$CH(CH_3)_2$	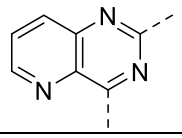	<4.3	<4.6	5.6	0.29	5.5	355	5.0
37	$CH(CH_3)_2$	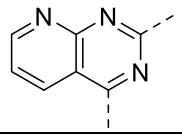	<4.3	<4.6	6.6	0.34	6.1	355	5.0
38	CF_3	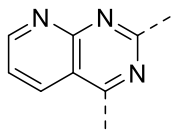	<4.3	<4.6	6.1	0.30	6.2	381	4.7
39	$CH(CH_3)_2$	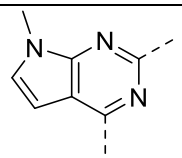	<4.3	ND	<4.3	0.22	ND	357	5.2
40	$CH(CH_3)_2$	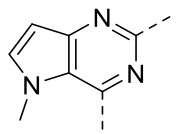	<4.3	<4.6	6.2	0.32	6.1	357	5.2
41	$CH(CH_3)_2$	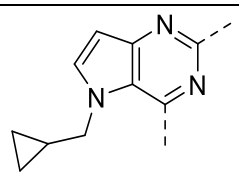	<4.3	ND	6.5	0.31	ND	398	6.0
42	$CH(CH_3)_2$	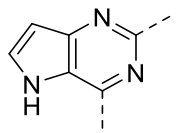	<4.3	<4.6	5.6	0.30	5.7	343	5.0

[a] determined by ADP-Glo; [b]determined by INCell Pulse in intact cells

In order to maximize the efficiency of the core, we sought to delete lipophilic atoms or replace these with heteroatoms. Intrigued by the parallels with the work by Dexheimer *et al.*[36], and the structural similarity of ML323 (Figure S2), we performed a truncation of the quinazoline core to afford compound **34**. In our assays, ML323 was inactive at both PI5P4Kα and PI5P4Kγ+ (data not shown), whereas **34** showed a pIC_{50} of 5.4 against PI5P4Kγ+ and no detectable inhibition of the α or β isoforms. A similar profile was seen with analogue **35** possessing a trifluoromethyl instead of the *iso*propyl (Table 3). The LE of compound **34** was an acceptable 0.31, but this truncation approach was not as productive as the introduction of heteroatoms to the core, at position 5 (**36**) and particularly at position 8 (**37, 38**). Pyridopyrimidine **37** showed an improved potency, a reduced clogP and good selectivity vs PI5P4Kα and PI5P4Kβ. Furthermore, **37** showed sub-micromolar activity in the cellular target engagement assay with PI5P4Kγ-WT.

Regioisomeric pyrrolopyrimidines **39** and **40** were also evaluated. Whilst compound **39** was inactive, compound **40** showed good potency and LE in the primary assay, as well as sub-micromolar activity in the cellular target

engagement assay. It also maintained selectivity vs PI5P4Kα and PI5P4Kβ, showed high levels of permeability and moderate microsomal stability (Table 2). The aliphatic substituent could be extended, as exemplified by **41**, but deletion of the *N*-methyl group (**42**) was not well tolerated.

Binding constants (K_Ds) were determined for compound **40** using commercially available assays for PI5P4Kγ-WT (68 nM) and PI5P4Kβ (>30,000 nM) and compared vs compound **1** (Table S6). This assay was not available for PI5P4Kα but a commercial IC_{50} determination was possible via Thermo Fisher to corroborate our own data (Table S7; IC_{50} > 30,000 nM for compounds **1** and **40**). Compound **40** was also tested for selectivity against a panel of 140 protein kinases and 15 lipid kinases (Tables S8 and S9, respectively). Only one of these targets (PAK2) showed <50% residual activity when tested at 10 μM.

In order to solve structures of co-complexes of PI5P4Kγ with examples from this chemical series, a number of protein constructs were expressed, purified and subjected to crystallisation trials. A truncated version of human PI5P4Kγ comprising residues His32 to Ala421, in accordance with the truncation used to generate X-ray structures of the other PI5P4K isoforms, was cloned into a bacterial expression vector. To increase the chances of obtaining crystals, three other truncated constructs were prepared in parallel, each with different length deletions of the previously unstructured region in the PI5P4Kβ structure. Purified recombinant protein was obtained for each of the four different truncations, and all were successful in crystallisation trials. Compound **40** was selected for crystallography owing to its balance of potency and solubility. A PI5P4Kγ protein construct comprising residues His32 to Ala421, with residues 300-341 deleted, was successfully co-crystallized with **40** at a 2.4 Å resolution (Figure 2, pdb code 7QIE).

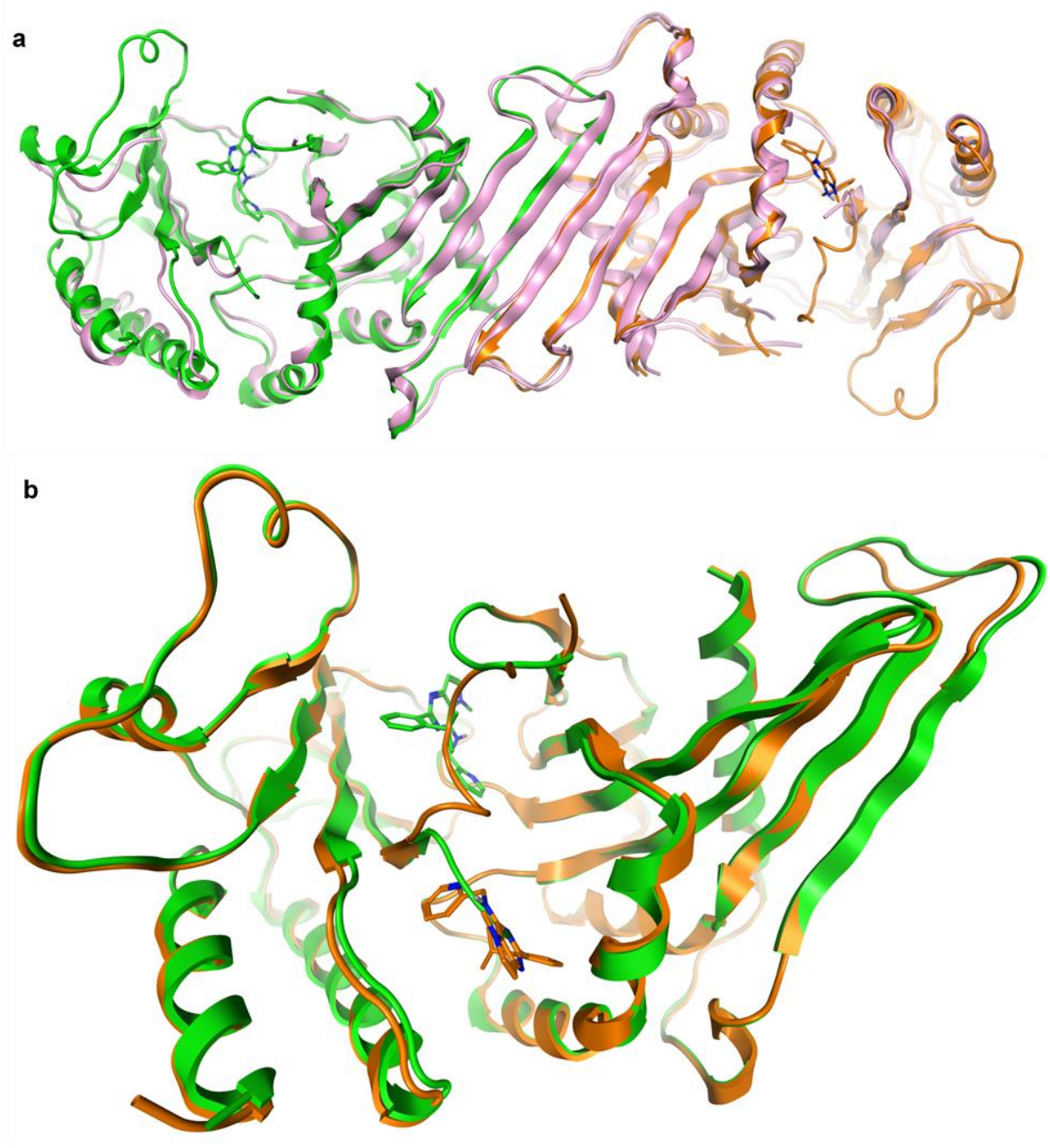

Figure 2. The crystal structure of PI5P4Kγ bound to **40** at 2.4Å (pdb: 7QIE). a) The dimer of chains A (orange) and B (green) with **40** bound superposed onto the dimer of chain B and C of apo PI5P4Kγ structure 2GK9 (in pink); b) Two binding sites for **40**: Chain A (orange, **40** in allosteric binding pocket) and chain B (green, **40** in ATP site) superposed with **40** in stick. The binding sites are mutually exclusive.

There are two PI5P4Kγ homodimers in the asymmetric unit, as is seen in the 2GK9 apo structure of PI5P4Kγ. Overall, the structure shows a high degree of similarity with that of apo structure 2GK9, although it has increased structural definition of some of the loop areas in the complex (Figure 2a). Most interesting is the presence of two distinct binding pockets for **40** in PI5P4Kγ that cannot be occupied simultaneously by the ligand (Figure 2b). In chain B, **40** occupies the pocket occupied by AMP/GMP in the PI5P4Kβ crystal structures (pdb codes 3X01, 3X02). The other three monomer chains (A, C and D) show the ligand located 18 Å away from the ATP site in a lipid binding pocket[37,38]. In this protein conformation, residues Gln378, Tyr379 and Asp380 of the activation loop occupy an inhibitory position in the ATP binding site (Figure 3a). The side chain of Tyr379 superposes closely onto the pyrimidine ring of AMP in 3X01, with the hydroxyl of Tyr379 forming some of the same hydrogen bonds. The side chain of Asp380 interacts with the Thr239 hydroxyl group, mimicking some of the interactions that the ribose of AMP makes. Thus, the binding of **40** into the allosteric pocket appears to stabilize a protein conformation where the activation loop inhibits access to the ATP site.

The allosteric binding site in the PI5P4Kγ protein is formed by residues Asp161, Met162, Asn165, Leu166, Tyr169, Leu182, Phe185, Phe272, Leu273, Leu276, Asp374 and Thr377 with the *iso*propylphenyl moiety of **40** inserting deep into a mostly lipophilic pocket (Figure 3). The pyridine substituent of **40** forms a hydrogen bond with the Thr377 hydroxyl group and the central pyrimidine ring forms a hydrogen bond with the side chain of Asn165 (Figure 3c). Finally, the NH linking the pyrrolopyrimidine core with the methylpyridine group interacts with the Asp374 carboxylate group. The ligand fits very snugly into the binding pocket, with only the methyl-pyrrole part of the bicyclic core solvent-accessible (Figure 3d). The *iso*propyl group of the ligand is in contact with the pyridine group, thus stabilizing the ligand conformation. In fact, *ab initio* quantum mechanical calculations suggest that the ligand conformation in the lipid binding site is very close to the lowest energy solution conformation for **40** (RMSD = 0.25 Å).

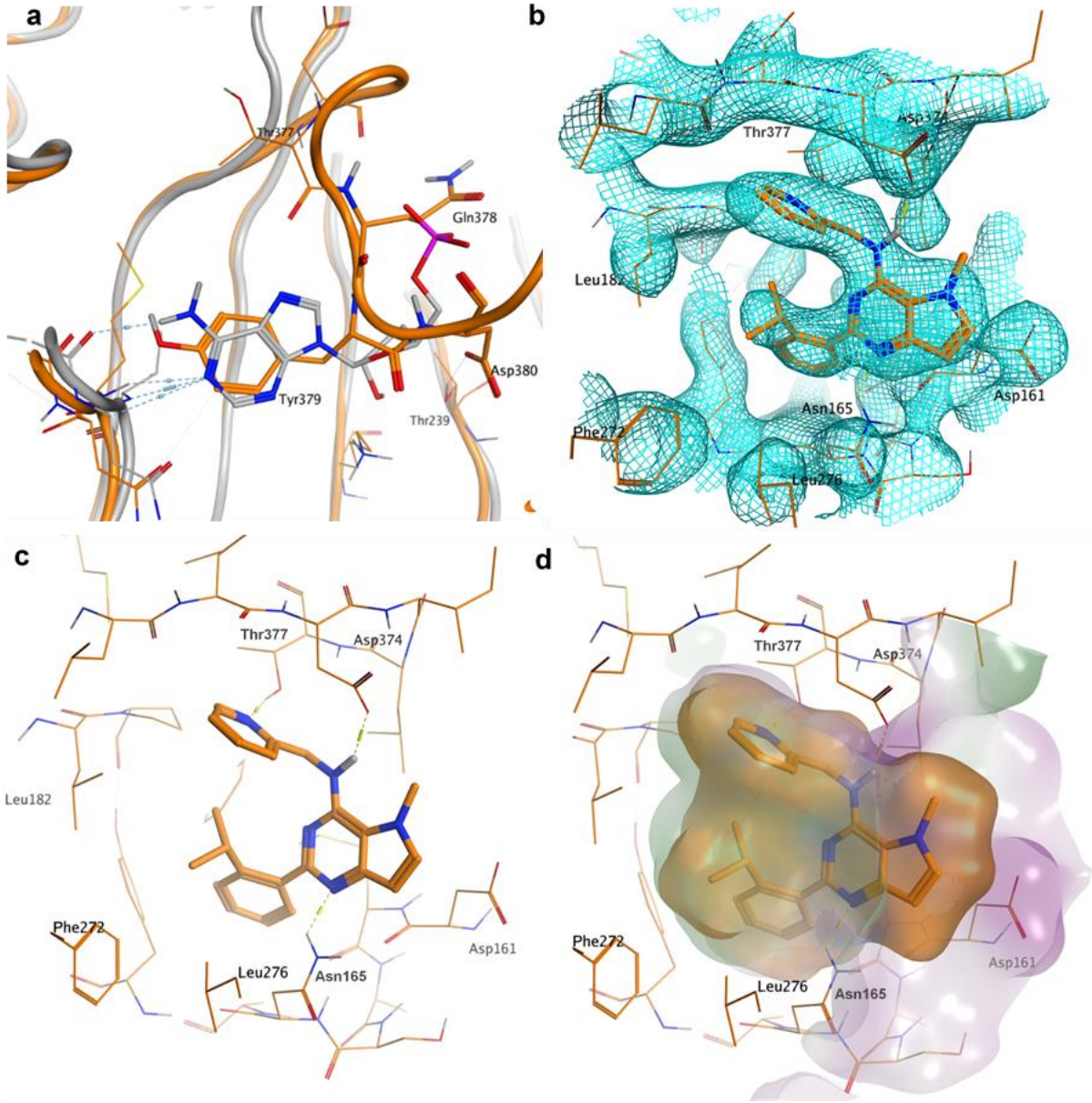

Figure 3. Focus on chain A of the crystal structure of PI5P4Kγ bound to **40** at 2.4Å with **40** in the allosteric binding pocket (pdb: 7QIE; orange). a) the AMP binding site of PI5P4Kβ (3X01, grey) superposed onto chain A (orange). Tyr379 of PI5P4Kγ overlays onto the pyrimidine ring of AMP; b) electron density at 1σ for the allosteric binding pocket in chain A of the **40**- PI5P4Kγ complex; c) the novel binding pocket in chain A of the **40**- PI5P4Kγ complex with key interactions highlighted; d) the allosteric binding pocket in chain A of the **40**- PI5P4Kγ complex with ligand and receptor molecular surfaces.

In chain B, where the ligand occupies the ATP site, the allosteric binding site is occupied by residues Ile375 and Leu376, which form the start of a loop that is mostly missing in PI5P4K crystal structures (Figure 4). Ile375 and Leu376 also occlude the substrate binding pocket in the apo structure 2GK9, explaining why this pocket was not

identified previously (Figure 4a). In the ATP-pocket, the ligand interacts with the Met206 backbone NH through the pyridine nitrogen, not the amino-pyrimidine moiety commonly associated with kinase hinge binding (Figure 4b). The pyridine ring also makes a hydrophobic contact with the Met206 side chain at the back of the ATP pocket (Figure 4d). Force-field based estimates of free energy of binding (MOE, GBVI/WSA dG) suggest that the binding energy for **40** in the allosteric pocket is 4.4 kcals/mol more favourable than in the ATP pocket. There is evidence from the electron density that there is some occupancy for both ligand binding modes in all chains.

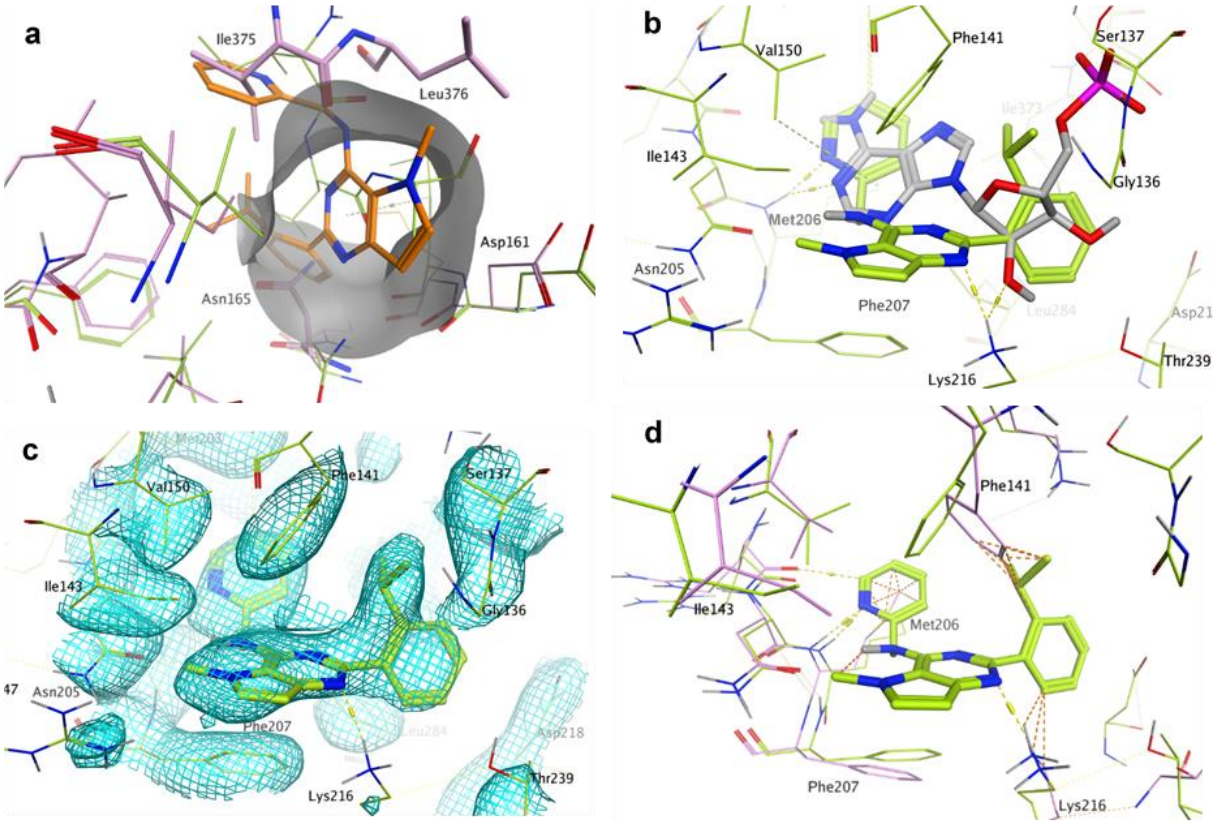

Figure 4. Focus on chain B of the crystal structure of PI5P4Kγ bound to **40** at 2.4Å (pdb: 7QIE; green). This chain has **40** bound in the ATP pocket. a) The allosteric binding pocket observed in chains A, C and D of PI5P4Kγ bound to **40** is (partially) occluded in the apo structure 2GK9 (pink) and chain B of the complex with **40** (green) by residues Ile375, Leu376 and Asn165 (apo only). **40** (orange sticks) from chain A of the PI5P4Kγ-**40** complex is superposed onto apo PI5P4Kγ (pink) and chain B of the PI5P4Kγ-**40** complex (green). b) **40** bound to the ATP pocket of chain B of the PI5P4Kγ complex in green with AMP as bound to PI5P4Kβ (pdb: 3X01) superposed in grey. The pyrimidine rings do not superpose. c) electron density at 1σ for the ATP binding pocket in chain B of the **40**- PI5P4Kγ complex. d) **40** bound to the ATP pocket of chain B of the PI5P4Kγ complex in green with apo

PI5P4Kγ (pdb: 2GK9) superposed in pink. Orange dotted lines indicate clashes between the ligand and the apo structure.

The **40**-PI5P4Kγ complex shows that one side of the ATP-binding pocket is formed by residues 134-141, when **40** is bound. In the apo structure 2GK9 residues 136 to 139 of this loop are missing, but these are clearly visible in chain B of the complex crystal structure, though some side chain density is poor (Figure 4c). The side chain of Phe141 of the loop contacts the *iso*propyl group and the pyrimidine core of **40**, and Gly136 also contacts the *iso*propyl group. It is likely that these interactions stabilize the loop. Chains A and C of the complex only show partial electron density for the loop. Some side chain adjustment to accommodate **40** can be observed in the ATP-binding pocket compared with apo-PI5P4Kγ. Phe141, Met206, and Lys216 have moved from their apo positions to create a pocket large enough for **40** to bind to (Figure 4d). This explains why our attempts to dock **1** and **40** to the ATP site of the apo structure were unsuccessful.

Discussion

The optimization of **1** delivered compounds with improved molecular properties and enabled a crystal structure of a complex of PI5P4Kγ with **40** to be obtained. A retrospective analysis of the measured potencies of examples in the series fits well with the observed binding mode of **40** in the allosteric binding pocket and on balance the data supports this as the binding site relevant to the observed inhibition. The *iso*propylphenyl group is shown to fit very tightly into this binding pocket, and Table 1 shows that substituents on the phenyl ring are not tolerated in the *meta* and *para* positions (**9**, **18** and **19**), except for F-atoms (**16** and **17**). It is not clear why compounds **20** and **21** show weak activity, but from the obtained crystal structure, binding to the ATP pocket cannot be ruled out. The *ortho iso*propyl group is important both for filling the lipophilic pocket formed by Leu182, Pro183, Phe185, Phe272 and Leu273 and stabilizing the binding conformation through internal hydrophobic contact. A trifluoromethyl group at the same position is also able to fill the pocket and stabilize the conformation, but all other groups tested were, in retrospect, too small (**6**, **7** and **8**) or too large (**25**) to fill the binding pocket or likely forced the ligand into a non-binding conformation (**26** and **27**). The SAR around the R^2 substituent in Table 1 shows that a 2-pyridine (**14**) is slightly favoured over a phenyl substituent (**11**), and the crystal structure suggests that this is due to the interaction with Thr377. The changes shown in Table 3 are modifications to parts of the core that are mostly outside the binding pocket, so it is not surprising that these changes are well-tolerated. Only **39** is inactive, and this is likely due to the *N*-methyl group clashing with the N165 side chain.

The binding mode of **40** found in Chains A, C and D of the complex fits well with the findings from mutational studies and hydrogen–deuterium exchange-MS (HDX-MS) experiments by Clarke *et al.* that suggested the putative PI5P-binding site of PI5P4Kγ, not the ATP-binding site, to be the likely region of interaction[30] of **1**. The HDX-MS method measures the rate of exchange of solvent accessible protons from protein amides with deuterium. Changes in exchange accessibility generated by binding of enzyme with inhibitor are detected by peptide mass spectrometry. The regions with reduced HDX-accessibility may indicate ligand binding sites or structural changes in the protein. The main sites showing an HDX-MS effect in Clarke *et al*.'s study are shown in Figure 5 projected onto the PI5P4Kγ-**40** complex, where site 1 comprises residues 158-162 and site 2 comprises residues 373-407. Both sites are in close proximity to **40** in the allosteric binding mode. Residues 378-380 in particular change their environment on binding with **40**, as they move from a flexible loop conformation without electron density in the apo structure and chain B to a buried location in the alternative protein conformation of chains A, C and D (Figure 5a, b). Clarke *et al*. also found that a N165I mutation removed sensitivity of PI5P4Kγ to **1**[30]. The NH_2 of Asn165 makes an H-bond interaction with the pyrimidine *N* of **40**, therefore mutating this to an *iso*leucine would reduce the binding energy significantly (Figure 5c). Asn165 is unique to the PI5P4Kγ isoform, the PI5P4Kα and PI5P4Kβ isoforms have an *iso*leucine in this position. This explains the selectivity of **40** and analogues for the PI5P4Kγ isoform.

Given that both of the binding modes of **40** observed in the X-ray structure have an occupied ATP binding site it might be expected that each of these would be associated with an ATP-competitive inhibition mechanism. In the chain-B structure the ATP site is directly occupied by **40** which would unambiguously lead to an ATP-competitive mode of inhibition. On the other hand, in chains A, C and D the ATP-binding site is occupied by the flexible loop. We hypothesise that the X-ray structure captures one possible conformation of this loop and that it is possible for this loop to adopt other conformations that would open up the ATP binding site and allow **40** to remain bound in conjunction with ATP.

Previous studies have shown that basal ATP turnover in the absence of PI5P is not inhibited by **1**, suggesting inhibitors from this chemical series can bind to the protein simultaneously with a nucleotide[30]. In an attempt to observe this phenomenon crystallographically, we set out to determine a ternary complex with PI5P4Kγ, **40** and the ATP derivative AMP-PNP. This resulted in a 1.95 Å crystal structure (pdb code 7QPN; Figure S3) that is highly similar to the one shown in Figures 2 and 3, but with AMP-PNP bound in a shallow pocket on the outside surface of the protein, not in the ATP pocket, as is also seen in PI5P4Kβ structure 3X04. Once again, **40** was observed to bind mainly to the allosteric pocket in this structure, with some density for **40** in the ATP pocket

(occupancy 0.35). However, we did not observe simultaneous binding of **40** to the allosteric pocket and AMP-PNP to the ATP pocket. Overall, the combined dataset is most consistent with the A/C/D chain binding mode, with support from the HDX data and with the SAR developed around this series.

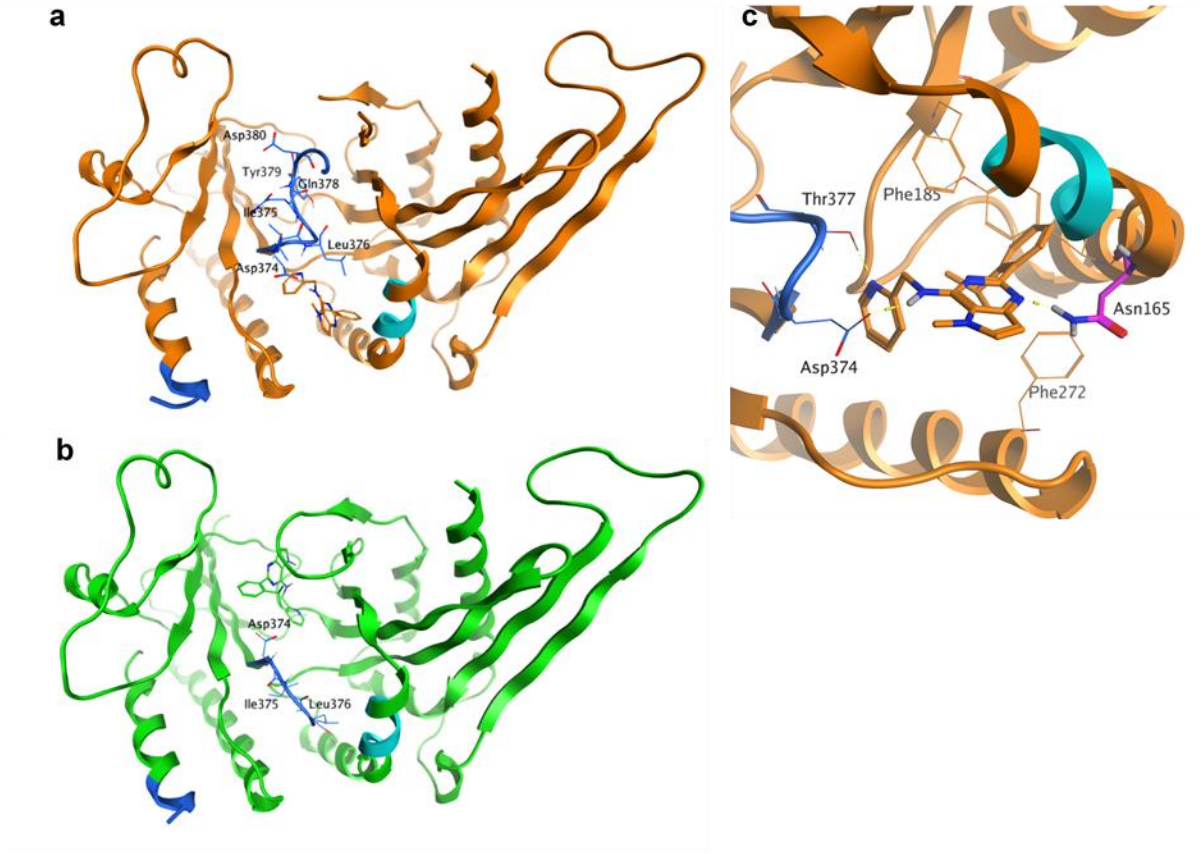

Figure 5. a) Chain A in orange (allosteric binding site occupied), b) Chain B in green (ATP site occupied) for 7QIE. HDX-MS sites identified are shown in cyan (site 1: residues 158-162) and blue (site 2: residues 373-407). Lys383A-Val403A and Thr377B-His404B, which connect the two regions of site 2, are not visible in the crystal structure. The *N*-terminal part of site 2 adopts different conformations in chains A and B. c) A close-up of chain A with **40** bound highlighting the location of Asn165. The N165I mutation was found to remove sensitivity of PI5P4Kγ to **40**.

In conclusion, we have optimised a series of selective small-molecule PI5P4Kγ inhibitors to improve both potency and physicochemical properties and enable structural biology studies. We have presented binding constants, thermal shift data and biochemical data, which show that, in general, this chemotype does not inhibit PI5P4Kα or β. In addition, we have shown that exemplars such as **40** are able to engage the PI5P4Kγ target in cells and that, in X-ray co-structures with PI5P4Kγ, **40** can adopt two distinct modes of inhibition, with binding to a distal lipid

binding site which is 18 Å from the ATP pocket preferred. The nature of this novel mode of inhibition remains to be further elucidated and may involve PI5P competition or conformational changes in the protein that manifest through changes in the interactions with distinct protein complexes. Further studies to understand the cell biology of these inhibitors and to identify novel chemotypes with further improved potencies and physicochemical properties are underway and will be the topic of future publications.

Experimental Section

Chemistry: Compound **9** was purchased from Ambinter (Amb16536894) and was determined by UPLC to have purity >95%. All other compounds were synthesised as described below, and all tested compounds have purity >95% by UPLC analysis. Compounds were synthesised according to schemes S1-S3 as described in the supporting information section.

X-ray crystallography and structure determination

Crystallography was performed by Peak Proteins Ltd. Truncated human PI5P4Kγ was expressed in *E.coli* BL21(DE3) Gold using a pET28b vector. Expression was induced using 0.1 mM IPTG and the cells cultured at 18 °C for 16 h before harvesting by centrifugation. The protein comprised of residues His32 to Ala421 with the region between and inclusive of residues 300-341 deleted. Purification of TEV-cleaved protein was by both affinity and size exclusion (Superdex 75) chromatography. The structure of the ligand complex was generated by co-crystallisation of human PI5P4Kγ in the presence of **40.** Purified protein (15.5mg/ml in 20mM HEPES pH7.5, 150 mM NaCl, 0.5mM TCEP) was incubated with 10 mM **40** (from 400 mM stock in DMSO) overnight at 4 °C. Crystals were grown from 22% w/v Peg3350, 0.3 M Ammonium Tartrate, 100mM PCPT (sodium propionate, sodium cacodylate trihydrate, bis-tris propane) pH 7.5 at 20 °C. Where AMP-PNP was used, the protein was first incubated with 4 mM AMP-PNP (in buffer) for 2 hours and then overnight with 10 mM **40** before setting crystal trays. For X-ray data collection they were flash-frozen and X-ray diffraction data were collected at 100K. (Diamond Light Source synchrotron facility, Oxford, UK, Beamlines (I03 and I24 for 7QIE and 7QPN, respectively.). Data were processed using the XDS and Aimless software. The phase information necessary to determine and analyse the structure was obtained by molecular replacement (PHASER, CCP4) using the previously solved structure of a human PI5P4Kγ (PDB code: 2GK9) as the search model. Subsequent model building and refinement was performed according to standard protocols with the software packages CCP4 and COOT. TLS refinement (REFMAC5, CCP4) has been carried out, which resulted in lower R-factors and higher

quality of the electron density map. The ligand parameterisation and the generation of the corresponding library files was carried out with ACEDRG (CCP4). The Ramachandran Plots of the final models show 91.3% and 92.3% of all residues in the most favoured regions and 7.0% and 5.0% in the additionally allowed regions, for 7QIE and 7QPN, respectively. Statistics of the final structure and the refinement process are listed in Table S5.

Computational modelling

The Maestro QM tautomer and conformer predictor (release 2019-3, Schrodinger, https://www.schrodinger.com/) was used to predict the 5 lowest energy conformers of **40**. The predictor generates conformers using macromodel, and then performs DFT geometry optimizations on the structures, using the B3LYP-D3/LACVP** level of theory. The structures were then ranked using optimization energies at the M06-2X/cc-pVTZ(-f) theory level in solution (water:PBF) calculated using the geometries from the previous step. The RMSD of the lowest energy conformer with the ligand from chain A of the minimized crystal structure (Maestro Protein Preparation, default settings) was then calculated using the Maximum Common Structure superposition algorithm in Maestro.

Free energy of binding was calculated using the Dock panel in MOE (release 2019.0101, Chemical Computing Group, www.chemcomp.com), using the crystal structure placement, with induced fit refinement guided by the GBVI/WSA dG scoring function. E_refine for the two binding modes of **40** was compared.

Marvin was used for clogP calculations using the consensus method, (Marvin 20.15, ChemAxon https://www.chemaxon.com).

Biochemical assays

Recombinant mutant PI5P4Kγ+ was prepared essentially as described previously[25]. Protein from *PIP4K2C* (UniGene 6280511), genetically modified to have a specific activity close to that of the active PI5P4Kα isoform[25] and cloned into the expression vector pGEX6P (Cytiva), was expressed and purified from *E. coli* BL21(DE3). Cultures were induced with 0.4 mM IPTG and probe-sonicated in the presence of protease inhibitors. GST fusion protein of PI5P4Kγ+ was harvested by binding to glutathione sepharose beads (Cytiva) and cleaved *in situ* with 50U of PreScission protease (Cytiva) for 4 hours at 4°C. Cleaved protein was further purified by size exclusion chromatography (AKTA Pure, Cytiva). Protein purity was confirmed by SDS-PAGE and concentration determined by colorimetric assay (Bio-Rad).

PI5P4Kγ+ activity in the presence of inhibitor compounds was determined by ADP-Glo assay (Promega). The assay was performed in a 384 well plate (Greiner 784201) with serial dilutions of test compound in 18µl of reaction

mix (20µM di-C8 PI5P, 10µM ATP, 33mM HEPES pH7.4, 0.1% CHAPS, 20mM $MgCl_2$ and 16.7µM EGTA). The plate was incubated for 60 minutes at room temperature after addition of purified PI5P4Kγ+ (150ng/well) and prior to the transfer of 4µl of the reaction mix into a second plate (Greiner 784904) containing 4µl of ADP-Glo Reagent™ for a further 40 minute incubation. After incubation with 8µl of Kinase Detection Reagent for 30 minutes, plate luminescence was read (Pherastar FSX, BMG Labtech).

Binding of compounds to PI5P4Kγ in intact cells was assessed using an INCell Pulse thermal stabilisation assay (DiscoverX). Hek293 cells stably expressing ePL-tagged PI5P4Kγ were incubated with 25nl of test compound in 100% DMSO in a black skirted PCR plate for 60 minutes at 38ºC. After incubation for 3 minutes at 46ºC, followed by cooling for 3 minutes at room temperature, 12µl of EA-3 reagent (prepared as per the manufactures guidelines) was added to each well. The plate was then incubated for 60 minutes in the dark prior to luminescence reading on a Pherastar FSX plate reader (BMG Labtech).

Data analysis

Statistical analysis was performed using non-parametric testing in Prism 8 (GraphPad). Activity pIC_{50} values and *in vivo* binding pEC_{50} values were estimated using a 4-parameter fit (Dotmatics).

Thermal shift assay: The thermal shift assay was performed with an Applied Biosystem StepOne Real-Time PCR system in 96-well plates sealed with optically clear lids. The fluorescent dye Sypro Orange was used to report on protein unfolding. The final concentration of PI5P4K protein was 4 µM, the ligand was at 63 µM, in a final volume of 20 µL. A 5000x stock solution of Sypro Orange was used, at a final concentration of 5x. The buffer was 50mM HEPES pH 7.4, 5mM $MgCl_2$, 100mM NaCl. The plates were heated from 25 °C to 90 °C at a rate of 0.5 °C/min. The thermal melting point was calculated for each well by monitoring the minimum point of the negative derivative of the fluorescence unfolding curves. Thermal shifts were calculated by comparison to control wells with no compound (5% DMSO). At least two chemical replicates of each ligand was performed, with control compounds used to check for consistency between plates.

ASSOCIATED CONTENT

Supporting Information

The Supporting Information is available free of charge on the ACS Publications website. Supplementary, tables and figures as well as further experimental details (ADMET, Chemical synthesis with schemes, selected NMR and HPLC spectra and molecular formula strings).

AUTHOR INFORMATION

Author Contributions

The manuscript was written through contributions of all authors. All authors have given approval to the final version of the manuscript. Stephen Andrews and Jonathan Clarke were program leaders, John Skidmore and James Duce offered further project leadership, Henriette Willems developed in silico models, analysed the X-structures and docked compounds, Helen Boffey, Simon Edwards and Timothy Rooney designed and synthesised the compounds, Duncan Scott developed thermal shift assays, David Winpenny, Tamara Romero and Christopher Green developed ADP-glo and INCell pulse assays and screened the compounds, Tina Howard and Derek Ogg planned and executed protein construct synthesis and X-ray crystallography studies.

Funding Sources

This work was funded by Alzheimer's Research UK (grant: ARUK-2015DDI-CAM), with support from the ALBORADA Trust. The ALBORADA Drug Discovery Institute is core funded by Alzheimer's Research UK (registered charity No. 1077089 and SC042474).

ACKNOWLEDGMENT

The authors wish to thank Professor David C. Rubinsztein for insightful discussions on the PI5P4K biology and suggestions for improving the manuscript.

ABBREVIATIONS

ATP, adenosine triphosphate; LE, ligand efficiency; mTOR, mechanistic target of rapamycin; PI5P4K, phosphatidylinositol 5-phosphate 4-kinase; SAR, structure-activity relationships; WT, wild-type

New PDB IDs

Authors will release the atomic coordinates upon article publication.

7QIE: 2.4Å structure of **40** bound to PI5P4Kγ

7QPN: 1.95Å structure of AMP-PNP and **40** bound to PI5P4Kγ

References

(1) Balla, T. Phosphoinositides: Tiny Lipids With Giant Impact on Cell Regulation. *Physiol Rev* **2013**, *93*, 1019–1137.

https://doi.org/10.1152/physrev.00028.2012.-Phosphoinositides.

(2) Burke, J. E. Structural Basis for Regulation of Phosphoinositide Kinases and Their Involvement in Human Disease. *Mol. Cell* **2018**, *71* (5), 653–673. https://doi.org/10.1016/j.molcel.2018.08.005.

(3) Halstead, J. R.; Jalink, K.; Divecha, N. An Emerging Role for PtdIns(4,5)P2-Mediated Signalling in Human Disease. *Trends Pharmacol. Sci.* **2005**, *26* (12), 654–660. https://doi.org/10.1016/j.tips.2005.10.004.

(4) Conduit, S. E.; Vanhaesebroeck, B. Phosphoinositide Lipids in Primary Cilia Biology. *Biochem. J.* **2020**, *477* (18), 3541–3565. https://doi.org/10.1042/BCJ20200277.

(5) van der Schaar, H. M.; Dorobantu, C. M.; Albulescu, L.; Strating, J. R. P. M.; van Kuppeveld, F. J. M. Fat(Al) Attraction: Picornaviruses Usurp Lipid Transfer at Membrane Contact Sites to Create Replication Organelles. *Trends Microbiol.* **2016**, *24* (7), 535–546. https://doi.org/10.1016/j.tim.2016.02.017.

(6) Rameh, L. E.; Tolias, K. F.; Duckworth, B. C.; Cantley, L. C. A New Pathway for Synthesis of Phosphatidylinositol-4,5-Bisphosphate. *Nature* **1997**, *390* (6656), 192–196. https://doi.org/10.1038/36621.

(7) Clarke, J. H.; Irvine, R. F. The Activity, Evolution and Association of Phosphatidylinositol 5-Phosphate 4-Kinases. *Advances in Biological Regulation*. Elsevier Ltd 2012, pp 40–45. https://doi.org/10.1016/j.advenzreg.2011.09.002.

(8) Wang, D. G.; Paddock, M. N.; Lundquist, M. R.; Sun, J. Y.; Mashadova, O.; Amadiume, S.; Bumpus, T. W.; Hodakoski, C.; Hopkins, B. D.; Fine, M.; Hill, A.; Yang, T. J.; Baskin, J. M.; Dow, L. E.; Cantley, L. C. PIP4Ks Suppress Insulin Signaling through a Catalytic-Independent Mechanism. *Cell Rep.* **2019**, *27* (7), 1991-2001.e5. https://doi.org/10.1016/j.celrep.2019.04.070.

(9) Zheng, L.; Conner, S. D. PI5P4Kγ Functions in DTX1-Mediated Notch Signaling. *Proc. Natl. Acad. Sci. U. S. A.* **2018**, *115* (9), E1983–E1990. https://doi.org/10.1073/pnas.1712142115.

(10) Gelato, K. A.; Tauber, M.; Ong, M. S.; Winter, S.; Hiragami-Hamada, K.; Sindlinger, J.; Lemak, A.; Bultsma, Y.; Houliston, S.; Schwarzer, D.; Divecha, N.; Arrowsmith, C. H.; Fischle, W. Accessibility of Different Histone H3-Binding Domains of UHRF1 Is Allosterically Regulated by Phosphatidylinositol 5-Phosphate. *Mol. Cell* **2014**, *54* (6), 905–919. https://doi.org/10.1016/j.molcel.2014.04.004.

(11) Keune, W. J.; Jones, D. R.; Bultsma, Y.; Sommer, L.; Zhou, X. Z.; Lu, K. P.; Divecha, N. Regulation of Phosphatidylinositol-5-Phosphate Signaling by Pin1 Determines Sensitivity to Oxidative Stress. *Sci. Signal.* **2012**, *5* (252). https://doi.org/10.1126/scisignal.2003223.

(12) Emerling, B. M.; Hurov, J. B.; Poulogiannis, G.; Tsukazawa, K. S.; Choo-Wing, R.; Wulf, G. M.; Bell, E. L.; Shim, H. S.; Lamia, K. A.; Rameh, L. E.; Bellinger, G.; Sasaki, A. T.; Asara, J. M.; Yuan, X.; Bullock, A.; Denicola, G. M.; Song, J.; Brown, V.; Signoretti, S.; Cantley, L. C. XDepletion of a Putatively Druggable Class of Phosphatidylinositol Kinases Inhibits Growth of P53-Null Tumors. *Cell* **2013**, *155* (4), 844. https://doi.org/10.1016/j.cell.2013.09.057.

(13) Jude, J. G.; Spencer, G. J.; Huang, X.; Somerville, T. D. D.; Jones, D. R.; Divecha, N.; Somervaille, T. C. P. A Targeted Knockdown Screen of Genes Coding for Phosphoinositide Modulators Identifies PIP4K2A as Required for Acute Myeloid Leukemia Cell Proliferation and Survival. *Oncogene* **2015**, *34* (10), 1253–1262. https://doi.org/10.1038/onc.2014.77.

(14) Lima, K.; Coelho-Silva, J. L.; Kinker, G. S.; Pereira-Martins, D. A.; Traina, F.; Fernandes, P. A. C. M.; Markus, R. P.; Lucena-Araujo, A. R.; Machado-Neto, J. A. PIP4K2A and PIP4K2C Transcript Levels Are Associated with Cytogenetic Risk and Survival Outcomes in Acute Myeloid Leukemia. *Cancer Genet.* **2019**, *233–234*, 56–66. https://doi.org/10.1016/j.cancergen.2019.04.002.

(15) Lamia, K. A.; Peroni, O. D.; Kim, Y.-B.; Rameh, L. E.; Kahn, B. B.; Cantley, L. C. Increased Insulin Sensitivity and Reduced Adiposity in Phosphatidylinositol 5-Phosphate 4-Kinase B−/− Mice. *Mol. Cell. Biol.* **2004**, *24* (11), 5080–5087.

https://doi.org/10.1128/mcb.24.11.5080-5087.2004.

(16) Shim, H.; Wu, C.; Ramsamooj, S.; Bosch, K. N.; Chen, Z.; Emerling, B. M.; Yun, J.; Liu, H.; Choo-Wing, R.; Yang, Z.; Wulf, G. M.; Kuchroo, V. K.; Cantley, L. C. Deletion of the Gene Pip4k2c, a Novel Phosphatidylinositol Kinase, Results in Hyperactivation of the Immune System. *Proc. Natl. Acad. Sci. U. S. A.* **2016**, *113* (27), 7596–7601. https://doi.org/10.1073/pnas.1600934113.

(17) Bulley, S. J.; Droubi, A.; Clarke, J. H.; Anderson, K. E.; Stephens, L. R.; Hawkins, P. T.; Irvine, R. F. In B Cells, Phosphatidylinositol 5-Phosphate 4-Kinase-α Synthesizes PI(4,5)P2 to Impact MTORC2 and Akt Signaling. *Proc. Natl. Acad. Sci. U. S. A.* **2016**, *113* (38), 10571–10576. https://doi.org/10.1073/pnas.1522478113.

(18) Gupta, A.; Toscano, S.; Trivedi, D.; Jones, D. R.; Mathre, S.; Clarke, J. H.; Divecha, N.; Raghu, P. Phosphatidylinositol 5-Phosphate 4-Kinase (PIP4K) Regulates TOR Signaling and Cell Growth during Drosophila Development. *Proc. Natl. Acad. Sci. U. S. A.* **2013**, *110* (15), 5963–5968. https://doi.org/10.1073/pnas.1219333110.

(19) Mackey, A. M.; Sarkes, D. A.; Bettencourt, I.; Asara, J. M.; Rameh, L. E. PIP4kγ Is a Substrate for MTORC1 That Maintains Basal MTORC1 Signaling during Starvation. *Sci. Signal.* **2014**, *7* (350). https://doi.org/10.1126/scisignal.2005191.

(20) Vicinanza, M.; Korolchuk, V. I.; Ashkenazi, A.; Puri, C.; Menzies, F. M.; Clarke, J. H.; Rubinsztein, D. C. PI(5)P Regulates Autophagosome Biogenesis. *Mol. Cell* **2015**, *57* (2), 219–234. https://doi.org/10.1016/j.molcel.2014.12.007.

(21) Lundquist, M. R.; Goncalves, M. D.; Loughran, R. M.; Possik, E.; Vijayaraghavan, T.; Yang, A.; Pauli, C.; Ravi, A.; Verma, A.; Yang, Z.; Johnson, J. L.; Wong, J. C. Y.; Ma, Y.; Hwang, K. S. K.; Weinkove, D.; Divecha, N.; Asara, J. M.; Elemento, O.; Rubin, M. A.; Kimmelman, A. C.; Pause, A.; Cantley, L. C.; Emerling, B. M. Phosphatidylinositol-5-Phosphate 4-Kinases Regulate Cellular Lipid Metabolism By Facilitating Autophagy. *Mol. Cell* **2018**, *70* (3), 531-544.e9. https://doi.org/10.1016/j.molcel.2018.03.037.

(22) Zhang, Y.; Wang, H.; Chen, T.; Wang, H.; Liang, X.; Zhang, Y.; Duan, J.; Qian, S.; Qiao, K.; Zhang, L.; Liu, Y.; Wang, J. C24-Ceramide Drives Gallbladder Cancer Progression Through Directly Targeting Phosphatidylinositol 5-Phosphate 4-Kinase Type-2 Gamma to Facilitate Mammalian Target of Rapamycin Signaling Activation. *Hepatology* **2021**, *73* (2), 692–712. https://doi.org/10.1002/hep.31304.

(23) Al-Ramahi, I.; Giridharan, S. S. P.; Chen, Y. C.; Patnaik, S.; Safren, N.; Hasegawa, J.; de Haro, M.; Gee, A. K. W.; Titus, S. A.; Jeong, H.; Clarke, J.; Krainc, D.; Zheng, W.; Irvine, R. F.; Barmada, S.; Ferrer, M.; Southall, N.; Weisman, L. S.; Botas, J.; Marugan, J. J. Inhibition of PIP4Kγ Ameliorates the Pathological Effects of Mutant Huntingtin Protein. *Elife* **2017**, *6*. https://doi.org/10.7554/eLife.29123.

(24) Roskoski, R. Classification of Small Molecule Protein Kinase Inhibitors Based upon the Structures of Their Drug-Enzyme Complexes. *Pharmacol. Res.* **2016**, *103*, 26–48. https://doi.org/10.1016/j.phrs.2015.10.021.

(25) Clarke, J. H.; Irvine, R. F. Evolutionarily Conserved Structural Changes in Phosphatidylinositol 5-Phosphate 4-Kinase (PI5P4K) Isoforms Are Responsible for Differences in Enzyme Activity and Localization. *Biochem. J.* **2013**, *454* (1), 49–57. https://doi.org/10.1042/BJ20130488.

(26) Rao, V. D.; Misra, S.; Boronenkov, I. V.; Anderson, R. A.; Hurley, J. H. Structure of Type IIβ Phosphatidylinositol Phosphate Kinase: A Protein Kinase Fold Flattened for Interfacial Phosphorylation. *Cell* **1998**, *94* (6), 829–839. https://doi.org/10.1016/S0092-8674(00)81741-9.

(27) Davis, M. I.; Hunt, J. P.; Herrgard, S.; Ciceri, P.; Wodicka, L. M.; Pallares, G.; Hocker, M.; Treiber, D. K.; Zarrinkar, P. P. Comprehensive Analysis of Kinase Inhibitor Selectivity. *Nat. Biotechnol.* **2011**, *29* (11), 1046–1051.

https://doi.org/10.1038/nbt.1990.

(28) Davis, M. I.; Sasaki, A. T.; Shen, M.; Emerling, B. M.; Thorne, N.; Michael, S.; Pragani, R.; Boxer, M.; Sumita, K.; Takeuchi, K.; Auld, D. S.; Li, Z.; Cantley, L. C.; Simeonov, A. A Homogeneous, High-Throughput Assay for Phosphatidylinositol 5-Phosphate 4-Kinase with a Novel, Rapid Substrate Preparation. *PLoS One* **2013**, *8* (1), e54127. https://doi.org/10.1371/journal.pone.0054127.

(29) Sumi, N. J.; Kuenzi, B. M.; Knezevic, C. E.; Remsing Rix, L. L.; Rix, U. Chemoproteomics Reveals Novel Protein and Lipid Kinase Targets of Clinical CDK4/6 Inhibitors in Lung Cancer. *ACS Chem. Biol.* **2015**, *10* (12), 2680–2686. https://doi.org/10.1021/acschembio.5b00368.

(30) Clarke, J. H.; Giudici, M.-L.; Burke, J. E.; Williams, R. L.; Maloney, D. J.; Marugan, J.; Irvine, R. F. The Function of Phosphatidylinositol 5-Phosphate 4-Kinase γ (PI5P4Kγ) Explored Using a Specific Inhibitor That Targets the PI5P-Binding Site. *Biochem. J.* **2015**, *466* (2), 359–367. https://doi.org/10.1042/BJ20141333.

(31) Sivakumaren, S. C.; Shim, H.; Zhang, T.; Ferguson, F. M.; Lundquist, M. R.; Browne, C. M.; Seo, H. S.; Paddock, M. N.; Manz, T. D.; Jiang, B.; Hao, M. F.; Krishnan, P.; Wang, D. G.; Yang, T. J.; Kwiatkowski, N. P.; Ficarro, S. B.; Cunningham, J. M.; Marto, J. A.; Dhe-Paganon, S.; Cantley, L. C.; Gray, N. S. Targeting the PI5P4K Lipid Kinase Family in Cancer Using Covalent Inhibitors. *Cell Chem. Biol.* **2020**. https://doi.org/10.1016/j.chembiol.2020.02.003.

(32) Manz, T. D.; Sivakumaren, S. C.; Yasgar, A.; Hall, M. D.; Davis, M. I.; Seo, H. S.; Card, J. D.; Ficarro, S. B.; Shim, H.; Marto, J. A.; Dhe-Paganon, S.; Sasaki, A. T.; Boxer, M. B.; Simeonov, A.; Cantley, L. C.; Shen, M.; Zhang, T.; Ferguson, F. M.; Gray, N. S. Structure-Activity Relationship Study of Covalent Pan-Phosphatidylinositol 5-Phosphate 4-Kinase Inhibitors. *ACS Med. Chem. Lett.* **2020**, *11* (3), 346–352. https://doi.org/10.1021/acsmedchemlett.9b00402.

(33) Manz, T. D.; Sivakumaren, S. C.; Ferguson, F. M.; Zhang, T.; Yasgar, A.; Seo, H. S.; Ficarro, S. B.; Card, J. D.; Shim, H.; Miduturu, C. V.; Simeonov, A.; Shen, M.; Marto, J. A.; Dhe-Paganon, S.; Hall, M. D.; Cantley, L. C.; Gray, N. S. Discovery and Structure-Activity Relationship Study of (z)-5-Methylenethiazolidin-4-One Derivatives as Potent and Selective Pan-Phosphatidylinositol 5-Phosphate 4-Kinase Inhibitors. *J. Med. Chem.* **2020**, *63* (9), 4880–4895. https://doi.org/10.1021/acs.jmedchem.0c00227.

(34) Manz, T. D.; Sivakumaren, S. C.; Yasgar, A.; Hall, M. D.; Davis, M. I.; Seo, H.-S.; Card, J. D.; Ficarro, S. B.; Shim, H.; Marto, J. A.; Dhe-Paganon, S.; Sasaki, A. T.; Boxer, M. B.; Simeonov, A.; Cantley, L. C.; Shen, M.; Zhang, T.; Ferguson, F. M.; Gray, N. S. Structure–Activity Relationship Study of Covalent Pan-Phosphatidylinositol 5-Phosphate 4-Kinase Inhibitors. *ACS Med. Chem. Lett.* **2019**, acsmedchemlett.9b00402. https://doi.org/10.1021/acsmedchemlett.9b00402.

(35) Sumita, K.; Lo, Y.-H.; Takeuchi, K.; Senda, M.; Kofuji, S.; Ikeda, Y.; Terakawa, J.; Sasaki, M.; Yoshino, H.; Majd, N.; Zheng, Y.; Kahoud, E. R.; Yokota, T.; Emerling, B. M.; Asara, J. M.; Ishida, T.; Locasale, J. W.; Daikoku, T.; Anastasiou, D.; Senda, T.; Sasaki, A. T. The Lipid Kinase PI5P4Kβ Is an Intracellular GTP Sensor for Metabolism and Tumorigenesis. *Mol. Cell* **2016**, *61* (2), 187–198. https://doi.org/10.1016/j.molcel.2015.12.011.

(36) Dexheimer, T. S.; Rosenthal, A. S.; Luci, D. K.; Liang, Q.; Villamil, M. A.; Chen, J.; Sun, H.; Kerns, E. H.; Simeonov, A.; Jadhav, A.; Zhuang, Z.; Maloney, D. J. Synthesis and Structure-Activity Relationship Studies of N -Benzyl-2-Phenylpyrimidin-4-Amine Derivatives as Potent Usp1/Uaf1 Deubiquitinase Inhibitors with Anticancer Activity against Nonsmall Cell Lung Cancer. *J. Med. Chem.* **2014**, *57* (19), 8099–8110. https://doi.org/10.1021/jm5010495.

(37) Kunz, J.; Wilson, M. P.; Kisseleva, M.; Hurley, J. H.; Majerus, P. W.; Anderson, R. A. The Activation Loop of Phosphatidylinositol Phosphate Kinases Determines Signaling Specificity. *Mol. Cell* **2000**, *5* (1), 1–11. https://doi.org/10.1016/S1097-2765(00)80398-6.

(38) Kunz, J.; Fuelling, A.; Kolbe, L.; Anderson, R. A. Stereo-Specific Substrate Recognition by Phosphatidylinositol Phosphate Kinases Is Swapped by Changing a Single Amino Acid Residue. *J. Biol. Chem.* **2002**, *277* (7), 5611–5619. https://doi.org/10.1074/jbc.M110775200.

Supporting Information

Development of Selective Phosphatidylinositol 5-Phosphate 4-Kinase γ (PI5P4Kγ) Inhibitors with a Non-ATP-competitive, Allosteric Binding Mode

Helen K. Boffey,[1‡] Timothy P. C. Rooney,[1‡] Henriette M. G. Willems,[1‡] Simon Edwards,[1‡] Christopher Green,[2] Tina Howard,[3] Derek Ogg,[3] Tamara Romero,[1] Duncan E. Scott,[1] David Winpenny,[1] James Duce,[1] John Skidmore,[1] Jonathan H. Clarke[1] and Stephen P Andrews[1]*

Addresses

[1]Jonathan Clarke, Helen Boffey, Simon Edwards, Tamara Romero, Timothy Rooney, Duncan Scott, Henriette Willems, David Winpenny, James Duce, John Skidmore and Stephen P Andrews: The ALBORADA Drug Discovery Institute, University of Cambridge, Island Research Building, Cambridge Biomedical Campus, Hills Road, Cambridge, CB2 0AH, United Kingdom

[2]Christopher Green: UK Dementia Research Institute, University of Cambridge, Island Research Building, Cambridge Biomedical Campus, Hills Road, Cambridge, CB2 0AH, United Kingdom

[3]Tina Howard, Derek Ogg: Peak Proteins, Alderley Park, Macclesfield, Cheshire, SK10 4TG, United Kingdom

Corresponding Author

*E-mail: spa26@cam.ac.uk

[‡]These authors contributed equally.

Table of Contents

Table S1. Comparison of PI5P4Kγ+ activity data generated in the ADP-Glo assays reported here, versus publicly available PI5P4Kγ data from kinase panels for six known kinase inhibitors.

Chemical Identifiers			**New Data[a]**			**public data for PI5P4Kγ (sourced from: DrugTargetCommons, ChEMBL, PUBMED)**	
Preferred Name	**SMILES**	**ChEMBL ID**	**PI5P4Kα pIC_{50}**	**PI5P4Kβ pIC_{50}**	**PI5P4Kγ+ pIC_{50}**	**pK_D**	**reference**
ML197	Cc1nc(cs1)CNc1ncnc2ccc(cc12)-c1ccc2c(c1)OCO2	CHEMBL1435542	<4.3	ND	5.4	6.6	Rosenthal AS, Tanega C, Shen M, Mott BT, Bougie JM, Nguyen DT, Misteli T, Auld DS, Maloney DJ, Thomas CJ, Potent and selective small molecule inhibitors of specific isoforms of Cdc2-like kinases (Clk) and dual specificity tyrosine-phosphorylation-regulated kinases (Dyrk), Bioorg. Med. Chem. Lett., 2011, 21, 10, 3152, 3158, 10.1016/j.bmcl.2011.02.114
ML106	CN(Cc1csc(n1)C)c1ncnc2ccc(cc12)-c1ccc2c(c1)OCO2	CHEMBL1474834	<4.3	ND	5.0	6.4	Rosenthal AS, Tanega C, Shen M, Mott BT, Bougie JM, Nguyen DT, Misteli T, Auld DS, Maloney DJ, Thomas CJ, Potent and selective small molecule inhibitors of specific isoforms of Cdc2-like kinases (Clk) and dual specificity tyrosine-phosphorylation-regulated kinases (Dyrk), Bioorg. Med. Chem. Lett., 2011, 21, 10, 3152, 3158, 10.1016/j.bmcl.2011.02.114
Foretinib	COc1cc2c(ccnc2cc1OCCCN1CCOCC1)Oc1ccc(cc1F)NC(=O)C1(CC1)C(=O)Nc1ccc(cc1)F	CHEMBL1230609	<4.3	ND	6.2	6.8	Davis MI, Hunt JP, Herrgard S, Ciceri P, Wodicka LM, Pallares G, Hocker M, Treiber DK, Zarrinkar PP, Comprehensive analysis of kinase inhibitor selectivity, Nat. Biotechnol., 2011, 29, 11, 1046, 1051, 10.1038/nbt.1990
BI-2536	CC[C@H]1N(C2CCCC2)c2nc(ncc2N(C)C1=O)Nc1ccc(cc1OC)C(=O)NC1CCN(C)CC1	CHEMBL513909	*4.6	ND	6.0	6.3	Davis MI, Hunt JP, Herrgard S, Ciceri P, Wodicka LM, Pallares G, Hocker M, Treiber DK, Zarrinkar PP, Comprehensive analysis of kinase inhibitor selectivity, Nat. Biotechnol., 2011, 29, 11, 1046, 1051, 10.1038/nbt.1990
Pazopanib	CN(c1ccc2c(n(nc2c1)C)C)c1ccnc(n1)Nc1cc(c(c1)S(=O)(=O)N)C	CHEMBL477772	*4.8	ND	6.0	6.6	Karaman MW, Herrgard S, Treiber DK, Gallant P, Atteridge CE, Campbell BT, Chan KW, Ciceri P, Davis MI, Edeen PT, Faraoni R, Floyd M, Hunt JP, Lockhart DJ, Milanov ZV, Morrison MJ, Pallares G, Patel HK, Pritchard S, Wodicka LM, Zarrinkar PP, A quantitative analysis of kinase inhibitor selectivity., Nat. Biotechnol., 2008, 26, 1, 127, 132, 10.1038/nbt1358
Palbociclib	CC(=O)C1=C(C)c2cnc(nc2N(C2CCCC2)C1=O)Nc1ccc(cn1)N1CCNCC1	CHEMBL189963	<4.3	<4.6	<4.3	5.8	Klaeger S, Heinzlmeir S and Wilhelm M et al., The target landscape of clinical kinase drugs, Science, 2017, 358, ean4368, 10.1126/science.aan4368

[a] pIC_{50}s determined in the ADP-Glo assays described herein

Table S2. Reported PI5P4K activity of compounds **1**-**5**, and comparison with data generated in the assays described in this article (where available).

Compound	**Previously published kinase inhibition data**				**New data**			
	PI5P4Kα activity (assay)	**PI5P4Kβ activity (assay)**	**PI5P4Kγ activity (assay)**	**ref**	**PI5P4Kα IC_{50} (μM)[a]**	**PI5P4Kβ IC_{50} (μM)[a]**	**PI5P4Kγ+ IC_{50} (μM)[a]**	**PI5P4Kγ- WT target engagement IC_{50} (μM)[b]**
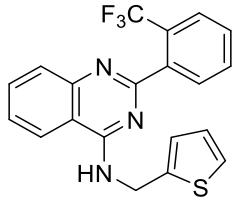 NIH-12848 (**1**)	>100 μM (^{32}P-ATP/PI5P incorporation)	>100 μM (^{32}P-ATP/PI5P incorporation)[c]	2-3 μM (^{32}P-ATP/PI5P incorporation)	1	>50	>25	0.79	2.5
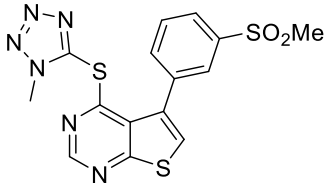 NCT-504 (**2**)	<35% inh @ 10 μM (KINONMEscan)	<65% inh @ 10 μM (KINONMEscan)	16 μM (^{32}P-ATP/PI5P incorporation)	2	2.0	>25	>50	>50
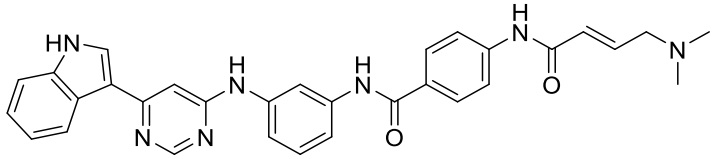 THZ-P1-2 (**3**)	0.95 μM (bioluminescence assay)	5.9 μM (FP assay)	91% inh. @ 1 μM (KINONMEscan)	3	0.13	1.0	0.13	1.3
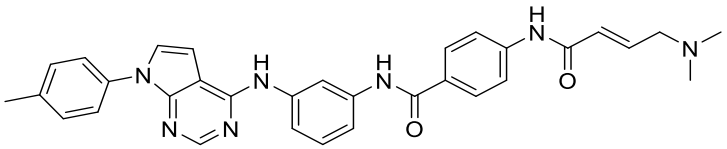 "compound 30" (**4**)	1.3 μM (bioluminescence assay)	9.9 μM (FP assay)	22% inh. @ 1 μM (KINONMEscan)	4	ND	ND	ND	ND
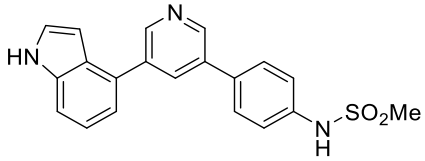 "compound 13" (**5**)	2 μM [c]bioluminescence assay)	22 μM (FP assay)	100% inh. @ 1 μM (KINONMEscan) 0.0034 μM (Ambit K_D)	3	ND	ND	ND	ND

[a]determined in the ADP-Glo assays described herein; [b]determined in the INCell Pulse assay described herein; [c]showed 'small but significant stimulation'.

Table S3: ADP-Glo pIC_{50} for compound against PI5P4Kγ+. Thermal shift (ΔT_m) values for compounds against PI5P4Kγ-WT with compound concentration at 63 µM

	PI5P4Kγ+ pIC_{50}	PI5P4Kγ-WT ΔT_m / °C
1	6.1 ± 0.3	4.7 ± 0.8
6	<4.3 ± 0.0	-1.1 ± 0.3
7	<4.5 ± 0.4	2.7 ± 0.0
8	<4.3 ± 0.0	0.1 ± 0.0
9	<4.3 ± 0.0	-1.6 ± 0.4
10	<4.3 ± 0.0	-0.8 ± 0.0
11	5.2 ± 1.0	4.6 ± 0.0
12	<4.3 ± 0.0	1.4 ± 0.4
13	5.5 ± 0.2	6.1 ± 0.0
14	5.5 ± 0.5	6.3 ± 0.6
15	<4.3 ± 0.0	-1.9 ± 0.0
18	<4.3 ± 0.0	1.3 ± 0.2
19	<4.3 ± 0.0	1.7 ± 0.7
20	5.1 ± 0.2	5.1 ± 0.0
21	5.1 ± 0.1	5.1 ± 0.0
22	6.5 ± 0.3	7.8 ± 0.7
24	5.3 ± 0.4	4.9 ± 0.7
25	5 ± 0.2	4.4 ± 0.7
26	<4.3 ± 0.0	2.9 ± 0.4
27	<4.3 ± 0.0	2.7 ± 0.4
29	<4.4 ± 0.3	0.2 ± 0.4
31	6.2 ± 0.3	7.0 ± 0.0
34	5.4 ± 0.2	4.4 ± 0.0
35	5 ± 0.3	3.9 ± 0.0
36	5.6 ± 0.6	4.4 ± 0.0
38	6.1 ± 0.2	5.5 ± 0.0
40	6.2 ± 0.3	6.9 ± 0.0
41	5.6 ± 0.3	4.9 ± 0.0
42	6.5 ± 0.3	6.8 ± 0.4

Table S4: Thermal shift (ΔT_m) profile of compounds **1**, **14** and **22** against α, β, γ-WT and γ+ isoforms of PI5P4K. Compound concentration was 63 µM.

	PI5P4Kα ΔT_m / °C	PI5P4Kβ ΔT_m / °C	PI5P4Kγ-WT ΔT_m / °C	PI5P4Kγ+ ΔT_m / °C
1	-0.2 ± 0.4	0.6 ± 0.3	4.7 ± 0.8	7.4 ± 0.6
14	-0.2 ± 0.4	0.4 ± 0.2	6.3 ± 0.6	n.d.
22	n.d.	n.d.	7.8 ± 0.8	12.1 ± 0.5

Table S5: Data collection and refinement statistics for X-ray crystal structures of PI5P4Kγ bound to **40**.

PDB ID	**7QIE**	**7QPN**
Protein/Ligand	PI5P4Kγ/**40**	PI5P4Kγ/**40**/AMP-PNP
Wavelength [Å]	0.976250	0.9999
Space group	P 21	P 21
a; b; c; [Å]	49.41; 114.79; 146.9	47.92; 65.62; 117.12
α; β; γ; [◦]	90.0; 95.1; 90.0	90.0; 93.16; 90.0
Resolution [Å]	146.17-2.39 (2.46-2.39)[a]	116.94-1.95 (2.14-1.95)
Unique reflections	62636 (18607)[2]	41286
Multiplicity	3.4 (3.3)[2]	5.5 (5.1)[2]
Completeness [%]	97.8 (99.4)	91.7 (56.5)
Rsym [%]	10 (271)[2]	11 (174)[2]
Rmeas [%]	12 (220)[2]	13 (199)[2]
Mean(I)/sd	4.7 (0.4)[2]	8.9 (1.1)[2]
CC(1/2)	0.998 (0.359)	0.996 (0.557)
Number of reflections (free)	34407 (1799)	37666 (1877)
R_{cryst} [%]	21.4	19.2
R_{free}[%]	26.6	26.2
Protein	9762	5132
Water	198	210
Ligand	108	116
Deviation from ideal geometry:		
Bond lengths [Å]	0.01	0.01
Bond angles [◦]	1.60	1.60

[a]values in parenthesis refer to the highest resolution bin.

Table S6: K_D values for **1** and **40**.[a]

Compound	PI5P4Kβ K_D (nM)	PI5P4Kγ K_D (nM)
1	>30,000	4000
40	>30,000	68

[a] Data were generated at Eurofins Discovery using DiscoverX KINOMEscan™ technology. Streptavidin-coated magnetic beads were treated with biotinylated small molecule ligands for 30 minutes at room temperature to generate affinity resins for kinase assays. The liganded beads were blocked with excess biotin and washed with blocking buffer (SeaBlock (Pierce), 1% BSA, 0.05% Tween 20, 1 mM DTT) to remove unbound ligand and to reduce non-specific binding. Binding reactions were assembled by combining kinases, liganded affinity beads, and test compounds in 1x binding buffer (20% SeaBlock, 0.17x PBS, 0.05% Tween 20, 6 mM DTT). Test compounds were prepared as 111X stocks in 100% DMSO. Kds were determined using an 11-point 3-fold compound dilution series with three DMSO control points. All compounds for Kd measurements are distributed by acoustic transfer (non-contact dispensing) in 100% DMSO. The compounds were then diluted directly into the assays such that the final concentration of DMSO was 0.9%. All reactions performed in polypropylene 384-well plate. Each was a final volume of 0.02 ml. The assay plates were incubated at room temperature with shaking for 1 hour and the affinity beads were washed with wash buffer (1x PBS, 0.05% Tween 20). The beads were then re-suspended in elution buffer (1x PBS, 0.05% Tween 20, 0.5 μM nonbiotinylated affinity ligand) and incubated at room temperature with shaking for 30 minutes. The kinase concentration in the eluates was measured by qPCR.

Table S7. PI5P4Kα adapta assay results for compounds **1** and **40**.[a]

Compound	PI5P4Kα adapta IC_{50} (nM)
1	>30,000
40	>30,000

[a] The experiments were run by Thermo Fisher. This assay is a TR-FRET based assay using an Eu-anti-ADP antibody, the conditions are: the 2X PIP4Kα/PI(5)P mixture is prepared in 50 mM HEPES pH 7.5, 0.1% CHAPS, 1 mM EGTA, 4 mM MgCl2. The final 10 μL Kinase Reaction consists of 1.5 - 6 ng PIP4Kα and 50 μM PI(5)P in 32.5 mM HEPES pH 7.5, 0.05% CHAPS, 0.5 mM EGTA, 2 mM MgCl2. After the 1 hour Kinase Reaction incubation, 5 μL of Detection Mix is added. The Detection mix consists of EDTA (30mM), Eu-anti-ADP antibody (6 nM) and ADP tracer in TR-FRET buffer. The detection mix contains the EC60 concentration of tracer for 5-150 mM ATP.

Table S8. Kinase selectivity screening for **40** at 10 μM against a general kinase panel of 140 targets in radiometric filter binding assay using 33P-g-ATPat the MRC PPU International Centre for Kinase Profiling, University of Dundee.

Kinase	**% activity remaining**	**s.d.**
MKK1	**92**	7
MKK2	**115**	1
MKK6	**90**	2
ERK1	**111**	11
ERK2	**98**	7
ERK5	**138**	13
JNK1	**86**	12
JNK2	**110**	14
JNK3	**97**	4
p38a MAPK	**100**	6
p38b MAPK	**94**	11
p38g MAPK	**105**	7
p38d MAPK	**117**	3
ERK8	**109**	1
RSK1	**99**	2
RSK2	**106**	8
PDK1	**103**	4
PKBa	**103**	4
PKBb	**75**	1
SGK1	**98**	7
S6K1	**95**	11
PKA	**109**	9
ROCK 2	**97**	14
PRK2	**83**	14
PKCa	**118**	9
PKCγ	**77**	4
PKCz	**111**	1
PKD1	**109**	10
STK33	**99**	1
MSK1	**95**	15
MNK1	**104**	8
MNK2	**117**	7

MAPKAP-K2	**123**	7
MAPKAP-K3	**102**	18
PRAK	**98**	1
CAMKKb	**99**	11
CAMK1	**97**	7
SmMLCK	**108**	12
PHK	**107**	11
DAPK1	**105**	2
CHK1	**96**	5
CHK2	**110**	0
GSK3b	**93**	14
CDK2-Cyclin A	**103**	3
CDK9-Cyclin T1	**108**	8
PLK1	**97**	1
Aurora A	**94**	10
Aurora B	**113**	14
TLK1	**115**	9
LKB1	**94**	6
AMPK (hum)	**88**	1
MARK1	**88**	6
MARK2	**101**	1
MARK3	**101**	6
MARK4	**105**	2
BRSK1	**115**	10
BRSK2	**83**	3
MELK	**95**	8
NUAK1	**88**	4
SIK2	**100**	5
SIK3	**111**	11
TSSK1	**96**	9
CK1γ2	**97**	1
CK1δ	**100**	3
CK2	**90**	15
TTBK1	**117**	3
TTBK2	**114**	8
DYRK1A	**101**	12
DYRK2	**106**	1

DYRK3	**128**	13
NEK2a	**103**	4
NEK6	**120**	2
IKKb	**100**	13
IKKe	**98**	11
TBK1	**93**	0
PIM1	**102**	3
PIM2	**110**	1
PIM3	**87**	3
SRPK1	**93**	5
EF2K	**98**	6
EIF2AK3	**103**	9
HIPK1	**104**	11
HIPK2	**114**	13
HIPK3	**92**	10
CLK2	**94**	6
PAK2	**45**	8
PAK4	**95**	1
PAK5	**120**	9
PAK6	**95**	2
MST2	**115**	7
MST3	**110**	13
MST4	**110**	17
GCK	**93**	6
MAP4K3	**91**	6
MAP4K5	**112**	1
MINK1	**95**	10
MEKK1	**68**	5
MLK1	**89**	10
MLK3	**90**	2
TESK1	**114**	1
TAO1	**115**	0
ASK1	**116**	0
TAK1	**110**	4
IRAK1	**114**	3
IRAK4	**114**	5
RIPK2	**92**	10

OSR1	**120**	14
TTK	**94**	7
MPSK1	**106**	14
WNK1	**112**	6
ULK1	**111**	3
ULK2	**91**	0
TGFBR1	**91**	4
Src	**135**	13
Lck	**102**	7
CSK	**94**	4
YES1	**115**	6
ABL	**108**	10
BTK	**111**	2
JAK3	**97**	3
SYK	**91**	2
ZAP70	**95**	5
TIE2	**89**	3
BRK	**112**	2
EPH-A2	**104**	12
EPH-A4	**96**	8
EPH-B1	**95**	9
EPH-B2	**78**	1
EPH-B3	**105**	13
EPH-B4	**120**	6
FGF-R1	**92**	3
HER4	**112**	2
IGF-1R	**107**	7
IR	**119**	13
IRR	**99**	12
TrkA	**100**	1
DDR2	**90**	8
VEG-FR	**125**	14
PDGFRA	**100**	1
PINK	**125**	10

Table S9. Lipid kinase selectivity screening for **40** at 10 μM against a kinase panel of 15 protein kinase targets using ADP-GloTM assay at the MRC PPU International Centre for Kinase Profiling, University of Dundee.

Kinase	**% activity remaining**	**s.d.**
PI3Kalpha	**91.4**	2.4
PI3K beta	**111.2**	1.2
PI3K gamma	**102.9**	2.3
Choline Kinase alpha	**101.6**	3.2
Choline Kinase beta	**97.3**	12.0
PIP5K2a	**100.3**	0.7
PI3Ka E524K +P85	**102.0**	10.7
PI3KA E545K +P85	**91.7**	0.9
PI4K2a	**93.5**	6.5
SPHK1	**91.8**	2.4
SPHK2	**83.8**	6.8
PIK4Ca	**81.1**	3.0
DGK beta	**102.0**	3.4
DGK gamma	**99.4**	4.6
DGK zeta	**106.2**	0.4

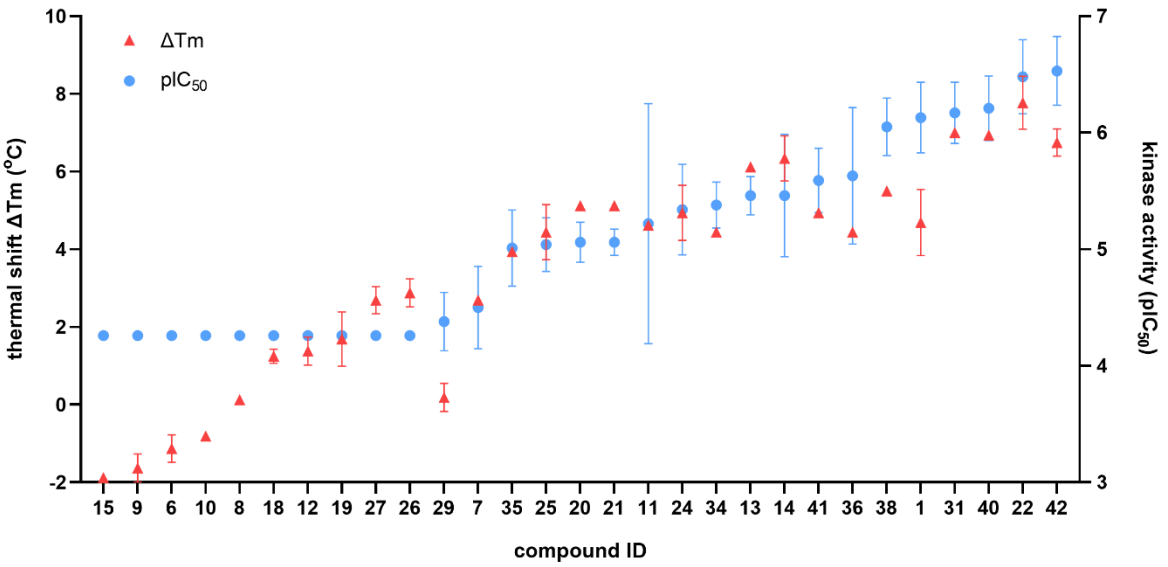

Figure S1: A comparison of compound pIC_{50} for PI5P4Kγ+ (red triangle, determined by ADP-Glo) to ΔTm for PI5P4Kγ-WT (blue circle, determined by thermal shift assay). Data are shown as mean value ± standard error.

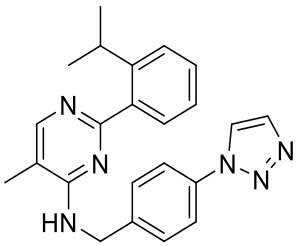

Figure S2: Structure of ML323.[5]

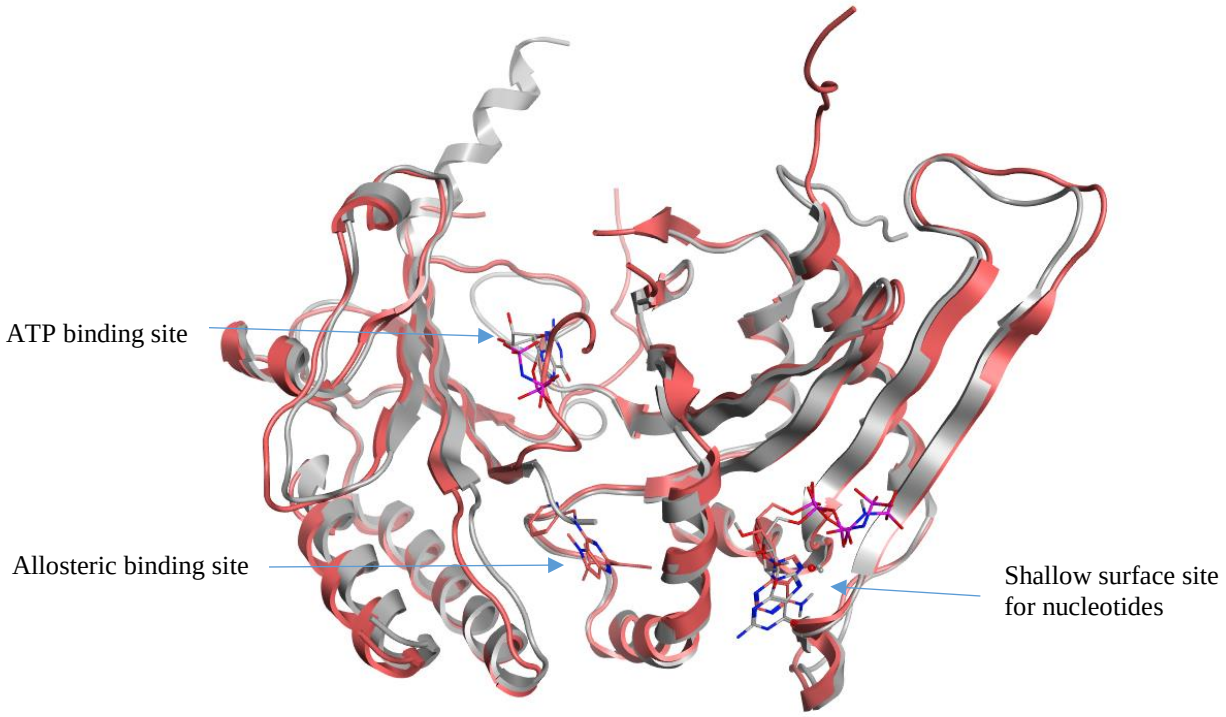

Figure S3. PI5P4Kγ/**40**/AMP-PNP (pdb 7QPN) in rose superposed onto PI5P4Kβ structure 3X04 chain A in grey. One GMP-PNP molecule binds in the ATP site of 3X04 binds and another one in a similar position to the AMP-PNP ligand of PI5P4Kγ/**40**/AMP-PNP on the surface of the protein (bottom right).

Supporting Experimental:

ADMET experimental

Microsomal stability analysis was performed by Charles River Laboratories Inc. (ADME-SOP-84). Briefly, test compounds in DMSO were incubated at a concentration of 1 µM (0.25% DMSO final) with mouse hepatic microsomes (0.5 mg protein/mL) in the presence of NADPH (1 mM) at 37 °C. Aliquots were taken at time intervals and analysed by mass spectrometry for compound remaining, allowing the determination of the half-life for the compound.

Plasma protein binding analysis was performed by Charles River Laboratories Inc. (ADME-SOP-90). Briefly, compounds in DMSO (10 µM, 0.5% DMSO final) were added to mouse plasma and dialysed against buffer for 4 hours at 37 °C. The compound concentration in each of the plasma and buffer compartments was determined by mass spectrometry and used to calculate the percentage compound bound.

Permeability: bi-directional Caco-2 cell permeability was performed by Charles River Laboratories Inc. (ADME-SOP-49). Briefly, compounds were administered at 10 µM (1% DMSO final) to the apical or basolateral side of a polarised Caco-2 cell monolayer, then incubated at 37 °C for 60 minutes before appearance on the opposite side of the monolayer was determined by mass spectrometry. The efflux ratio (ER) is calculated from the ratio of B-A to A-B permeabilities.

Kinetic solubility analysis was performed by Charles River Laboratories Inc. (ADME-SOP-01). Compound in DMSO at 10 mM was diluted to 200 µM in both DMSO and buffer (0.1 M PBS, pH 7.4, 2% DMSO final), and an aliquot of the 200 µM DMSO solution was diluted to 10 µM, and all dilutions were equilibrated for 2 hours. Compound concentration in the PBS filtrate was determined by LC-UV and comparing to the DMSO dilutions as calibration standards.

mchrom_LogD: The chromatographic LogD value was determined from the chromatographic hydrophobicity index (CHI) value using the equation $mchromLogD_{7.4} = 0.0857\ CHI_{7.4} - 2$(ref 6)[6] The CHI value of an individual compound was measured on a Waters Aquity UPLC system, XSelect HSS C18 5 µm 4.6x150 mm HPLC column, 5-100% gradient of MeCN in 50mM NH4OAc in H_2O adjusted to pH 7.4. Retention times of standards with known CHI were used to establish the linear regression expression for use on the test compounds[7].

Chemistry General Experimental:

Compound **9** was purchased from Ambinter (Amb16536894) and was determined by UPLC to have purity >95%. All other compounds were synthesised as described below, and all tested compounds have purity >95% by UPLC

analysis. Reagents and solvents were of commercially available reagent grade quality and used without further purification. Reactions requiring anhydrous conditions were carried out in oven dried glassware under an atmosphere of N_2. Reactions were monitored by thin-layer chromatography on silica gel 60 F_{254} aluminium or glass supported sheets, or by liquid chromatography-mass spectrometry (LCMS). Flash column chromatography was carried out on a Biotage Isolera One system using normal phase (SiO_2) cartridges. Compounds were loaded in solution or adsorbed onto Celite® 545, and eluted using a linear gradient of the specified solvents. Purification by C18 reverse phase HPLC was carried using an Agilent 1260 Infinity machine and a Waters XBridge BEH C18 OBD column (130 Å, 5 µm, 30 mm × 100 mm) with a linear gradient of H_2O (with 0.1% NH_3) and MeCN (with 0.1% NH_3). LCMS analysis was performed on a Waters Aquity HClass UPLC system with an Aquity QDa for mass detection. High-resolution mass spectra (HRMS) were measured on a Waters Vion IMS QTof spectrometer. NMR spectra were recorded on a Bruker Advance III (^1H = 300 MHz, ^{19}F = 282 MHz, ^{13}C = 75 MHz) spectrometer using the requisite solvent as a reference for internal deuterium lock. The chemical shift data for each signal are given as δ chemical shift (multiplicity, *J* values in Hz, integration) in units of parts per million (ppm) relative to tetramethylsilane (TMS) where δH (TMS) = 0.00 ppm. The multiplicity of each signal is indicated by: s (singlet), d (doublet), t (triplet), q (quartet), quin (quintet), hept (heptet) or m (multiplet). Signals from exchangeable protons were not always detected. UPLC analysis of final compounds was performed on a Waters Aquity HClass UPLC system and is reported as method name, retention time, UV % purity. The method parameters are as follows;

Method	Column	Additive	Flow rate	Gradient (time, %MeCN in H_2O)
A	BEH C18 (130 Å, 1.7 µm, 2.1 mm × 50 mm)	10 mM NH_3	0.6 mL/min	0 min, 5%; 0.8 min, 5%; 3.3 min, 95%; 4.3 min, 95%; 4.5 min, 5%; 5.5 min, 5%.
B	HSS C18 (100 Å, 1.8 µm, 2.1 mm × 50 mm)	0.1% HCO_2H	0.6 mL/min	0 min, 5%; 0.8 min, 5%; 3.3 min, 95%; 4.3 min, 95%; 4.5 min, 5%; 5.5 min, 5%.
C	BEH C18 (130 Å, 1.7 µm, 2.1 mm × 50 mm)	10 mM NH_3	0.6 mL/min	0 min, 5%; 0.8 min, 5%; 8.3 min, 95%; 9.3 min, 95%; 9.5 min, 5%; 10.5 min, 5%.
D	HSS C18 (100 Å, 1.8 µm, 2.1 mm × 50 mm)	0.1% HCO_2H	0.6 mL/min	0 min, 5%; 0.8 min, 5%; 8.3 min, 95%; 9.3 min, 95%; 9.5 min, 5%; 10.5 min, 5%.

Abbreviations: DME: 1,2-dimethoxyethane, DMF: *N*,*N*-dimethylformamide, DMSO: dimethyl sulfoxide, HPLC: high performance liquid chromatography, HRMS: high-resolution mass spectra, LCMS: liquid chromatography-mass spectrometry, rt: room temperature, SEM: 2-(trimethylsilyl)ethoxymethyl, TFA: Trifluoroacetic acid, TMS: tetramethylsilane, UPLC: ultra-performance liquid chromatography.

General procedure 1:

A solution of the requisite aryl chloride (1.0 eq), the requisite amine (1.1 eq) and triethylamine (3.0 eq) in CH_2Cl_2 (0.5 M) was stirred at rt for the stated period of time. Then the reaction was diluted with CH_2Cl_2, washed with brine (2 ×), then dried ($MgSO_4$) and concentrated *in vacuo*.

General procedure 2:

A microwave flask was charged with the requisite aryl chloride (1.0 eq) dissolved in DME (2 mL). Then the requisite boronic acid (1.5 eq) and Na_2CO_3 (2.0 eq) were added, followed by H_2O (0.5 mL), and the mixture was degassed with N_2. Tetrakis(triphenylphosphine)palladium (0.1 eq) was added, the reaction further degassed, then sealed and heated under microwave irradiation for the stated time and temperature. Purification was achieved *via* the stated method.

General procedure 3:

A microwave flask was charged with the requisite aryl chloride (1.0 eq) dissolved in DME (2 mL). Then the requisite boronic acid (1.5 eq) and Na_2CO_3 (2.0 eq) were added, followed by H_2O (0.5 mL), and the mixture was degassed with N_2. Tetrakis(triphenylphosphine)palladium (0.05 eq) was added, the reaction further degassed, then sealed and heated thermally for 4 hours 30 minutes at 90 °C. Purification was achieved *via* the stated method.

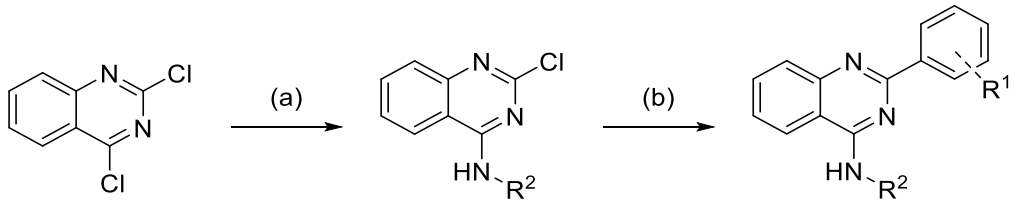

43 **44-54** **1, 6-8, 10-31**

R^1	R^2	Step (a) product	Step (b) product
2-CF_3	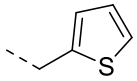	**44**	**1**
H	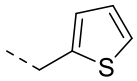	**44**	**6**
2-CH_3	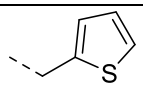	**44**	**7**
2-OCH_3	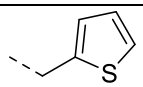	**44**	**8**
2-CF_3	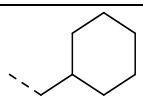	**45**	**10**
2-CF_3	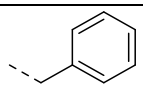	**46**	**11**
2-CF_3	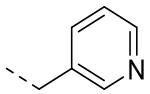	**47**	**12**
2-CF_3	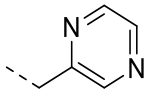	**48**	**13**
2-CF_3	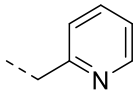	**49**	**14**
2-CF_3	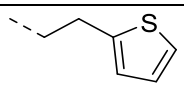	**50**	**15**
2-CF_3-4-F	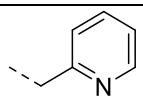	**49**	**16**
2-CF_3-5-F	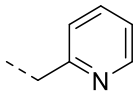	**49**	**17**
3-CF_3	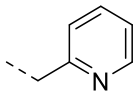	**49**	**18**
4-CF_3	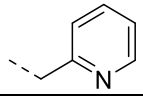	**49**	**19**
3-OMe	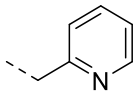	**49**	**20**
4-OMe	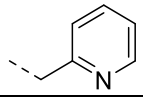	**49**	**21**

R^1	R^2	Step (a) product	Step (b) product
2-$CH(CH_3)_2$	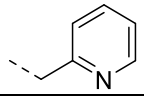	**49**	**22**
2-cyclopropyl	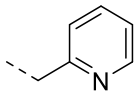	**49**	**23**
2-CH_2CH_3	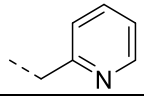	**49**	**24**
2-Ph	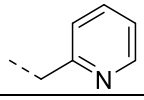	**49**	**25**
2-CN	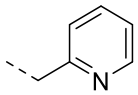	**49**	**26**
2-NMe_2	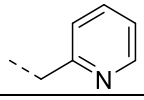	**49**	**27**
2-$CH(CH_3)_2$	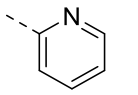	**51**	**28**
2-$CH(CH_3)_2$	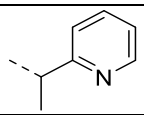	**52**	**29**
2-$CH(CH_3)_2$	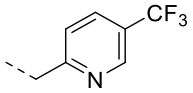	**53**	**30**
2-$CH(CH_3)_2$	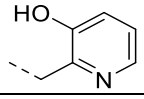	**54**	**31**

Supporting Scheme S1: *Reagents and conditions*: (a) R^2-NH_2, NEt_3, CH_2Cl_2, rt. (b) R^1-$B(OH)_2$, $Pd(PPh_3)_4$, Na_2CO_3, DME, H_2O, 120 °C.

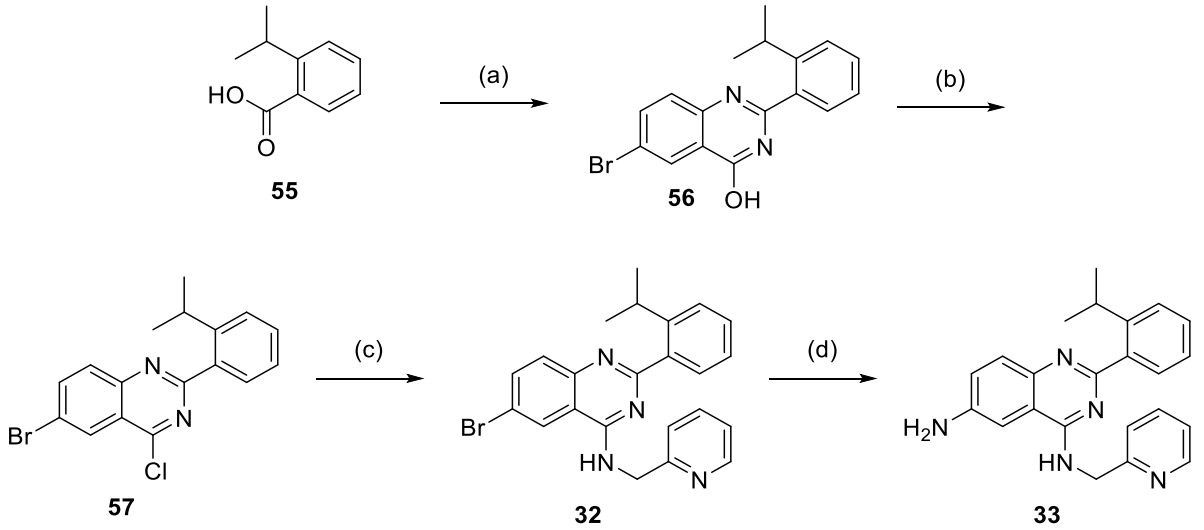

Supporting Scheme S2: *Reagents and conditions*: (a) i) $SOCl_2$, DMF, CH_2Cl_2, 0 °C to 50 °C. ii) 2-amino-5-bromobenzamide, NEt_3, CH_2Cl_2, 0 °C to rt. iii) NaOH, H_2O, 100 °C. b) $POCl_3$, toluene, 90 °C. c) pyridin-2-ylmethanamine, NEt_3, CH_2Cl_2, rt. d) NaN_3, CuI, sodium ascorbate, *trans*-*N*,*N*'-dimethylcyclohexane-1,2-diamine, EtOH, H_2O, 100 °C.

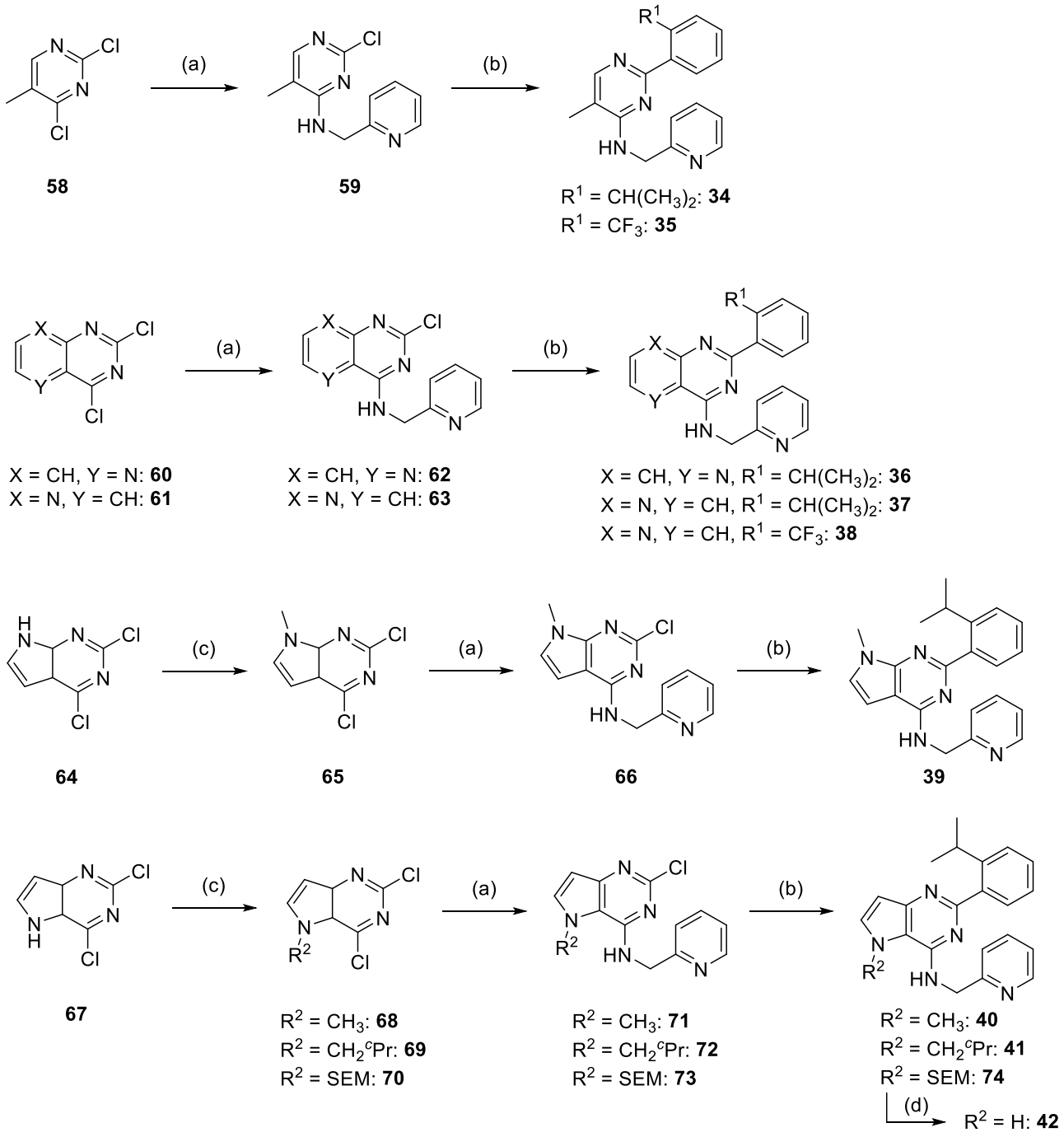

Supporting Scheme S3: *Reagents and conditions*: (a) pyridin-2-ylmethanamine, NEt_3, CH_2Cl_2, rt. (b) (2-propan-2-ylphenyl)boronic acid or (2-trifluoromethyl)phenylboronic acid, $Pd(PPh_3)_4$, Na_2CO_3, DME, H_2O, 120 °C. (c) CH_3I or $^cPrCH_2Br$ or SEM-Cl, NaH, DMF, rt. (d) i) TFA, CH_2Cl_2, rt. ii) NH_3, MeOH, rt.

*2-Chloro-N-(thiophen-2-ylmethyl)quinazolin-4-amine (**44**).*

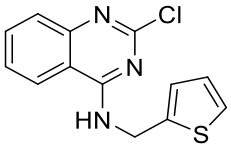

2,4-Dichloroquinazoline **43** (1.00 g, 5.02 mmol) and thiophen-2-ylmethanamine (425 µL, 683 mg, 6.03 mmol) were reacted according to general procedure 1 for 24 hours to give 2-chloro-*N*-(thiophen-2-ylmethyl)quinazolin-4-amine **44** (1.21 g, 4.39 mmol, 87%) as a cream coloured solid which was used without further purification. ^{1}H NMR (300 MHz, Chloroform-*d*) δ 7.85 – 7.73 (m, 2H), 7.68 (d, *J* = 8.1 Hz, 1H), 7.48 (ddd, *J* = 8.3, 6.6, 1.6 Hz, 1H), 7.31 (dd, *J* = 5.1, 1.2 Hz, 1H), 7.18 – 7.14 (m, 1H), 7.03 (dd, *J* = 5.1, 3.5 Hz, 1H), 6.11 (s, 1H), 5.06 (dd, *J* = 5.3, 0.8 Hz, 2H). Data in accordance with published data.[5]

*N-(Thiophen-2-ylmethyl)-2-(2-(trifluoromethyl)phenyl)quinazolin-4-amine (**1**).*

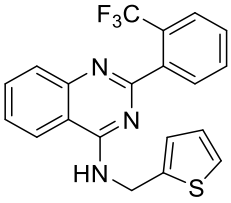

2-Chloro-*N*-(thiophen-2-ylmethyl)quinazolin-4-amine **44** (100 mg, 0.36 mmol) and (2-(trifluoromethyl)phenyl)boronic acid (207 mg, 1.09 mmol) were reacted according to general procedure 2 for 30 min at 120 °C. After concentrating *in vacuo*, purification *via* silica gel chromatography (gradient elution 5 to 40% EtOAc in petroleum ether), followed by preparatory HPLC (gradient elution 25 to 95% MeCN in H_2O with 0.1% NH_3) yielded *N*-(thiophen-2-ylmethyl)-2-(2-(trifluoromethyl)phenyl)quinazolin-4-amine **1** (40 mg, 0.10 mmol, 29%) as a white solid. MS (ESI+) *m/z* calcd. for $C_{20}H_{15}N_3F_3S$ $[M+H]^+$ 386.1; found 385.8. HRMS (ESI+) *m/z* calcd. for $C_{20}H_{15}N_3F_3S^+$ 386.0933 $[M+H]^+$; found 386.0934. UPLC (method C) t_R = 5.76 min, >98%. ^{1}H NMR (300 MHz, DMSO-d_6) δ 9.03 (t, *J* = 5.9 Hz, 1H), 8.36 – 8.26 (m, 1H), 7.90 – 7.62 (m, 6H), 7.57 (ddd, *J* = 8.3, 6.8, 1.4 Hz, 1H), 7.36 (dd, *J* = 5.1, 1.3 Hz, 1H), 7.06 (dd, *J* = 3.4, 1.2 Hz, 1H), 6.95 (dd, *J* = 5.1, 3.4 Hz, 1H), 4.97 (d, *J* = 5.6 Hz, 2H). ^{13}C NMR (75 MHz, DMSO-d_6) δ 161.9, 159.4, 150.0, 142.6, 140.3, 133.5 (*C*H), 132.5 (*C*H), 131.7 (*C*H), 129.4 (*C*H), 128.3 (*C*H), 127.5 (q, J = 30.6 Hz), 127.0 (*C*H), 126.9 (q, J = 5.2 Hz, *C*H), 126.6 (*C*H), 126.3 (*C*H), 125.6 (*C*H), 123.1 (*C*H), 122.9, 113.7, 39.1 (CH_2). ^{19}F NMR (282 MHz, DMSO-d_6) δ -55.89.

*2-Phenyl-N-(thiophen-2-ylmethyl)quinazolin-4-amine (**6**).*

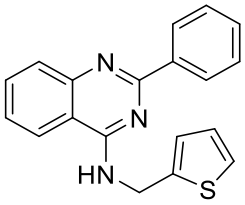

2-Chloro-*N*-(thiophen-2-ylmethyl)quinazolin-4-amine **44** (100 mg, 0.36 mmol) and phenylboronic acid (88 mg, 0.72 mmol) were reacted according to general procedure 2 for 30 min at 120 °C. After concentrating *in vacuo*, purification *via* silica gel chromatography (gradient elution 5 to 40% EtOAc in petroleum ether) yielded 2-phenyl-*N*-(thiophen-2-ylmethyl)quinazolin-4-amine **6** (65 mg, 0.21 mmol, 56%) as a white solid. MS (ESI+) *m*/*z* calcd for $C_{19}H_{16}N_3S$ $[M + H]^+$ 318.1; found 318.1. UPLC (method C) t_R = 5.89 min, >98%. ^{1}H NMR (300 MHz, Chloroform-*d*) δ 8.72 – 8.59 (m, 2H), 8.02 – 7.93 (m, 1H), 7.82 – 7.66 (m, 2H), 7.59 – 7.38 (m, 4H), 7.28 – 7.25 (m, 1H), 7.17 (dd, *J* = 3.5, 1.1 Hz, 1H), 7.02 (dd, *J* = 5.1, 3.5 Hz, 1H), 6.09 – 5.94 (m, 1H), 5.21 (d, *J* = 5.5 Hz, 2H).

*N-(Thiophen-2-ylmethyl)-2-(o-tolyl)quinazolin-4-amine (**7**).*

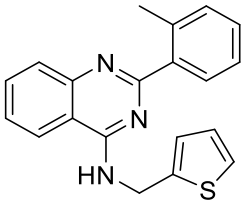

2-Chloro-*N*-(thiophen-2-ylmethyl)quinazolin-4-amine **44** (100 mg, 0.36 mmol) and 2-methylphenylboronic acid (99 mg, 0.72 mmol) were reacted according to general procedure 2 for 30 min at 120 °C. After concentrating *in vacuo*, purification *via* silica gel chromatography (gradient elution 5 to 40% EtOAc in petroleum ether) yielded *N*-(thiophen-2-ylmethyl)-2-(o-tolyl)quinazolin-4-amine **7** (12 mg, 0.036 mmol, 10%) as a white oily solid. MS (ESI+) *m*/*z* calcd for $C_{20}H_{18}N_3S$ $[M + H]^+$ 332.1; found 332.1. UPLC (method C) t_R = 5.73 min, >98%. ^{1}H NMR (300 MHz, Chloroform-*d*) δ 8.00 – 7.90 (m, 2H), 7.82 – 7.69 (m, 2H), 7.48 (ddd, *J* = 8.2, 6.9, 1.3 Hz, 1H), 7.39 – 7.25 (m, 4H), 7.12 (dt, *J* = 3.0, 1.1 Hz, 1H), 7.02 (dd, *J* = 5.1, 3.5 Hz, 1H), 6.02 – 5.89 (m, 1H), 5.14 (dd, *J* = 5.3, 0.9 Hz, 2H), 2.64 (s, 3H).

*2-(2-Methoxyphenyl)-N-(thiophen-2-ylmethyl)quinazolin-4-amine (**8**).*

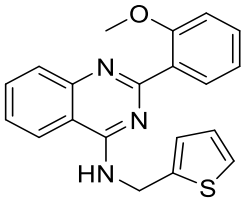

2-Chloro-*N*-(thiophen-2-ylmethyl)quinazolin-4-amine **44** (100 mg, 0.36 mmol) and 2-methoxyphenylboronic acid (110 mg, 0.72 mmol) were reacted according to general procedure 2 for 30 min at 120 °C. After concentrating *in vacuo*, purification *via* silica gel chromatography (gradient elution 5 to 80% EtOAc in petroleum ether) yielded 2-(2-methoxyphenyl)-*N*-(thiophen-2-ylmethyl)quinazolin-4-amine **8** (103 mg, 0.296 mmol, 82%) as a yellow solid. MS (ESI+) *m*/*z* calcd for $C_{20}H_{18}N_3OS$ $[M + H]^+$ 348.1; found 348.1. UPLC (method C) t_R = 5.02 min, >98%. ^{1}H NMR (300 MHz, Chloroform-*d*) δ 8.01 – 7.94 (m, 1H), 7.85 (dd, *J* = 7.5, 1.8 Hz, 1H), 7.80 – 7.69 (m, 2H), 7.51 – 7.36 (m, 2H), 7.27 (dd, *J* = 5.1, 1.2 Hz, 1H), 7.18 – 6.96 (m, 4H), 6.01 (s, 1H), 5.11 (d, *J* = 4.0 Hz, 2H), 3.90 (s, 3H).

*2-Chloro-N-(cyclohexylmethyl)quinazolin-4-amine (**45**).*

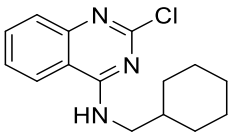

2,4-Dichloroquinazoline **43** (1.00 g, 5.03 mmol) and cyclohexanemethanamine (783 µL, 681 mg, 6.03 mmol) were reacted according to general procedure 1 for 18 hours. Purification *via* silica gel chromatography (gradient elution 0 to 50% EtOAc in petroleum ether) yielded 2-chloro-*N*-(cyclohexylmethyl)quinazolin-4-amine **45** (1.33 g, 4.82 mmol, 96%). MS (ESI+) *m*/*z* calcd for $C_{15}H_{19}ClN_3$ $[M + H]^+$ 276.1; found 276.0. UPLC (method A) t_R = 3.27 min, >95%.

*N-(Cyclohexylmethyl)-2-(2-(trifluoromethyl)phenyl)quinazolin-4-amine (**10**).*

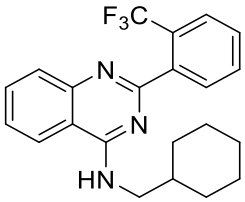

2-Chloro-*N*-(cyclohexylmethyl)quinazolin-4-amine **45** (100 mg, 0.36 mmol) and (2-(trifluoromethyl)phenyl)boronic acid (104 mg, 0.55 mmol) were reacted according to general procedure 2 for 40 min at 125 °C. After concentrating *in vacuo*, purification *via* silica gel chromatography (gradient elution 0 to 50% EtOAc in petroleum ether) yielded *N*-(cyclohexylmethyl)-2-(2-(trifluoromethyl)phenyl)quinazolin-4-amine **10** (87 mg, 0.23 mmol, 63%) as a white solid. MS (ESI+) *m*/*z* calcd for $C_{22}H_{23}F_3N_3$ $[M + H]^+$ 386.2; found 386.0. UPLC (method C) t_R = 6.64 min, 98%. ^{1}H NMR (300 MHz, Chloroform-*d*) δ 7.94 (dt, *J* = 8.2, 1.0 Hz, 1H), 7.88 – 7.71 (m, 4H), 7.64 (td, *J* = 7.5, 1.4 Hz, 1H), 7.57 – 7.49 (m, 2H), 5.84 (s, 1H), 3.58 (dd, *J* = 6.8, 5.7 Hz, 2H), 1.90 – 1.55 (m, 7H), 1.38 – 1.13 (m, 4H).

*N-Benzyl-2-chloroquinazolin-4-amine (**46**).*

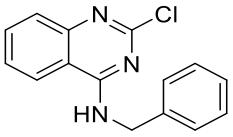

2,4-Dichloroquinazoline **43** (1.00 g, 5.03 mmol) and benzylamine (602 µL, 591 mg, 5.52 mmol) were reacted according to general procedure 1 for 3 hours. Purification *via* silica gel chromatography (gradient elution 0 to 50% EtOAc in petroleum ether) yielded *N*-benzyl-2-chloroquinazolin-4-amine **46** (1.32 g, 4.89 mmol, 97%). MS (ESI+) *m*/*z* calcd for $C_{15}H_{13}ClN_3$ $[M + H]^+$ 270.1; found 269.9. UPLC (method A) t_R = 2.94 min, 90%.

*N-Benzyl-2-(2-(trifluoromethyl)phenyl)quinazolin-4-amine (**11**).*

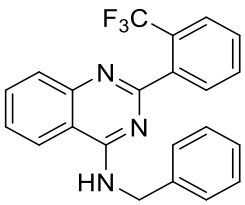

N-Benzyl-2-chloroquinazolin-4-amine **46** (100 mg, 0.37 mmol) and (2-(trifluoromethyl)phenyl)boronic acid (106 mg, 0.56 mmol) were reacted according to general procedure 2 for 35 min at 125 °C. After concentrating *in vacuo*, purification *via* silica gel chromatography (gradient elution 0 to 50% EtOAc in petroleum ether) yielded

N-benzyl-2-(2-(trifluoromethyl)phenyl)quinazolin-4-amine **11** (127 mg, 0.336 mmol, 91%) as a white solid. MS (ESI+) *m*/*z* calcd for $C_{22}H_{17}F_3N_3$ $[M + H]^+$ 380.1; found 379.9. UPLC (method C) t_R = 5.89 min, >98%. ^{1}H NMR (300 MHz, Chloroform-*d*) δ ^{1}H NMR (300 MHz, Chloroform-*d*) δ 8.01 – 7.92 (m, 1H), 7.92 – 7.61 (m, 5H), 7.61 – 7.30 (m, 7H), 5.95 (s, 1H), 4.94 (d, *J* = 5.3 Hz, 2H).

*2-Chloro-N-(pyridin-3-ylmethyl)quinazolin-4-amine (**47**).*

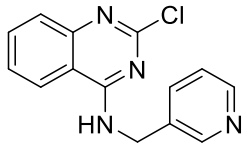

2,4-Dichloroquinazoline **43** (1.50 g, 7.54 mmol) and 3-aminomethylpyridine (844 µL, 897 mg, 8.29 mmol) were reacted according to general procedure 1 for 18 hours. Purification *via* silica gel chromatography (gradient elution 0 to 100% EtOAc in petroleum ether) yielded 2-chloro-*N*-(pyridin-3-ylmethyl)quinazolin-4-amine **47** (1.83 g, 6.74 mmol, 89%). MS (ESI+) *m*/*z* calcd for $C_{14}H_{12}ClN_4$ $[M + H]^+$ 271.1; found 271.1. UPLC (method A) t_R = 2.45 min, 80%.

*N-(Pyridin-3-ylmethyl)-2-(2-(trifluoromethyl)phenyl)quinazolin-4-amine (**12**).*

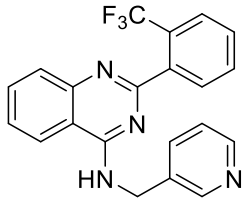

2-Chloro-*N*-(pyridin-3-ylmethyl)quinazolin-4-amine **47** (100 mg, 0.37 mmol) and (2-(trifluoromethyl)phenyl)boronic acid (106 mg, 0.56 mmol) were reacted according to general procedure 2 for 40 min at 125 °C. After concentrating *in vacuo*, purification *via* silica gel chromatography (gradient elution 0 to 100% EtOAc in petroleum ether) yielded *N*-(pyridin-3-ylmethyl)-2-(2-(trifluoromethyl)phenyl)quinazolin-4-amine **12** (111 mg, 0.292 mmol, 79%) as a white solid. MS (ESI+) *m*/*z* calcd for $C_{21}H_{16}F_3N_4$ $[M + H]^+$ 381.1; found 381.1. UPLC (method C) t_R = 4.72 min, >98%. ^{1}H NMR (300 MHz, DMSO-d_6) δ 8.99 (t, *J* = 5.9 Hz, 1H), 8.62 – 8.51 (m, 1H), 8.44 (dd, *J* = 4.8, 1.7 Hz, 1H), 8.38 – 8.24 (m, 1H), 7.86 – 7.71 (m, 5H), 7.70 – 7.50 (m, 3H), 7.32 (ddd, *J* = 7.9, 4.8, 0.9 Hz, 1H), 4.83 (d, *J* = 5.7 Hz, 2H).

*2-Chloro-N-(pyrazin-2-ylmethyl)quinazolin-4-amine (**48**).*

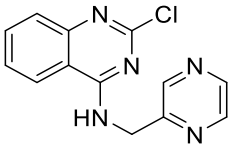

2,4-Dichloroquinazoline **43** (1.50 g, 7.54 mmol) and 2-aminomethylpyrazine (794 µL, 904 mg, 8.29 mmol) were reacted according to general procedure 1 for 2 hours. Purification *via* silica gel chromatography (gradient elution 0 to 100% EtOAc in petroleum ether) yielded 2-chloro-*N*-(pyrazin-2-ylmethyl)quinazolin-4-amine **48** (1.26 g, 4.64 mmol, 62%). MS (ESI+) *m*/*z* calcd for $C_{13}H_{11}ClN_5$ $[M + H]^+$ 272.1; found 272.0. UPLC (method A) t_R = 2.33 min, 72%.

*N-(Pyrazin-2-ylmethyl)-2-(2-(trifluoromethyl)phenyl)quinazolin-4-amine (**13**).*

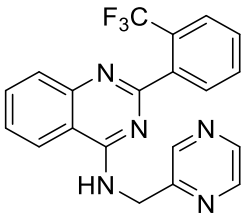

2-Chloro-*N*-(pyrazin-2-ylmethyl)quinazolin-4-amine **48** (100 mg, 0.37 mmol) and (2-(trifluoromethyl)phenyl)boronic acid (104 mg, 0.55 mmol) were reacted according to general procedure 2 for 40 min at 125 °C. After concentrating *in vacuo*, purification *via* silica gel chromatography (gradient elution 0 to 100% EtOAc in petroleum ether) yielded *N*-(pyrazin-2-ylmethyl)-2-(2-(trifluoromethyl)phenyl)quinazolin-4-amine **13** (71 mg, 0.19 mmol, 51%) as a white solid. MS (ESI+) *m*/*z* calcd for $C_{20}H_{15}F_3N_5$ $[M + H]^+$ 382.1; found 382.1. UPLC (method C) t_R = 4.45 min, >98%. ^{1}H NMR (300 MHz, Methanol-d4) δ 8.61 (d, J = 1.5 Hz, 1H), 8.56 (dd, J = 2.6, 1.5 Hz, 1H), 8.51 – 8.43 (m, 1H), 8.26 (ddd, J = 8.3, 1.4, 0.7 Hz, 1H), 7.87 (ddd, J = 8.1, 6.6, 1.4 Hz, 1H), 7.81 (ddd, J = 8.4, 1.6, 0.7 Hz, 1H), 7.79 – 7.74 (m, 1H), 7.73 – 7.66 (m, 1H), 7.63 (ddt, J = 7.5, 6.8, 1.5 Hz, 3H), 5.02 (s, 2H).

*2-Chloro-N-(pyridin-2-ylmethyl)quinazolin-4-amine (**49**).*

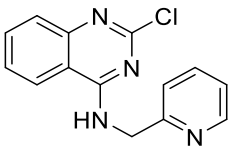

2,4-Dichloroquinazoline **43** (1.00 g, 5.03 mmol) and 2-aminomethylpyridine (569 µL, 597 mg, 5.53 mmol) were reacted according to general procedure 1 for 18 hours. Purification *via* silica gel chromatography (gradient elution 0 to 100% EtOAc in petroleum ether) yielded 2-chloro-*N*-(pyridin-2-ylmethyl)quinazolin-4-amine **49** (852 mg, 3.15 mmol, 63%). MS (ESI+) *m/z* calcd for $C_{14}H_{12}ClN_4$ $[M + H]^+$ 271.1; found 270.9. UPLC (method A) t_R = 2.54 min, 86%.

*N-(Pyridin-2-ylmethyl)-2-(2-(trifluoromethyl)phenyl)quinazolin-4-amine (**14**).*

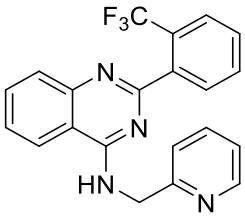

2-Chloro-*N*-(pyridin-2-ylmethyl)quinazolin-4-amine **49** (100 mg, 0.37 mmol) and (2-(trifluoromethyl)phenyl)boronic acid (106 mg, 0.56 mmol) were reacted according to general procedure 2 for 35 min at 125 °C. After concentrating *in vacuo*, purification *via* silica gel chromatography (gradient elution 0 to 100% EtOAc in petroleum ether) yielded *N*-(pyridin-2-ylmethyl)-2-(2-(trifluoromethyl)phenyl)quinazolin-4-amine **14** (102 mg, 0.268 mmol, 72%) as a colourless solid. MS (ESI+) *m/z* calcd. for $C_{21}H_{16}N_4F_3$ $[M+H]^+$ 381.1; found 380.9. HRMS (ES+) *m/z* calcd. for $C_{21}H_{16}N_4F_3^+$ $[M+H]^+$ 381.1322; found 381.1324. UPLC (method A) t_R = 4.94 min, >98%. ^{1}H NMR (300 MHz, Chloroform-*d*) δ 8.65 (ddd, *J* = 5.0, 1.8, 1.0 Hz, 1H), 8.04 – 7.92 (m, 2H), 7.91 – 7.61 (m, 6H), 7.60 – 7.52 (m, 2H), 7.36 (dt, *J* = 7.9, 1.0 Hz, 1H), 7.29 – 7.24 (m, 1H), 4.99 (d, *J* = 4.3 Hz, 2H). ^{13}C NMR (75 MHz, DMSO-d_6) δ 162.0, 159.9, 159.1, 150.1, 149.3, 140.3 (q, *J* = 2.2 Hz), 137.0, 133.5, 132.4, 131.7, 129.3, 128.3, 127.5 (q, *J* = 30.6 Hz), 126.8 (q, *J* = 5.2 Hz), 126.5, 124.6 (q, *J* = 273.6 Hz), 123.2, 122.5, 121.4, 113.8, 46.0. ^{19}F NMR (282 MHz, DMSO-d_6) δ -56.10.

*2-Chloro-N-(2-(thiophen-2-yl)ethyl)quinazolin-4-amine (**50**).*

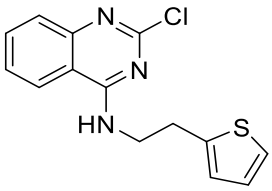

2,4-Dichloroquinazoline **43** (1.00 g, 5.03 mmol) and thiophen-2-ethylamine (705 µL, 766 mg, 6.03 mmol) were reacted according to general procedure 1 for 3 hours to give 2-chloro-*N*-(2-(thiophen-2-yl)ethyl)quinazolin-4-

amine **50** (1.45 g, 5.00 mmol, 99%) which was used without further purification. MS (ESI+) *m/z* calcd for $C_{14}H_{13}ClN_3S$ $[M + H]^+$ 290.1; found 289.9. UPLC (method A) t_R = 3.07 min, 93%.

*N-(2-(Thiophen-2-yl)ethyl)-2-(2-(trifluoromethyl)phenyl)quinazolin-4-amine (**15**).*

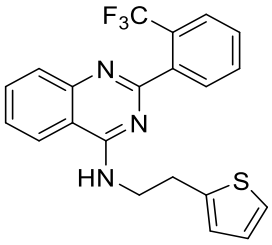

2-Chloro-*N*-(2-(thiophen-2-yl)ethyl)quinazolin-4-amine **50** (100 mg, 0.35 mmol) and (2-(trifluoromethyl)phenyl)boronic acid (99 mg, 0.52 mmol) were reacted according to general procedure 2 for 45 min at 125 °C. After concentrating *in vacuo*, purification *via* silica gel chromatography (gradient elution 0 to 50% EtOAc in petroleum ether) yielded *N*-(2-(thiophen-2-yl)ethyl)-2-(2-(trifluoromethyl)phenyl)quinazolin-4-amine **15** (121 mg, 0.303 mmol, 87%) as a white solid. MS (ESI+) *m/z* calcd for $C_{21}H_{17}F_3N_3S$ $[M + H]^+$ 400.1; found 399.9. UPLC (method C) t_R = 6.02 min, >98%. ^{1}H NMR (300 MHz, Chloroform-*d*) δ 7.99 – 7.72 (m, 4H), 7.72 – 7.60 (m, 2H), 7.63 – 7.42 (m, 2H), 7.22 (dd, *J* = 5.1, 1.2 Hz, 1H), 7.00 (dd, *J* = 5.1, 3.4 Hz, 1H), 6.91 (dt, *J* = 3.4, 1.0Hz, 1H), 5.93 (s, 1H), 4.01 (q, *J* = 6.3 Hz, 2H), 3.27 (td, *J* = 6.5, 0.8 Hz, 2H).

*2-(4-Fluoro-2-(trifluoromethyl)phenyl)-N-(pyridin-2-ylmethyl)quinazolin-4-amine (**16**).*

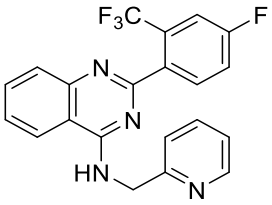

2-Chloro-*N*-(pyridin-2-ylmethyl)quinazolin-4-amine **49** (50 mg, 0.180 mmol) and 4-fluoro-2-(trifluoromethyl)phenyl]boronic acid (57.6 mg, 0.280 mmol) were reacted according to general procedure 2 for 45 mins at 120 °C. Upon cooling to room temperature the reaction mixture was loaded onto an SCX-II column, washed with MeOH, then eluted with 0.5 M NH_3 in MeOH and concentrated *in vacuo*. Purification *via* preparatory HPLC (gradient elution 30 to 70% MeCN in H_2O with 0.1% NH_3) yielded 2-(4-fluoro-2-(trifluoromethyl)phenyl)-*N*-(pyridin-2-ylmethyl)quinazolin-4-amine **16** (46.5 mg, 0.117 mmol, 63%) as a white solid. MS (ESI+) *m/z* calcd for $C_{21}H_{15}F_4N_4$ $[M + H]^+$ 399.1; found 399.2. UPLC (method C) t_R = 5.25 min, >98%. ^{1}H NMR (300 MHz,

Chloroform-d) δ 8.66 (dt, *J* = 4.7, 1.4 Hz, 1H), 8.00 (dd, *J* = 8.3, 1.3 Hz, 1H), 7.92 (td, *J* = 5.5, 2.7 Hz, 2H), 7.80 (ddd, *J* = 8.3, 7.0, 1.4 Hz, 1H), 7.73 (td, *J* = 7.7, 1.8 Hz, 1H), 7.66 (s, 1H), 7.63 – 7.47 (m, 2H), 7.41 – 7.32 (m, 2H), 7.32 – 7.24 (m, 1H), 4.97 (d, *J* = 4.3 Hz, 2H).

*2-(5-Fluoro-2-(trifluoromethyl)phenyl)-N-(pyridin-2-ylmethyl)quinazolin-4-amine (**17**).*

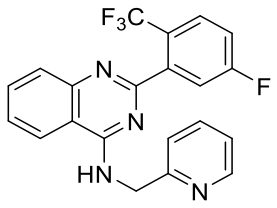

2-Chloro-*N*-(pyridin-2-ylmethyl)quinazolin-4-amine **49** (100 mg, 0.370 mmol) and 5-fluoro-2-(trifluoromethyl)phenyl]boronic acid (115 mg, 0.550 mmol) were reacted according to general procedure 2 for 45 mins at 120 °C. Upon cooling to room temperature the reaction mixture was loaded onto an SCX-II column, washed with MeOH, then eluted with 0.5 M NH_3 in MeOH and concentrated *in vacuo*. Purification *via* preparatory HPLC (gradient elution 30 to 70% MeCN in H_2O with 0.1% NH_3) yielded 2-(5-fluoro-2-(trifluoromethyl)phenyl)-*N*-(pyridin-2-ylmethyl)quinazolin-4-amine **17** (82.3 mg, 0.413 mmol, 56%) as a white solid. MS (ESI+) *m/z* calcd for $C_{21}H_{15}F_4N_4$ $[M + H]^+$ 399.1; found 399.2. UPLC (method C) t_R = 5.28 min, >98%. ^{1}H NMR (300 MHz, Chloroform-d) δ 8.65 (d, *J* = 5.0 Hz, 1H), 7.96 (dd, *J* = 21.7, 8.3 Hz, 2H), 7.88 – 7.67 (m, 4H), 7.67 – 7.48 (m, 2H), 7.36 (d, *J* = 7.9 Hz, 1H), 7.26 (dt, *J* = 17.8, 5.4 Hz, 2H), 4.97 (d, *J* = 4.4 Hz, 2H).

*N-(Pyridin-2-ylmethyl)-2-(3-(trifluoromethyl)phenyl)quinazolin-4-amine (**18**).*

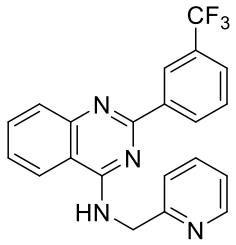

2-Chloro-*N*-(pyridin-2-ylmethyl)quinazolin-4-amine **49** (50 mg, 0.185 mmol) and [3-(trifluoromethyl)phenyl]boronic acid (53.0 mg, 0.22 mmol) were reacted according to general procedure 3,

resulting in partial conversion to desired product. A further 1 equivalent of [3-(trifluoromethyl)phenyl]boronic acid (35.5 mg, 0.15 mmol) and 0.05 equivalents of tetrakis(triphenylphosphine)palladium (10 mg, 0.01 mmol) were added to the reaction mixture with degassing and further heating for 18 hours at 90 °C, followed by 3 hours at 110 °C. Upon cooling to room temperature the reaction mixture purified directly *via* silica gel chromatography (gradient elution 10 to 80% EtOAc in petroleum ether) followed by preparatory HPLC (gradient elution 30 to 80% MeCN in H_2O with 0.1% NH_3) yielding *N*-(pyridin-2-ylmethyl)-2-(3-(trifluoromethyl)phenyl)quinazolin-4-amine **18** (13.0 mg, 0.034 mmol, 19%) as a white solid. MS (ESI+) *m/z* calcd for $C_{21}H_{16}F_3N_4$ $[M + H]^+$ 381.1; found 381.2. UPLC (method C) t_R = 5.97 min, >98%. ^{1}H NMR (300 MHz, Chloroform-*d*) δ 8.92 – 8.76 (m, 2H), 8.67 (ddd, *J* = 4.9, 1.8, 0.9 Hz, 1H), 8.01 – 7.91 (m, 2H), 7.79 (ddd, *J* = 8.9, 7.2, 1.5 Hz, 2H), 7.75 – 7.71 (m, 1H), 7.70 – 7.58 (m, 1H), 7.58 – 7.45 (m, 3H), 7.34 – 7.23 (m, 1H, obsc. by solvent peak), 5.09 (d, *J* = 4.5 Hz, 2H).

*N-(Pyridin-2-ylmethyl)-2-(4-(trifluoromethyl)phenyl)quinazolin-4-amine (**19**).*

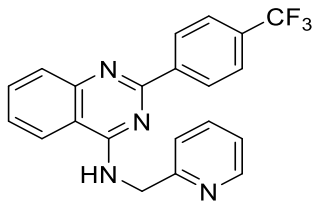

2-Chloro-*N*-(pyridin-2-ylmethyl)quinazolin-4-amine **49** (50.0 mg, 0.185 mmol) and [4-(trifluoromethyl)phenyl]boronic acid (53.0 mg, 0.22 mmol) were reacted according to general procedure 3, resulting in partial conversion to desired product. A further 1 equivalent of [4-(trifluoromethyl)phenyl]boronic acid (35.5 mg, 0.15 mmol) and 0.05 equivalents of tetrakis(triphenylphosphine)palladium (10 mg, 0.01 mmol) were added to the reaction mixture with degassing and further heating for 18 hours at 90 °C, followed by 3 hours at 110 °C. Upon cooling to room temperature the reaction mixture was purified directly *via* silica gel chromatography (gradient elution 10 to 80% EtOAc in petroleum ether) followed by preparatory HPLC (gradient elution 30 to 80% MeCN in H_2O with 0.1% NH_3) yielding *N*-(pyridin-2-ylmethyl)-2-(4-(trifluoromethyl)phenyl)quinazolin-4-amine **19** (18.0 mg, 0.047 mmol, 26%) as a white solid. MS (ESI+) *m/z* calcd for $C_{21}H_{16}F_3N_4$ $[M + H]^+$ 381.1; found 381.2. UPLC (method C) t_R = 6.04 min, >98%. ^{1}H NMR (300 MHz, Chloroform-*d*) δ 8.72 (dp, *J* = 7.6, 0.9 Hz, 2H), 8.68 (ddd, *J* = 4.9, 1.8, 1.0 Hz, 1H), 7.97 (dq, *J* = 7.9, 0.6 Hz, 2H), 7.86 – 7.69 (m, 4H), 7.56-7.50 (m, 1H), 7.49 (brs, 1H), 7.48-7.44 (m, 1H), 7.35 – 7.24 (m, 1H, obsc. by solvent peak), 5.09 (d, *J* = 4.5 Hz, 2H).

*2-(3-Methoxyphenyl)-N-(pyridin-2-ylmethyl)quinazolin-4-amine (**20**).*

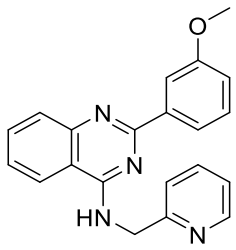

2-Chloro-*N*-(pyridin-2-ylmethyl)quinazolin-4-amine **49** (50 mg, 0.185 mmol) and (3-methoxyphenyl)boronic acid (41.0 mg, 0.22 mmol) were reacted according to general procedure 3, resulting in partial conversion to desired product. A further 1 equivalent of (3-methoxyphenyl)boronic acid (27.3 mg, 0.15 mmol) and 0.05 equivalents of tetrakis(triphenylphosphine)palladium (10 mg, 0.01 mmol) were added to the reaction mixture with degassing and further heating for 18 hours at 90 °C, followed by 3 hours at 110 °C. Upon cooling to room temperature the reaction mixture purified directly *via* silica gel chromatography (gradient elution 10 to 80% EtOAc in petroleum ether) followed by preparatory HPLC (gradient elution 30 to 80% MeCN in H_2O with 0.1% NH_3) yielded 2-(3-methoxyphenyl)-*N*-(pyridin-2-ylmethyl)quinazolin-4-amine **20** (22.0 mg, 0.064 mmol, 36%) as a white solid. MS (ESI+) *m/z* calcd for $C_{21}H_{19}N_4O$ $[M + H]^+$ 343.2; found 343.2. UPLC (method C) t_R = 4.98 min, >98%. ^{1}H NMR (300 MHz, Chloroform-*d*) δ 8.67 (ddd, *J* = 5.0, 1.8, 0.9 Hz, 1H), 8.23 (dt, *J* = 7.7, 1.2 Hz, 1H), 8.19 (dd, *J* = 2.7, 1.4 Hz, 1H), 8.01 – 7.89 (m, 2H), 7.83 – 7.68 (m, 2H), 7.53 – 7.41 (m, 3H), 7.41-7.34 (m, 1H), 7.31 – 7.24 (m, 1H, obsc. by solvent peak), 7.05 (ddd, *J* = 8.2, 2.7, 1.0 Hz, 1H), 5.10 (d, *J* = 4.5 Hz, 2H), 3.97 (s, 3H).

*2-(4-Methoxyphenyl)-N-(pyridin-2-ylmethyl)quinazolin-4-amine (**21**).*

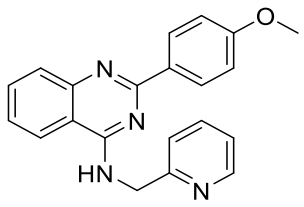

2-Chloro-*N*-(pyridin-2-ylmethyl)quinazolin-4-amine **49** (50 mg, 0.185 mmol) and (4-methoxyphenyl)boronic acid (41.0 mg, 0.22 mmol) were reacted according to general procedure 3. Upon cooling to room temperature the reaction mixture was purified directly *via* silica gel chromatography (gradient elution 10 to 80% EtOAc in petroleum ether) yielding 2-(4-methoxyphenyl)-*N*-(pyridin-2-ylmethyl)quinazolin-4-amine **21** (20.0 mg, 0.058

mmol, 32%) as a white solid. MS (ESI+) *m/z* calcd for $C_{21}H_{19}N_4O$ $[M + H]^+$ 343.2; found 343.1. UPLC (method C) t_R = 4.98 min, 98%. ^{1}H NMR (300 MHz, Chloroform-*d*) δ 8.66 (ddd, *J* = 4.9, 1.8, 0.9 Hz, 1H), 8.22 (ddd, *J* = 7.7, 1.5, 1.0 Hz, 1H), 8.18 (dd, *J* = 2.6, 1.5 Hz, 1H), 8.01 – 7.89 (m, 2H), 7.80 – 7.70 (m, 2H), 7.53 – 7.41 (m, 3H), 7.40 (s, 1H), 7.33 – 7.22 (m, 1H, obsc. by solvent peak), 7.05 (ddd, *J* = 8.2, 2.7, 1.0 Hz, 1H), 5.10 (d, *J* = 4.5 Hz, 2H), 3.96 (s, 3H).

*2-(2-Isopropylphenyl)-N-(pyridin-2-ylmethyl)quinazolin-4-amine (**22**).*

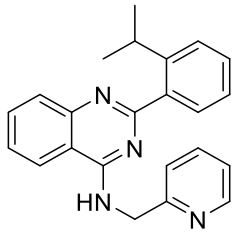

2-Chloro-*N*-(pyridin-2-ylmethyl)quinazolin-4-amine **49** (50 mg, 0.185 mmol) and (2-propan-2-ylphenyl)boronic acid (45.0 mg, 0.22 mmol) were reacted according to general procedure 3, resulting in partial conversion to desired product. A further 1 equivalent of (2-propan-2-ylphenyl)boronic acid (30 mg, 0.15 mmol) and 0.05 equivalents of tetrakis(triphenylphosphine)palladium (10 mg, 0.01 mmol) were added to the reaction mixture with degassing and further heating for 18 hours at 90 °C. Upon cooling to room temperature the reaction mixture was purified directly *via* silica gel chromatography (gradient elution 10 to 80% EtOAc in petroleum ether) yielding 2-(2-isopropylphenyl)-*N*-(pyridin-2-ylmethyl)quinazolin-4-amine **22** (31.0 mg, 0.087 mmol, 49%) as a white solid. MS (ESI+) *m/z* calcd. for $C_{23}H_{23}N_4$ $[M + H]^+$ 355.2; found 355.1. HRMS (ES+) *m/z* calcd. for $C_{23}H_{23}N_4^+$ $[M + H]^+$ 355.1917; found 355.1923. UPLC (method C) t_R = 5.31 min, 97%. ^{1}H NMR (300 MHz, DMSO-d_6) δ 8.99 (t, *J* = 6.0 Hz, 1H), 8.51 (ddd, *J* = 4.9, 1.9, 1.0 Hz, 1H), 8.43 – 8.34 (m, 1H), 7.86 – 7.68 (m, 3H), 7.61 – 7.54 (m, 1H), 7.47 (dt, *J* = 7.6, 1.1 Hz, 1H), 7.39 – 7.14 (m, 5H), 4.90 (d, *J* = 5.8 Hz, 2H), 3.46 (p, *J* = 6.9 Hz, 1H), 0.96 (d, *J* = 6.9 Hz, 6H). ^{13}C NMR (75 MHz, DMSO-d_6) δ 164.0, 159.8, 159.3, 150.3, 149.4, 147.2, 139.7, 137.1, 133.3, 130.3, 129.0, 128.3, 126.1, 125.8, 125.5, 123.1, 122.4, 121.0, 113.6, 46.0, 29.0, 24.2.

*2-(2-Cyclopropylphenyl)-N-(pyridin-2-ylmethyl)quinazolin-4-amine (**23**).*

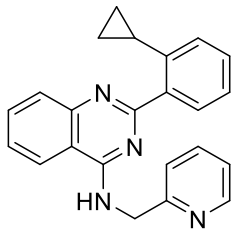

2-Chloro-*N*-(pyridin-2-ylmethyl)quinazolin-4-amine **49** (50 mg, 0.180 mmol) and (2-cyclopropylphenyl)boronic acid (44.7 mg, 0.276 mmol) were reacted according to general procedure 2 for 45 mins at 120 °C. Upon cooling to room temperature the reaction mixture was loaded onto an SCX-II column, washed with MeOH, then eluted with 0.5 M NH_3 in MeOH and concentrated *in vacuo*. Purification *via* preparatory HPLC (gradient elution 40 to 80% MeCN in H_2O with 0.1% NH_3) yielded 2-(2-cyclopropylphenyl)-*N*-(pyridin-2-ylmethyl)quinazolin-4-amine **23** (29.9 mg, 0.085 mmol, 46%) as a white solid. MS (ESI+) *m/z* calcd for $C_{23}H_{21}N_4$ $[M + H]^+$ 353.2; found 353.2. UPLC (method C) t_R = 5.00 min, 99%. ^{1}H NMR (300 MHz, Chloroform-d) δ 8.65 (dt, *J* = 4.9, 1.3 Hz, 1H), 7.97 (td, *J* = 8.5, 1.3 Hz, 2H), 7.84 – 7.65 (m, 3H), 7.58 – 7.45 (m, 2H), 7.41 – 7.21 (m, 4H), 7.04 (dd, *J* = 7.6, 1.5 Hz, 1H), 5.02 (d, *J* = 4.4 Hz, 2H), 2.62 (tt, *J* = 8.5, 5.4 Hz, 1H), 0.85 – 0.73 (m, 2H), 0.69 (ddd, *J* = 7.0, 5.4, 3.4 Hz, 2H).

*2-(2-Ethylphenyl)-N-(pyridin-2-ylmethyl)quinazolin-4-amine (**24**).*

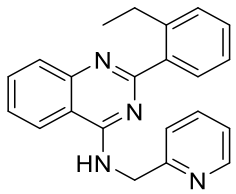

2-Chloro-*N*-(pyridin-2-ylmethyl)quinazolin-4-amine **49** (50 mg, 0.185 mmol) and (2-ethylphenyl)boronic acid (55.4 mg, 0.369 mmol) were reacted according to general procedure 2 for 2 hours at 120 °C. Upon cooling to room temperature the reaction mixture was loaded onto an SCX-II column, washed with MeOH, then eluted with 0.5 M NH_3 in MeOH and concentrated *in vacuo*. Purification *via* preparatory HPLC (gradient elution 5 to 95% MeCN in H_2O with 0.1% NH_3) yielded 2-(2-ethylphenyl)-*N*-(pyridin-2-ylmethyl)quinazolin-4-amine **24** (50.3 mg, 0.148 mmol, 80%) as a white solid. MS (ESI+) *m/z* calcd for $C_{22}H_{21}N_4$ $[M + H]^+$ 341.2; found 341.1. UPLC (method C) t_R = 5.15 min, >98%. ^{1}H NMR (300 MHz, Chloroform-d) δ 8.66 (ddd, *J* = 4.9, 1.8, 1.0 Hz, 1H), 8.01

– 7.97 (m, 1H), 7.95 (ddd, *J* = 8.3, 1.3, 0.6 Hz, 1H), 7.83 – 7.75 (m, 2H), 7.72 (td, *J* = 7.7, 1.8 Hz, 1H), 7.53 (ddd, *J* = 8.2, 7.0, 1.3 Hz, 1H), 7.48 (s, 1H), 7.42 – 7.23 (m, 5H), 5.01 (d, *J* = 4.4 Hz, 2H), 3.02 (q, *J* = 7.5 Hz, 2H), 1.22 (t, *J* = 7.5 Hz, 3H).

*2-([1,1'-Biphenyl]-2-yl)-N-(pyridin-2-ylmethyl)quinazolin-4-amine (**25**).*

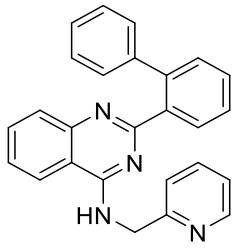

2-Chloro-*N*-(pyridin-2-ylmethyl)quinazolin-4-amine **49** (50 mg, 0.185 mmol) and biphenylboronic acid (73.2 mg, 0.369 mmol) were reacted according to general procedure 2 for 45 min at 120 °C. Upon cooling to room temperature the reaction mixture was loaded onto an SCX-II column, washed with MeOH, then eluted with 0.5 M NH_3 in MeOH and concentrated *in vacuo*. Purification *via* preparatory HPLC (gradient elution 5 to 95% MeCN in H_2O with 0.1% NH_3) yielded 2-(2-phenylphenyl)-*N*-(pyridin-2-ylmethyl)quinazolin-4-amine **25** (55.0 mg, 0.142 mmol, 77%) as a white solid. MS (ESI+) *m/z* calcd for $C_{26}H_{21}N_4$ $[M + H]^+$ 389.2; found 389.1. UPLC (method C) t_R = 5.34 min, >98%. ^{1}H NMR (300 MHz, Chloroform-*d*) δ 8.59 (dt, *J* = 4.9, 1.3 Hz, 1H), 8.18 – 8.06 (m, 1H), 7.88 (ddd, *J* = 20.8, 8.4, 1.2 Hz, 2H), 7.71 (dtd, *J* = 22.5, 7.3, 1.6 Hz, 2H), 7.59 – 7.41 (m, 4H), 7.38 – 7.30 (m, 2H), 7.30 – 7.08 (m, 6H), 4.14 (d, *J* = 4.2 Hz, 2H).

*2-(4-((Pyridin-2-ylmethyl)amino)quinazolin-2-yl)benzonitrile (**26**).*

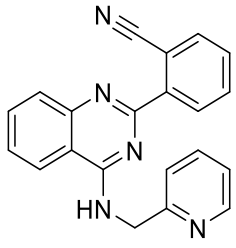

2-Chloro-*N*-(pyridin-2-ylmethyl)quinazolin-4-amine **49** (50 mg, 0.185 mmol) and 2-cyanophenylboronic acid (35.0 mg, 0.22 mmol) were reacted according to general procedure 3. Upon cooling to room temperature the

reaction mixture was purified directly *via* silica gel chromatography (gradient elution 10 to 80% EtOAc in petroleum ether) yielding 2-(4-((pyridin-2-ylmethyl)amino)quinazolin-2-yl)benzonitrile **26** (9.0 mg, 0.027 mmol, 15%) as a white solid. MS (ESI+) *m/z* calcd for $C_{21}H_{16}N_5$ $[M + H]^+$ 338.1; found 338.1. UPLC (method C) t_R = 4.78 min, >98%. ^{1}H NMR (300 MHz, Chloroform-*d*) δ 8.65 (ddd, *J* = 4.9, 1.8, 1.0 Hz, 1H), 8.60 (ddd, *J* = 8.0, 1.3, 0.5 Hz, 1H), 8.05 – 7.93 (m, 2H), 7.88 (ddd, *J* = 7.7, 1.4, 0.5 Hz, 1H), 7.84 – 7.79 (m, 1H), 7.77 – 7.66 (m, 3H), 7.60 – 7.52 (m, 2H), 7.52 – 7.46 (m, 1H), 7.33 – 7.21 (m, 1H, obsc. by solvent peak), 5.23 (d, *J* = 4.4 Hz, 2H).

*2-(2-(Dimethylamino)phenyl)-N-(pyridin-2-ylmethyl)quinazolin-4-amine (**27**).*

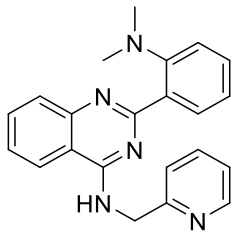

2-Chloro-*N*-(pyridin-2-ylmethyl)quinazolin-4-amine **49** (100 mg, 0.36 mmol) and N,N-dimethyl-2-(4,4,5,5-tetramethyl-1,3,2-dioxaborolan-2-yl)aniline (134 mg, 0.54 mmol) were reacted according to general procedure 2 overnight at 120 °C. Upon cooling to room temperature the reaction mixture was loaded onto an SCX-II column, washed with MeOH, then eluted with 0.5 M NH_3 in MeOH and concentrated *in vacuo*. Purification *via* preparatory HPLC (gradient elution 5 to 95% MeCN in H_2O with 0.1% NH_3) yielded 2-(2-(dimethylamino)phenyl)-*N*-(pyridin-2-ylmethyl)quinazolin-4-amine **27** (3.0 mg, 0.008 mmol, 2.3%) as a white solid. MS (ESI+) *m*/*z* calcd for $C_{22}H_{22}N_5$ $[M + H]^+$ 356.2; found 356.1. UPLC (method D) t_R = 3.18 min, >98%. ^{1}H NMR (300 MHz, Chloroform-d) δ 8.69 – 8.61 (m, 1H), 8.01 – 7.91 (m, 2H), 7.80 – 7.74 (m, 1H), 7.74 – 7.65 (m, 2H), 7.51 (ddd, J = 8.2, 7.0, 1.3 Hz, 1H), 7.44 – 7.37 (m, 2H), 7.33 (ddd, J = 8.3, 7.2, 1.8 Hz, 1H), 7.26 (d, J = 6.5 Hz, 1H), 7.04 (dd, J = 8.3, 1.1 Hz, 1H), 6.98 (td, J = 7.4, 1.1 Hz, 1H), 5.01 (s, 2H), 2.73 (s, 6H).

*2-Chloro-N-(pyridin-2-yl)quinazolin-4-amine (**51**).*

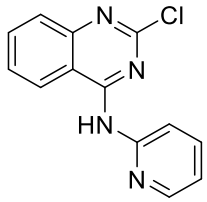

2,4-Dichloroquinazoline **43** (0.50 g, 2.51 mmol) and 2-aminopyridine (0.24 g, 2.51 mmol) were reacted according to general procedure 1 in $CHCl_3$ (10 mL) at 80°C for 18 h. Purification *via* silica gel chromatography (gradient elution 5 to 100% EtOAc in petroleum ether) gave 2-chloro-*N*-(pyridin-2-yl)quinazolin-4-amine **51** (0.64 g, 2.49 mmol, 99%) as a white solid. MS (ESI+) *m*/*z* calcd for $C_{13}H_{10}ClN_4$ $[M + H]^+$ 257.1; found 257.2. UPLC (method A) t_R = 2.95 min, 96%.

*2-(2-Isopropylphenyl)-N-(pyridin-2-yl)quinazolin-4-amine (**28**).*

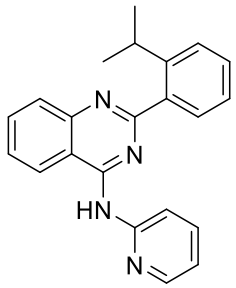

2-Chloro-*N*-(pyridin-2-yl)quinazolin-4-amine **51** (100 mg, 0.39 mmol) and (2-isopropylphenyl)boronic acid (96 mg, 0.58 mmol) were reacted according to general procedure 2 for 3.5 h at 130 °C. Upon cooling to room temperature the reaction mixture was loaded onto an SCX-II column, washed with MeOH, then eluted with 0.5 M NH_3 in MeOH and concentrated *in vacuo*. Purification *via* preparatory HPLC (gradient elution 5 to 95% MeCN in H_2O with 0.1% NH_3) yielded 2-(2-isopropylphenyl)-*N*-(pyridin-2-yl)quinazolin-4-amine **28** (24 mg, 0.07 mmol, 19%) as a white solid. MS (ESI+) *m*/*z* calcd for $C_{22}H_{21}N_4$ $[M + H]^+$ 341.2; found 341.2. UPLC (method C) t_R = 6.18 min, >98%. ^{1}H NMR (300 MHz, Chloroform-d) δ 8.88 – 8.78 (m, 0.7H), 8.65 (d, *J* = 7.9 Hz, 0.3H), 8.41 – 8.32 (m, 0.7H), 8.22 (d, *J* = 5.3 Hz, 0.3H), 8.05 (m, 1.3H), 7.88 (ddd, *J* = 8.2, 6.9, 1.3 Hz, 0.7H), 7.79 – 7.56 (m, 3H), 7.56 – 7.45 (m, 2H), 7.45 – 7.28 (m, 2H), 7.11 – 6.92 (m, 1H), 3.72 (p, *J* = 6.9 Hz, 0.7H), 3.53 – 3.39 (m, 0.3H), 1.29 (m, 6H), rotamers observed.

*2-Chloro-N-(1-(pyridin-2-yl)ethyl)quinazolin-4-amine (**52**).*

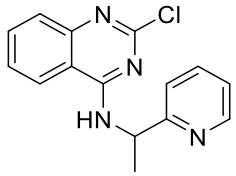

2,4-Dichloroquinazoline **43** (1.00 g, 5.02 mmol) and 1-(pyridin-2-yl)ethan-1-amine (0.68 g, 5.53 mmol) were reacted according to general procedure 1 for 18 h to give 2-chloro-*N*-(1-(pyridin-2-yl)ethyl)quinazolin-4-amine **52** (0.89 g, 3.12 mmol, 62%) as a cream coloured solid which was used without further purification. MS (ESI+) *m*/*z* calcd for $C_{15}H_{14}ClN_4$ $[M + H]^+$ 285.1; found 285.0. UPLC (method A) t_R = 2.57 min, 68%.

*2-(2-Isopropylphenyl)-N-(1-(pyridin-2-yl)ethyl)quinazolin-4-amine (**29**).*

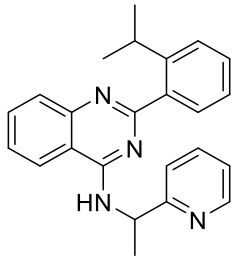

2-Chloro-*N*-(1-(pyridin-2-yl)ethyl)quinazolin-4-amine **52** (100 mg, 0.36 mmol) and (2-isopropylphenyl)boronic acid (89 mg, 0.54 mmol) were reacted according to general procedure 2 for 40 mins at 120 °C. Upon cooling to room temperature the reaction mixture was loaded onto an SCX-II column, washed with MeOH, then eluted with 0.5 M NH_3 in MeOH and concentrated *in vacuo*. Purification *via* preparatory HPLC (gradient elution 5 to 95% MeCN in H_2O with 0.1% NH_3) yielded 2-(2-isopropylphenyl)-*N*-(1-(pyridin-2-yl)ethyl)quinazolin-4-amine **29** (50 mg, 0.14 mmol, 38%) as a white solid. MS (ESI+) *m*/*z* calcd for $C_{24}H_{25}N_4$ $[M + H]^+$ 369.2; found 369.2. UPLC (method D) t_R = 4.05 min, >98%. 1H NMR (300 MHz, Chloroform-d) δ 8.66 (ddd, J = 4.9, 1.8, 0.9 Hz, 1H), 8.02 – 7.87 (m, 2H), 7.81 – 7.72 (m, 1H), 7.72 – 7.65 (m, 2H), 7.62 (d, J = 7.0 Hz, 1H), 7.52 (ddd, J = 8.2, 7.0, 1.3 Hz, 1H), 7.49 – 7.45 (m, 1H), 7.42 (td, J = 8.0, 7.4, 1.5 Hz, 1H), 7.34 – 7.29 (m, 2H), 7.26 (ddd, J = 7.5, 4.9, 1.1 Hz, 1H), 5.69 (p, J = 6.7 Hz, 1H), 3.76 – 3.60 (m, 1H), 1.66 (d, J = 6.7 Hz, 3H), 1.32 (d, J = 6.8 Hz, 3H), 1.26 (d, J = 6.9 Hz, 3H).

*2-Chloro-N-((5-(trifluoromethyl)pyridin-2-yl)methyl)quinazolin-4-amine (**53**).*

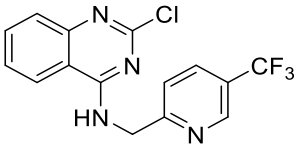

2,4-Dichloroquinazoline **43** (0.20 g, 1.00 mmol) and [5-(trifluoromethyl)pyridin-2-yl]methanamine hydrochloride (0.22 g, 1.06 mmol) were reacted according to general procedure 1 with 4 eq of triethylamine for 60 h to give 2-chloro-*N*-[[5-(trifluoromethyl)-2-pyridyl]methyl]quinazolin-4-amine **53** (0.19 g, 0.57 mmol, 57%) as a cream coloured solid which was used without further purification. MS (ESI+) *m/z* calcd for $C_{15}H_{11}ClF_3N_4$ $[M + H]^+$ 339.1; found 339.0. UPLC (method A) t_R = 2.92 min, 91%.

*2-(2-Isopropylphenyl)-N-((5-(trifluoromethyl)pyridin-2-yl)methyl)quinazolin-4-amine (**30**).*

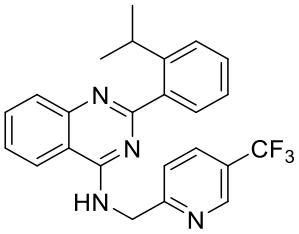

2-Chloro-*N*-((5-(trifluoromethyl)pyridin-2-yl)methyl)quinazolin-4-amine **53** (80 mg, 0.24 mmol) and (2-isopropylphenyl)boronic acid (58 mg, 0.35 mmol) were reacted according to general procedure 2 for 40 mins at 125 °C. Upon cooling to room temperature the reaction mixture was loaded onto an SCX-II column, washed with MeOH, then eluted with 0.5 M NH_3 in MeOH and concentrated *in vacuo*. Purification *via* preparatory HPLC (gradient elution 5 to 95% MeCN in H_2O with 0.1% NH_3) yielded 2-(2-isopropylphenyl)-*N*-((5-(trifluoromethyl)pyridin-2-yl)methyl)quinazolin-4-amine **30** (31 mg, 0.07 mmol, 31%) as a white solid. MS (ESI+) *m/z* calcd for $C_{24}H_{22}F_3N_4$ $[M + H]^+$ 423.2; found 423.3. UPLC (method C) t_R = 6.14 min, >98%. ^{1}H NMR (300 MHz, Chloroform-d) δ 8.93 (dt, *J* = 2.0, 0.9 Hz, 1H), 8.02 – 7.89 (m, 3H), 7.81 (ddd, *J* = 8.2, 7.0, 1.4 Hz, 1H), 7.66 (ddd, *J* = 7.6, 1.4, 0.6 Hz, 1H), 7.56 (ddd, *J* = 8.3, 7.0, 1.2 Hz, 1H), 7.51 – 7.36 (m, 3H), 7.33-7.25 (m, 2H), 5.09 (d, *J* = 4.6 Hz, 2H), 3.58 (hept, *J* = 6.8 Hz, 1H), 1.25 (d, *J* = 6.9 Hz, 6H).

*2-(((2-Chloroquinazolin-4-yl)amino)methyl)pyridin-3-ol (**54**).*

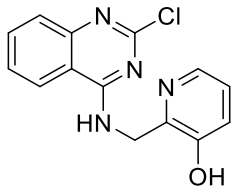

2,4-Dichloroquinazoline **43** (200 mg, 1.00 mmol) and 2-(aminomethyl)pyridin-3-ol dihydrochloride (208 mg, 1.06 mmol) were reacted according to general procedure 1 with 5 eq of triethylamine for 60 h to give 2-(((2-chloroquinazolin-4-yl)amino)methyl)pyridin-3-ol **54** (216 mg, 0.75 mmol, 75%) as a white solid which was used without further purification. MS (ESI+) *m*/*z* calcd for $C_{14}H_{12}ClN_4O$ $[M + H]^+$ 287.1; found 287.0. UPLC (method A) t_R = 1.79 min, 32%.

*2-(((2-(2-Isopropylphenyl)quinazolin-4-yl)amino)methyl)pyridin-3-ol (**31**).*

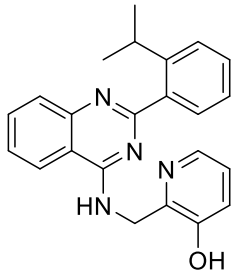

2-(((2-Chloroquinazolin-4-yl)amino)methyl)pyridin-3-ol **54** (80 mg, 0.28 mmol) and (2-isopropylphenyl)boronic acid (69 mg, 0.42 mmol) were reacted according to general procedure 2 for 40 mins at 125 °C. Upon cooling to room temperature the reaction mixture was loaded onto an SCX-II column, washed with MeOH, then eluted with 0.5 M NH_3 in MeOH and concentrated *in vacuo*. Purification *via* preparatory HPLC (gradient elution 5 to 95% MeCN in H_2O with 0.1% NH_3) yielded 2-(((2-(2-isopropylphenyl)quinazolin-4-yl)amino)methyl)pyridin-3-ol **31** (8 mg, 0.02 mmol, 8%) as a white solid. MS (ESI+) *m*/*z* calcd for $C_{23}H_{23}N_4O$ $[M + H]+$ 371.2; found 371.3. UPLC (method C) t_R = 4.03 min, >95%. ^{1}H NMR (300 MHz, Chloroform-d) δ 11.18 (s, 1H), 8.08 (dd, *J* = 3.9, 2.1 Hz, 1H), 7.93 (dt, *J* = 8.2, 1.1 Hz, 1H), 7.82 (tdd, *J* = 8.3, 7.1, 1.1 Hz, 2H), 7.59 (dt, *J* = 7.4, 1.0 Hz, 1H), 7.55 – 7.41 (m, 4H), 7.35 (ddd, *J* = 7.6, 5.5, 3.1 Hz, 1H), 7.22 – 7.09 (m, 2H), 4.95 (d, *J* = 6.4 Hz, 2H), 3.45 – 3.29 (m, 1H), 1.28 (d, *J* = 6.8 Hz, 6H).

*6-Bromo-2-(2-isopropylphenyl)quinazolin-4-ol (**56**).*

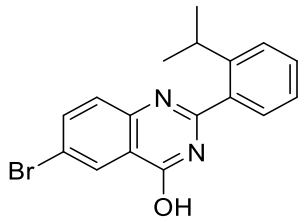

2-(Propan-2-yl)benzoic acid **55** (200 mg, 1.22mmol) was taken up in anhydrous DCM (5 mL) with 3 drops of anhydrous DMF, and cooled on an ice bath. Thionyl dichloride (0.34 mL, 4.65 mmol) was added dropwise and the mixture heated to 50 °C for 4 hours. The solvent was removed *in vacuo* and co-evaporated with toluene. The prepared acid chloride was taken up in DCM (1 mL) and added dropwise to a suspension of 2-amino-5-bromobenzamide (250 mg, 1.16mmol) and triethylamine (0.32 mL, 2.33 mmol) in DCM (5 mL) at 0 °C. After addition, the reaction was warmed to room temperature and left to stir overnight. DMF (2 mL) was added to achieve full dissolution and the reaction stirred at room temperature for a further 4 hours. EtOAc was added to the reaction mixture and washed with sat. aq. $NaHCO_3$ (x1), H_2O (x1), 1M aq. HCl (x1) and brine (x1), then dried ($MgSO_4$), and solvent removed to give a brown residue. Purification *via* silica gel chromatography (gradient elution 0 to 40% EtOAc in petroleum ether) yielded the intermediate *N*-(4-bromo-2-carbamoylphenyl)-2-isopropylbenzamide. MS (ESI+) *m/z* calcd for $C_{17}H_{17}BrN_2O_2$ $[M + H]^+$ 361.1; found 361.2. This material was taken up in 5% NaOH (217 mg, 5.42 mmol) in H_2O (4.7 mL) and heated to reflux for 3 hours. The reaction was cooled and acidified to ~pH 5 with acetic acid. The resulting white solid was filtered and washed with H_2O and dried under high vacuum to afford 6-bromo-2-(2-isopropylphenyl)quinazolin-4-ol **56** (350 mg, 1.02 mmol, 88%) as an off-white solid. MS (ESI+) *m/z* calcd for $C_{17}H_{15}BrN_2O$ $[M + H]^+$ 343.0; found 343.1. UPLC (method A) t_R = 2.82 min, 97%. ^{1}H NMR (300 MHz, Chloroform-*d*) δ 8.21 (s, 1H), 7.80 (d, *J* = 9.0 Hz, 1H), 7.64 (d, *J* = 8.8 Hz, 1H), 7.40 (d, *J* = 4.2 Hz, 2H), 7.36-7.27 (m, 2H, obsc. by solvent peak), 7.20-7.11 (m, 1H), 3.27 (p, *J* = 6.8 Hz, 1H), 1.18 (d, *J* = 6.8 Hz, 6H).

*6-Bromo-4-chloro-2-(2-isopropylphenyl)quinazoline (**57**).*

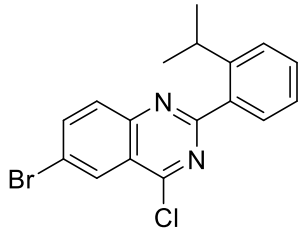

6-Bromo-2-(2-isopropylphenyl)quinazolin-4-ol **56** (380 mg, 1.11 mmol) was taken up in toluene (5 mL) and phosphorus oxychloride (3.5 mL, 37.3 mmol) was added. The mixture was heated for 18 hours at 90 °C. Reaction cooled and added slowly to cooled sat. aq. $NaHCO_3$, stirred for 30 mins on ice and extracted with EtOAc (2 ×), dried ($MgSO_4$) and solvent removed to give 6-bromo-4-chloro-2-(2-isopropylphenyl)quinazoline **57** (356 mg, 0.984 mmol, 89%) of an oil that solidified on standing. Not purified further. MS (ESI+) *m*/*z* calcd for $C_{17}H_{14}BrClN_2$ $[M + H]^+$ 361.0; found 361.1. UPLC (method A) t_R = 3.97 min, 95%. ^1H NMR (300 MHz, Chloroform-*d*) δ 8.49 (dd, *J* = 2.1, 0.6 Hz, 1H), 8.06 (dd, *J* = 8.9, 2.1 Hz, 1H), 8.00 (d, *J* = 8.9 Hz, 1H), 7.82 – 7.72 (m, 1H), 7.56 – 7.43 (m, 2H), 7.34 (ddd, *J* = 7.7, 6.1, 2.6 Hz, 1H), 3.59 (hept, *J* = 6.8 Hz, 1H), 1.30 (d, *J* = 6.8 Hz, 6H).

*6-Bromo-2-(2-isopropylphenyl)-N-(pyridin-2-ylmethyl)quinazolin-4-amine (**32**).*

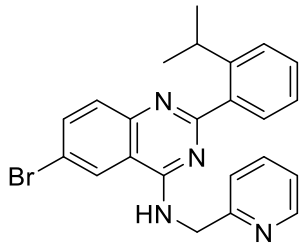

6-Bromo-4-chloro-2-(2-isopropylphenyl)quinazoline **57** (350 mg, 0.970 mmol) and pyridin-2-ylmethanamine (0.12 mL, 1.16 mmol) were reacted according to general procedure 1 for 18 hours. A further 0.5 eq of pyridin-2-ylmethanamine (0.05 mL, 0.48 mmol) was added and the reaction stirred at room temperature for a further 3 hours. The reaction was diluted with CH_2Cl_2, washed with brine (2 ×), then dried ($MgSO_4$) and concentrated *in vacuo*. 50 mg of crude material was purified *via* preparatory HPLC (gradient elution 40 to 80% MeCN in H_2O with 0.1% NH_3) yielding 6-bromo-2-(2-isopropylphenyl)-*N*-(pyridin-2-ylmethyl)quinazolin-4-amine **32** (29.5 mg, 0.068 mmol, 7%) to be used for biological testing. MS (ESI+) *m*/*z* calcd for $C_{23}H_{22}BrN_4$ $[M + H]^+$ 433.1; found

433.2. UPLC (method C) t_R = 6.16 min, >98%. ^{1}H NMR (300 MHz, Chloroform-d) δ 8.68 (ddd, *J* = 5.0, 1.8, 1.0 Hz, 1H), 8.13 (dd, *J* = 1.9, 0.7 Hz, 1H), 7.85 (dd, *J* = 8.9, 1.9 Hz, 1H), 7.81 (dd, *J* = 8.9, 0.7 Hz, 1H), 7.73 (td, *J* = 7.7, 1.8 Hz, 1H), 7.68 (ddd, *J* = 7.6, 1.5, 0.6 Hz, 1H), 7.52 (s, 1H), 7.49 – 7.38 (m, 2H), 7.37 – 7.24 (m, 3H), 4.97 (d, *J* = 4.3 Hz, 2H), 3.60 (hept, *J* = 6.9 Hz, 1H), 1.28 (d, *J* = 6.9 Hz, 6H).

The remaining crude material was purified *via* silica gel chromatography (gradient elution 0 to 100% EtOAc in petroleum ether) yielding 6-bromo-2-(2-isopropylphenyl)-*N*-(pyridin-2-ylmethyl)quinazolin-4-amine **32** (0.26 g, 0.60 mmol, 62%) as a white solid for use as an intermediate. MS (ESI+) *m/z* 433 and 435 $[M + H]^+$. Combined yield (0.29g, 0.67 mmol, 69%).

*2-(2-Isopropylphenyl)-N^4-(pyridin-2-ylmethyl)quinazoline-4,6-diamine (**33**).*

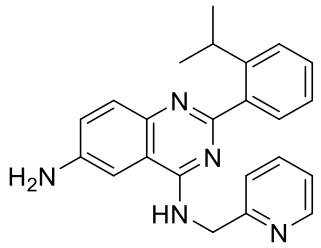

6-Bromo-2-(2-isopropylphenyl)-*N*-(pyridin-2-ylmethyl)quinazolin-4-amine **32** (30 mg, 0.070 mmol, 1.0 eq) was dissolved in EtOH:H_2O 7:3 (1 mL) in a MW vial and sodium azide (9.0 mg, 0.14 mmol, 2.0 eq.) and copper(I) iodide (1.3 mg, 0.010 mmol, 0.1 eq.) were added, followed by sodium ascorbate (0.8 mg, 0.004 mmol, 0.06 eq.). The mixture was thoroughly degassed and *trans*-*N*,*N*'-dimethylcyclohexane-1,2-diamine (0.002 mL, 0.01 mmol, 0.2 eq.) was added followed by capping. Further degassing (including cooling and evacuating the vessel, and rewarming to rt, repeat) and the mixture was heated to 100 °C overnight. LCMS suggested ~40% conversion to azide and ~25% conversion to amine. The reaction mixture was loaded onto an SCX-2 column and washed through with MeOH. Product eluted with 0.5 M NH_3 in MeOH and solvent removed to give crude material which was purified *via* preparatory HPLC (gradient elution 30 to 70% MeCN in H_2O with 0.1% NH_3) to give 2-(2-isopropylphenyl)-N^4-(pyridin-2-ylmethyl)quinazoline-4,6-diamine **33** (2.5 mg, 0.0068 mmol, 9.8%) as a pale brown solid. MS (ESI+) *m/z* calcd for $C_{23}H_{24}N_5$ $[M + H]^+$ 370.2; found 370.3. UPLC (method D) t_R = 3.63 min, >98%. ^{1}H NMR (300 MHz, Chloroform-d) δ 8.65 (dt, *J* = 5.0, 1.3 Hz, 1H), 7.79 (d, *J* = 8.8 Hz, 1H), 7.71 (td, *J* = 7.7, 1.8 Hz, 1H), 7.65 (dd, *J* = 7.5, 1.5 Hz, 1H), 7.44 (dd, *J* = 7.8, 1.7 Hz, 1H), 7.39 (td, *J* = 8.0, 7.5, 1.6 Hz, 1H),

7.34 (d, *J* = 7.8 Hz, 1H), 7.31 – 7.24 (m, 2H), 7.21 (dd, *J* = 8.8, 2.4 Hz, 1H), 7.11 (s, 1H), 7.08 (d, *J* = 2.5 Hz, 1H), 4.97 (d, *J* = 4.4 Hz, 2H), 4.01 (s, 2H), 3.61 (hept, *J* = 6.9 Hz, 1H), 1.26 (d, *J* = 6.9 Hz, 6H).

*2-Chloro-5-methyl-N-(pyridin-2-ylmethyl)pyrimidin-4-amine (**59**).*

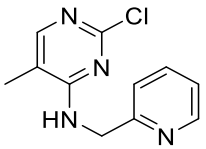

2,4-Dichloro-5-methylpyrimidine **58** (0.10 g, 0.62 mmol) and pyridin-2-ylmethanamine (77 µL, 80 mg, 0.74 mmol) were reacted according to general procedure 1 for 18 hours, followed by purification *via* silica gel chromatography (gradient elution 20 to 100% EtOAc in petroleum ether) to give 2-chloro-5-methyl-*N*-(pyridin-2-ylmethyl)pyrimidin-4-amine **59** (97 mg, 0.41 mmol, 67%) as a white solid. MS (ESI+) *m*/*z* calcd for $C_{11}H_{11}ClN_4$ $[M + H]^+$ 235.1; found 235.1. UPLC (method A) t_R = 2.30 min, 97%.

*2-(2-Isopropylphenyl)-5-methyl-N-(pyridin-2-ylmethyl)pyrimidin-4-amine (**34**).*

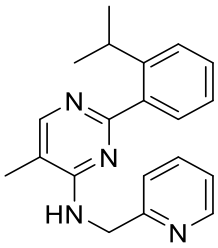

2-Chloro-5-methyl-*N*-(pyridin-2-ylmethyl)pyrimidin-4-amine **59** (45.2 mg, 0.193 mmol) and (2-propan-2-ylphenyl)boronic acid (47.4 mg, 0.289 mmol) were reacted according to general procedure 2 for 45 min at 120 °C, resulting in partial conversion to desired product. A further 0.5 equivalents of (2-propan-2-ylphenyl)boronic acid (12.0 mg, 0.072 mmol) and 0.1 equivalents of tetrakis(triphenylphosphine)palladium (22.2 mg, 0.019 mmol) were added to the reaction mixture with degassing and further heating for 30 min at 120 °C. Upon cooling to rt the reaction mixture was loaded onto an SCX-II column, washed with MeOH, then eluted with 0.5 M NH_3 in MeOH and concentrated *in vacuo*, yielding 2-(2-isopropylphenyl)-5-methyl-*N*-(pyridin-2-ylmethyl)pyrimidin-4-amine **34** (55.3 mg, 0.174 mmol, 90%) as a white solid. MS (ESI+) *m*/*z* calcd for $C_{20}H_{23}N_4^+$ $[M + H]^+$ 319.1917; found 319.2. HRMS (ESI+) *m*/*z* calcd for $C_{20}H_{23}N_4^+$ $[M + H]^+$ 319.1917; found 319.1915. UPLC (method C) t_R = 4.89 min, 97%. ^{1}H NMR (300 MHz, Chloroform-*d*) δ 8.61 (ddd, *J* = 4.9, 1.8, 1.0 Hz, 1H), 8.17 (d, *J* = 1.0 Hz, 1H), 7.74 – 7.63 (m, 1H), 7.63 – 7.57 (m, 1H), 7.57 – 7.43 (m, 1H), 7.43 – 7.34 (m, 2H), 7.33 – 7.20 (m, 2H), 6.27 (s, 1H), 4.87 (d, *J* = 4.6 Hz, 2H), 3.57 (h, *J* = 6.8 Hz, 1H), 2.23 (d, *J* = 0.9 Hz, 3H), 1.24 (d, *J* = 6.9 Hz, 6H).

*5-Methyl-N-(pyridin-2-ylmethyl)-2-(2-(trifluoromethyl)phenyl)pyrimidin-4-amine (**35**).*

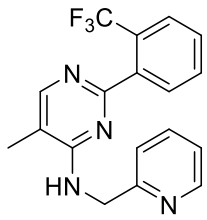

2-Chloro-5-methyl-*N*-(pyridin-2-ylmethyl)pyrimidin-4-amine **59** (45.2 mg, 0.193 mmol) and (2-trifluoromethyl)phenylboronic acid (54.9 mg, 0.289 mmol) were reacted according to general procedure 2 for 45 min at 120 °C. Upon cooling to room temperature the reaction mixture was loaded onto an SCX-II column, washed with MeOH, then eluted with 0.5 M NH_3 in MeOH and concentrated *in vacuo* yielding 5-methyl-*N*-(pyridin-2-ylmethyl)-2-[2-(trifluoromethyl)phenyl]pyrimidin-4-amine **35** (60.0 mg, 0.174 mmol, 90.5%) as a white solid. MS (ESI+) *m/z* calcd for $C_{18}H_{16}F_3N_4$ $[M + H]^+$ 345.1; found 345.1. HRMS (ESI+) *m/z* calcd for $C_{18}H_{16}F_3N_4^+$ $[M + H]^+$ 345.1322; found 345.1323. UPLC (method C) t_R = 4.56 min, 98%. ^{1}H NMR (300 MHz, DMSO-d_6) δ 8.49 (ddd, *J* = 4.8, 1.9, 1.0 Hz, 1H), 8.10 (d, *J* = 1.0 Hz, 1H), 7.80 – 7.51 (m, 6H), 7.29 – 7.18 (m, 2H), 4.73 (d, *J* = 5.8 Hz, 2H), 2.15 (d, *J* = 0.9 Hz, 3H). ^{13}C NMR (75 MHz, DMSO-d_6) δ 163.0, 160.9, 159.6, 153.8, 149.2, 139.9, 136.9, 132.3, 131.6, 129.2, 127.3 (q, *J* = 30.6 Hz), 126.8 (q, *J* = 5.4 Hz), 122.3, 121.1, 112.8, 45.7, 14.0. ^{19}F NMR (282 MHz, DMSO-d_6) δ -56.08.

*2-Chloro-N-(pyridin-2-ylmethyl)pyrido[3,2-d]pyrimidin-4-amine (**62**).*

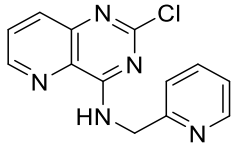

2,4-Dichloropyrido[3,2-d]pyrimidine **60** (0.15 g, 0.75 mmol) and pyridin-2-ylmethanamine (81 µL, 85 mg, 0.79 mmol) were reacted according to general procedure 1 for 18 hours, followed by purification *via* silica gel chromatography (gradient elution 20 to 100% EtOAc in petroleum ether) to give 2-chloro-*N*-(pyridin-2-ylmethyl)pyrido[3,2-d]pyrimidin-4-amine **62** (169 mg, 0.62 mmol, 83%) as a pale yellow solid. MS (ESI+) *m/z* calcd for $C_{13}H_{10}ClN_5$ $[M + H]^+$ 272.1; found 272.0. UPLC (method A) t_R = 2.52 min, >98%. ^{1}H NMR (300 MHz,

Chloroform-*d*) δ 8.77 (dd, *J* = 4.3, 1.6 Hz, 1H), 8.69 (ddd, *J* = 4.9, 1.8, 1.0 Hz, 1H), 8.65 (brs, 1H), 8.06 (dd, *J* = 8.5, 1.5 Hz, 1H), 7.74 (td, *J* = 7.8, 4.3 Hz, 1H), 7.69 (dd, *J* = 8.5, 4.3 Hz, 1H), 7.39 (dt, *J* = 7.9, 1.0 Hz, 1H), 7.34 – 7.23 (m, 1H, obsc. by solvent peak), 4.98 (d, *J* = 5.0 Hz, 2H).

*2-(2-Isopropylphenyl)-N-(pyridin-2-ylmethyl)pyrido[3,2-d]pyrimidin-4-amine (**36**).*

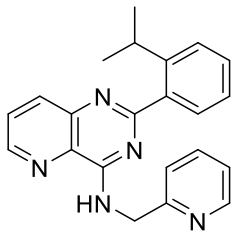

2-Chloro-*N*-(pyridin-2-ylmethyl)pyrido[3,2-d]pyrimidin-4-amine **62** (50.0 mg, 0.181 mmol) and (2-propan-2-ylphenyl)boronic acid (59.3 mg, 0.361 mmol) were reacted according to general procedure 2 for 45 min at 120 °C, resulting in partial conversion to desired product. A further 2 equivalents of (2-propan-2-ylphenyl)boronic acid (59.3 mg, 0.36 mmol) and 0.1 equivalents of tetrakis(triphenylphosphine)palladium (20.9 mg, 0.018 mmol) were added to the reaction mixture with degassing and further heating for 30 min at 120 °C. The reaction mixture was loaded onto an SCX-II column, washed with MeOH, then eluted with 0.5 M NH_3 in MeOH and concentrated *in vacuo*. Purification *via* preparatory HPLC (gradient elution 5 to 95% MeCN in H_2O with 0.1% NH_3) yielded 2-(2-isopropylphenyl)-*N*-(pyridin-2-ylmethyl)pyrido[3,2-d]pyrimidin-4-amine **36** (44.2 mg, 0.124 mmol, 68%) as a beige solid. MS (ESI+) *m/z* calcd for $C_{22}H_{22}N_5$ $[M + H]^+$ 356.2; found 356.1. UPLC (method C) t_R = 5.02 min, >98%. ^{1}H NMR (300 MHz, Chloroform-d) δ 8.79 (ddd, *J* = 4.2, 1.6, 0.7 Hz, 1H), 8.67 (ddd, *J* = 4.9, 1.8, 0.9 Hz, 1H), 8.26 (s, 1H), 8.19 (ddd, *J* = 8.5, 1.6, 0.7 Hz, 1H), 7.76 – 7.62 (m, 3H), 7.49 – 7.33 (m, 3H), 7.33 – 7.20 (m, 2H), 5.04 (d, *J* = 5.4 Hz, 2H), 3.59 (dq, *J* = 13.7, 6.8 Hz, 1H), 1.25 (dd, *J* = 6.9, 0.7 Hz, 6H).

*2-Chloro-N-(pyridin-2-ylmethyl)pyrido[2,3-d]pyrimidin-4-amine (**63**).*

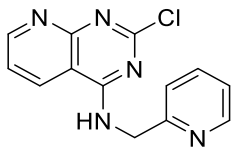

2,4-Dichloropyrido[2,3-d]pyrimidine **61** (0.25 g, 1.25 mmol) and pyridin-2-ylmethanamine (0.15 g, 1.37 mmol) were reacted according to general procedure 1 for 18 hours to give 2-chloro-*N*-(pyridin-2-ylmethyl)pyrido[2,3-d]pyrimidin-4-amine **63** (125 mg, 0.83 mmol, 66%) as a pale yellow solid which was used without further purification. MS (ESI+) *m/z* calcd for $C_{13}H_{10}ClN_5$ $[M + H]^+$ 272.1; found 272.1. UPLC (method A) t_R = 2.20 min, >95%. ^{1}H NMR (300 MHz, Chloroform-*d*) δ 9.08 (dd, *J* = 4.4, 1.8 Hz, 1H), 8.69 – 8.60 (m, 1H), 8.34 (dd, *J* = 8.2, 1.9 Hz, 1H), 8.16 (s, 1H), 7.78 (td, *J* = 7.7, 1.8 Hz, 1H), 7.48 (dd, *J* = 8.2, 4.4 Hz, 1H), 7.40 (dt, *J* = 7.9, 1.0 Hz, 1H), 7.36 – 7.29 (m, 1H), 4.95 (d, *J* = 4.1 Hz, 2H).

*2-(2-Isopropylphenyl)-N-(pyridin-2-ylmethyl)pyrido[2,3-d]pyrimidin-4-amine (**37**).*

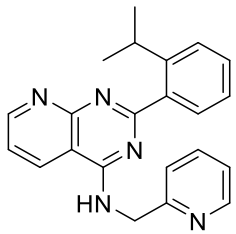

2-Chloro-*N*-(pyridin-2-ylmethyl)pyrido[2,3-d]pyrimidin-4-amine **63** (50 mg, 0.184 mmol) and (2-propan-2-ylphenyl)boronic acid (45.3 mg, 0.276 mmol) were reacted according to general procedure 2 for 45 mins at 120 °C. Upon cooling to room temperature the reaction mixture was loaded onto an SCX-II column, washed with MeOH, then eluted with 0.5 M NH_3 in MeOH and concentrated *in vacuo*. Purification *via* preparatory HPLC (gradient elution 5 to 95% MeCN in H_2O with 0.1% NH_3) yielded 2-(2-isopropylphenyl)-*N*-(pyridin-2-ylmethyl)pyrido[2,3-d]pyrimidin-4-amine **37** (17.7 mg, 0.05 mmol, 27% yield) as a white solid. MS (ESI+) *m/z* calcd for $C_{22}H_{22}N_5$ $[M + H]^+$ 356.2; found 356.2. HRMS (ESI+) *m/z* calcd for $C_{22}H_{22}N_5^+$ $[M + H]^+$ 356.1870; found 356.1869. UPLC (method C) t_R = 5.28 min, >98%. ^{1}H NMR (300 MHz, Chloroform-d) δ 9.12 (dd, *J* = 4.4, 1.9 Hz, 1H), 8.65 (dt, *J* = 4.8, 1.4 Hz, 1H), 8.38 (dd, *J* = 8.2, 1.9 Hz, 1H), 7.90 – 7.80 (m, 1H), 7.78 – 7.68 (m, 2H), 7.49 – 7.39 (m, 3H), 7.35 (dt, *J* = 7.8, 1.0 Hz, 1H), 7.33 – 7.26 (m, 2H), 4.99 (d, *J* = 4.3 Hz, 2H), 3.86 (dq, *J* = 13.7, 6.9 Hz, 1H), 1.31 (d, *J* = 6.9 Hz, 6H).

*N-(Pyridin-2-ylmethyl)-2-[2-(trifluoromethyl)phenyl]pyrido[2,3-d]pyrimidin-4-amine (**38**).*

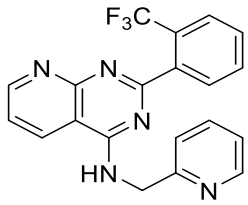

2-Chloro-*N*-(pyridin-2-ylmethyl)pyrido[2,3-d]pyrimidin-4-amine **63** (50 mg, 0.184 mmol) and (2-trifluoromethyl)phenylboronic acid (52.4 mg, 0.276 mmol) were reacted according to general procedure 2 for 45 mins at 120 °C. Upon cooling to room temperature the reaction mixture was loaded onto an SCX-II column, washed with MeOH, then eluted with 0.5 M NH_3 in MeOH and concentrated *in vacuo*. Purification *via* preparatory HPLC (gradient elution 5 to 95% MeCN in H_2O with 0.1% NH_3) yielded *N*-(pyridin-2-ylmethyl)-2-[2-(trifluoromethyl)phenyl]pyrido[2,3-d]pyrimidin-4-amine **38** (26.3 mg, 0.69 mmol, 37.5% yield) as a white solid. MS (ESI+) *m/z* calcd for $C_{20}H_{15}F_3N_5$ $[M + H]^+$ 382.1; found 382.2. HRMS (ESI+) *m/z* calcd for $C_{20}H_{15}F_3N_5^+$ $[M + H]^+$ 382.1274; found 382.1275. UPLC (method D) t_R = 4.17 min, >98%. ^{1}H NMR (300 MHz, Chloroform-d) δ 9.12 (dd, J = 4.4, 1.9 Hz, 1H), 8.69 – 8.60 (m, 1H), 8.40 (dd, J = 8.2, 1.9 Hz, 1H), 8.10 – 8.01 (m, 1H), 7.88 (s, 1H), 7.83 (dd, J = 7.8, 1.3 Hz, 1H), 7.74 (td, J = 7.7, 1.8 Hz, 1H), 7.67 (dd, J = 8.3, 6.9 Hz, 1H), 7.63 – 7.54 (m, 1H), 7.49 (dd, J = 8.2, 4.4 Hz, 1H), 7.39 – 7.34 (m, 1H), 7.32-7.26 (m, 1H), 4.99 (d, J = 4.3 Hz, 2H). ^{13}C NMR (75 MHz, DMSO-d_6) δ 165.3, 161.2, 159.0, 158.6, 156.6, 149.4, 139.9 (q, *J* = 2.0 Hz), 137.1, 133.1, 132.5, 131.7, 129.6, 127.4 (q, *J* = 30.7 Hz), 126.9 (q, *J* = 5.1 Hz), 124.6 (q, *J* = 273.6 Hz), 122.6, 122.2, 121.5, 108.6, 46.2. ^{19}F NMR (282 MHz, DMSO-d_6) δ -56.02.

*2,4-Dichloro-7-methyl-7H-pyrrolo[2,3-d]pyrimidine (**65**).*

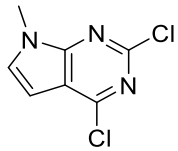

To a stirred solution of 2,4-dichloro-7*H*-pyrrolo[2,3-d]pyrimidine **64** (1.00 g, 5.32mmol) in DMF (8 mL) at room temperature was added sodium hydride (60% dispersion in mineral oil) (0.23 g, 5.85 mmol) in one portion and the reaction allowed to stir for 20 minutes before iodomethane (0.40 mL, 0.91 g, 6.38 mmol) was added *via* syringe and the reaction stirred at room temperature overnight. The reaction was diluted with water and EtOAc, extracted into EtOAc (x3), dried over sodium sulfate, filtered and concentrated *in vacuo*. Purification *via* silica gel

chromatography (gradient elution 5 to 100% EtOAc in petroleum ether) yielded 2,4-dichloro-7-methyl-7*H*-pyrrolo[2,3-d]pyrimidine **65** (1.01 g, 5.00 mmol, 94%) as a white solid. MS (ESI+) *m/z* calcd for $C_7H_6Cl_2N_3$ [M + H]$^+$ 202.0; not observed. UPLC (method A) t_R = 2.72 min, 89%.

*2-Chloro-7-methyl-N-(pyridin-2-ylmethyl)-7H-pyrrolo[2,3-d]pyrimidin-4-amine (**66**).*

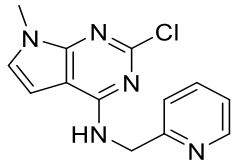

2,4-Dichloro-7-methyl-7*H*-pyrrolo[2,3-d]pyrimidine **65** (255 mg, 1.26 mmol) and pyridin-2-ylmethanamine (143 mg, 1.33 mmol) were reacted according to general procedure 1 in chloroform (8 mL) at 80 ºC for 18 h. Purification *via* silica gel chromatography (gradient elution 5 to 100% EtOAc in petroleum ether) gave 2-Chloro-7-methyl-N-(pyridin-2-ylmethyl)-7H-pyrrolo[2,3-d]pyrimidin-4-amine **66** (238 mg, 0.87 mmol, 69%) as a white solid. MS (ESI+) *m/z* calcd for $C_{13}H_{13}ClN_5$ [M + H]$^+$ 274.1; found 274.1. UPLC (method A) t_R = 2.52 min, 73%.

*2-(2-Isopropylphenyl)-7-methyl-N-(pyridin-2-ylmethyl)-7H-pyrrolo[2,3-d]pyrimidin-4-amine (**39**).*

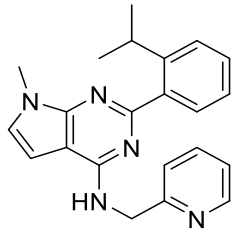

2-Chloro-7-methyl-N-(pyridin-2-ylmethyl)-7H-pyrrolo[2,3-d]pyrimidin-4-amine **66** (60 mg, 0.22 mmol) and (2-isopropylphenyl)boronic acid (54 mg, 0.33 mmol) were reacted according to general procedure 2 for 1 h at 125 °C. Upon cooling to room temperature the reaction mixture was loaded onto an SCX-II column, washed with MeOH, then eluted with 0.5 M NH_3 in MeOH and concentrated *in vacuo*. Purification *via* preparatory HPLC (gradient elution 5 to 95% MeCN in H_2O with 0.1% NH_3) yielded 2-(2-isopropylphenyl)-5-methyl-*N*-(pyridin-2-ylmethyl)-5*H*-pyrrolo[3,2-d]pyrimidin-4-amine **39** (51 mg, 0.14 mmol, 65%) as a white solid. MS (ESI+) *m/z*

calcd for $C_{22}H_{24}N_5$ $[M + H]^+$ 358.2; found 358.3. UPLC (method D) t_R = 4.21 min, >98%. ^{1}H NMR (300 MHz, Chloroform-d) δ 8.62 (ddd, *J* = 4.9, 1.8, 1.0 Hz, 1H), 7.74 – 7.61 (m, 2H), 7.49 – 7.17 (m, 6H), 6.96 (d, *J* = 3.5 Hz, 1H), 6.48 (d, *J* = 3.5 Hz, 1H), 6.25 (t, *J* = 5.2 Hz, 1H), 5.00 (d, *J* = 5.2 Hz, 2H), 3.85 (s, 3H), 3.65 (p, *J* = 6.9 Hz, 1H), 1.26 (d, *J* = 6.9 Hz, 6H). 1H NMR (300 MHz, Chloroform-d) δ 8.62 (ddd, J = 4.9, 1.8, 1.0 Hz, 1H), 7.74 – 7.61 (m, 2H), 7.44 (dd, J = 7.9, 1.6 Hz, 1H), 7.38 (ddd, J = 8.0, 7.0, 1.5 Hz, 2H), 7.31 – 7.24 (m, 1H), 7.24 – 7.19 (m, 1H), 6.96 (d, J = 3.5 Hz, 1H), 6.48 (d, J = 3.5 Hz, 1H), 6.25 (t, J = 5.2 Hz, 1H), 5.00 (d, J = 5.2 Hz, 2H), 3.85 (s, 3H), 3.65 (p, J = 6.9 Hz, 1H), 1.26 (d, J = 6.9 Hz, 6H).

*2,4-Dichloro-5-methyl-5H-pyrrolo[3,2-d]pyrimidine (**68**).*

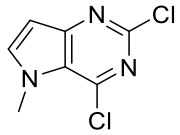

To a stirred solution of 2,4-dichloro-5*H*-pyrrolo[3,2-d]pyrimidine **67** (1.00 g, 5.32mmol) in DMF (10 mL) at room temperature was added sodium hydride (60% dispersion in mineral oil) (0.23 g, 5.85 mmol) in one portion and the reaction allowed to stir for 20 minutes before iodomethane (0.40 mL, 0.91 g, 6.38 mmol) was added *via* syringe and the reaction stirred at room temperature for 2 h. The reaction was diluted with water and EtOAc, extracted into EtOAc (x3), dried over sodium sulfate, filtered and concentrated *in vacuo*. Purification *via* silica gel chromatography (gradient elution 5 to 100% EtOAc in petroleum ether) yielded 2,4-Dichloro-5-methyl-5H-pyrrolo[3,2-d]pyrimidine **68** (0.98 g, 4.83 mmol, 91%) as a white solid. MS (ESI+) *m/z* calcd for $C_7H_6Cl_2N_3$ $[M + H]^+$ 202.0; found 202.0 (50%). UPLC (method A) t_R = 2.47 min, 89%.

*2-Chloro-5-methyl-N-(pyridin-2-ylmethyl)-5H-pyrrolo[3,2-d]pyrimidin-4-amine (**71**).*

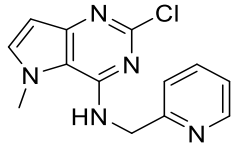

2,4-Dichloro-5-methyl-5H-pyrrolo[3,2-d]pyrimidine **68** (0.98 g, 4.83 mmol) and pyridin-2-ylmethanamine (0.55 g, 5.07 mmol) were reacted according to general procedure 1 in chloroform (12 mL) at reflux overnight to give 2-chloro-5-methyl-*N*-(pyridin-2-ylmethyl)-5*H*-pyrrolo[3,2-d]pyrimidin-4-amine **71** (0.97 g, 3.54 mmol, 73%) as a white solid which was used without further purification. MS (ESI+) *m/z* calcd for $C_{13}H_{13}ClN_5$ $[M + H]^+$ 274.1; found 274.0. UPLC (method B) t_R = 1.91 min, >90%.

*2-(2-Isopropylphenyl)-5-methyl-N-(pyridin-2-ylmethyl)-5H-pyrrolo[3,2-d]pyrimidin-4-amine (**40**).*

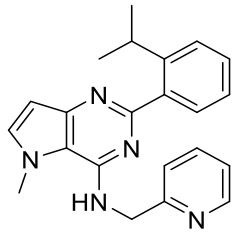

2-Chloro-5-methyl-*N*-(pyridin-2-ylmethyl)-5*H*-pyrrolo[3,2-d]pyrimidin-4-amine **71** (100 mg, 0.37 mmol) and (2-isopropylphenyl)boronic acid (90 mg, 0.55 mmol) were reacted according to general procedure 2 for 40 mins at 125 °C. Upon cooling to room temperature the reaction mixture was loaded onto an SCX-II column, washed with MeOH, then eluted with 0.5 M NH_3 in MeOH and concentrated *in vacuo*. Purification *via* preparatory HPLC (gradient elution 5 to 95% MeCN in H_2O with 0.1% NH_3) yielded 2-(2-isopropylphenyl)-5-methyl-*N*-(pyridin-2-ylmethyl)-5*H*-pyrrolo[3,2-d]pyrimidin-4-amine **40** (36 mg, 0.10 mmol, 28%) as a white solid. MS (ESI+) *m/z* calcd for $C_{22}H_{24}N_5$ $[M + H]^+$ 358.2; found 358.1. HRMS (ESI+) *m/z* calcd for $C_{22}H_{24}N_5^+$ $[M + H]^+$ 358.2026; found 358.2033. UPLC (method C) t_R = 4.87 min, >98%. ^{1}H NMR (300 MHz, DMSO-d_6) δ 8.51 (ddd, *J* = 4.9, 1.8, 0.9 Hz, 1H), 7.72 (td, *J* = 7.7, 1.8 Hz, 1H), 7.47 (d, *J* = 3.0 Hz, 1H), 7.45 – 7.19 (m, 6H), 7.13 (ddd, *J* = 7.6, 5.2, 3.4 Hz, 1H), 6.37 (d, *J* = 3.0 Hz, 1H), 4.83 (d, *J* = 5.6 Hz, 2H), 4.16 (s, 3H), 3.44 (p, *J* = 6.9 Hz, 1H), 0.92 (d, *J* = 6.9 Hz, 6H). ^{13}C NMR (75 MHz, DMSO-d_6) δ 160.0, 159.1, 149.8, 149.6, 149.2, 146.9, 140.4, 136.9, 134.1, 130.4, 128.2, 125.5, 125.2, 122.2, 121.0, 113.8, 101.1, 45.7, 37.0, 28.7, 24.2.

*2,4-Dichloro-5-(cyclopropylmethyl)-5H-pyrrolo[3,2-d]pyrimidine (**69**).*

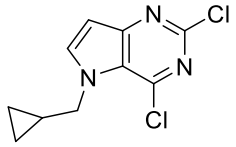

To a stirred solution of 2,4-dichloro-5*H*-pyrrolo[3,2-d]pyrimidine **67** (1.00 g, 5.32mmol) in DMF (10 mL) at room temperature was added sodium hydride (60% dispersion in mineral oil) (0.23 g, 5.85 mmol) in one portion and the reaction allowed to stir for 20 minutes before (bromomethyl)cyclopropane (0.62 mL, 0.86 g, 6.38 mmol) was added *via* syringe and the reaction stirred at room temperature overnight. The reaction was diluted with water and EtOAc, extracted into EtOAc (x3), dried over sodium sulfate, filtered and concentrated *in vacuo*. Purification *via* silica gel chromatography (gradient elution 5 to 100% EtOAc in petroleum ether) yielded 2,4-dichloro-5-(cyclopropylmethyl)-5*H*-pyrrolo[3,2-d]pyrimidine **69** (1.05 g, 4.33 mmol, 82%) as a white solid. MS (ESI+) *m/z* calcd for $C_{10}H_{10}Cl_2N_3$ $[M + H]^+$ 242.0; found 242.1. UPLC (method A) t_R = 2.95 min, 88%.

*2-Chloro-5-(cyclopropylmethyl)-N-(pyridin-2-ylmethyl)-5H-pyrrolo[3,2-d]pyrimidin-4-amine (**72**).*

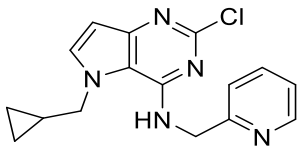

2,4-Dichloro-5-(cyclopropylmethyl)-5*H*-pyrrolo[3,2-d]pyrimidine **69** (0.55 g, 2.27 mmol) and pyridin-2-ylmethanamine (0.26 g, 2.39 mmol) were reacted according to general procedure 1 in chloroform (10 mL) at 90 °C for 48 h. Purification *via* silica gel chromatography (gradient elution 5 to 100% EtOAc in petroleum ether) gave 2-Chloro-5-(cyclopropylmethyl)-N-(pyridin-2-ylmethyl)-5H-pyrrolo[3,2-d]pyrimidin-4-amine **72** (0.58 g, 1.84 mmol, 81%) as a cream coloured solid. MS (ESI+) *m/z* calcd for $C_{16}H_{17}ClN_5$ $[M + H]^+$ 314.1; found 314.2. UPLC (method A) t_R = 2.45 min, 80%.

*5-(Cyclopropylmethyl)-2-(2-isopropylphenyl)-N-(pyridin-2-ylmethyl)-5H-pyrrolo[3,2-d]pyrimidin-4-amine (**41**).*

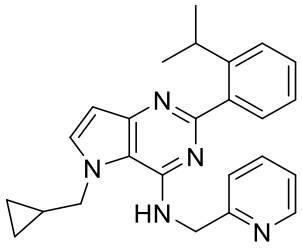

2-Chloro-5-(cyclopropylmethyl)-*N*-(pyridin-2-ylmethyl)-5*H*-pyrrolo[3,2-d]pyrimidin-4-amine **72** (80 mg, 0.26 mmol) and (2-isopropylphenyl)boronic acid (63 mg, 0.38 mmol) were reacted according to general procedure 2 for 40 mins at 125 °C. Upon cooling to room temperature the reaction mixture was loaded onto an SCX-II column, washed with MeOH, then eluted with 0.5 M NH_3 in MeOH and concentrated *in vacuo*. Purification *via* preparatory HPLC (gradient elution 5 to 95% MeCN in H_2O with 0.1% NH_3) yielded 5-(cyclopropylmethyl)-2-(2-isopropylphenyl)-*N*-(pyridin-2-ylmethyl)-5*H*-pyrrolo[3,2-d]pyrimidin-4-amine **41** (80 mg, 0.20 mmol, 79%) as a white solid. MS (ESI+) *m/z* calcd for $C_{25}H_{28}N_5$ $[M + H]^+$ 398.2; found 398.4. UPLC (method C) t_R = 5.58 min, >98%. ^{1}H NMR (300 MHz, Chloroform-d) δ 8.60 (ddd, J = 4.9, 1.8, 1.0 Hz, 1H), 7.70 (td, J = 7.7, 1.8 Hz, 1H), 7.63 (ddd, J = 7.5, 1.5, 0.5 Hz, 1H), 7.43 (dd, J = 7.8, 1.6 Hz, 1H), 7.38 (dd, J = 7.1, 1.5 Hz, 1H), 7.33 (dt, J = 7.9, 1.1 Hz, 1H), 7.30 – 7.27 (m, 1H), 7.26-7.25 (m, 1H), 7.25 – 7.21 (m, 1H), 6.92 (t, J = 4.3 Hz, 1H), 6.59 (d, J = 3.1 Hz, 1H), 4.97 (d, J = 4.2 Hz, 2H), 4.35 (d, J = 6.6 Hz, 2H), 3.60 (hept, J = 6.9 Hz, 1H), 1.48 (ttt, J = 8.0, 6.6, 4.9 Hz, 1H), 1.26 (d, J = 6.9 Hz, 6H), 0.80 – 0.63 (m, 2H), 0.58 – 0.43 (m, 2H).

*2,4-Dichloro-5-((2-(trimethylsilyl)ethoxy)methyl)-5H-pyrrolo[3,2-d]pyrimidine (**70**).*

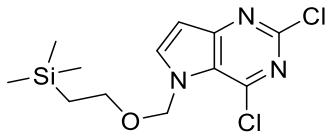

To a stirred solution of 2,4-dichloro-5*H*-pyrrolo[3,2-d]pyrimidine **67** (1.00 g, 5.32mmol) in DMF (12mL) at room temperature was added sodium hydride (60% dispersion in mineral oil) (0.26 g, 6.38mmol) in one portion and the reaction allowed to stir for 15 minutes before 2-(chloromethoxyethyl)trimethyl silane (1.03 mL, 0.98 g, 5.85mmol) was added *via* syringe and the reaction stirred at room temperature overnight. The reaction was diluted with water and EtOAc, extracted into EtOAc (x3), dried over sodium sulfate, filtered and concentrated *in vacuo*. Purification *via* silica gel chromatography (gradient elution 5 to 100% EtOAc in petroleum ether) yielded 2,4-dichloro-5-((2-(trimethylsilyl)ethoxy)methyl)-5*H*-pyrrolo[3,2-d]pyrimidine **70** (0.80 g, 2.51 mmol, 47%) as a white solid. MS (ESI+) *m/z* calcd for $C_{12}H_{18}Cl_2N_3OSi$ $[M + H]^+$ 318.1; found 318.0. UPLC (method B) t_R = 3.57 min, 86%.

*2-Chloro-N-(pyridin-2-ylmethyl)-5-((2-(trimethylsilyl)ethoxy)methyl)-5H-pyrrolo[3,2-d]pyrimidin-4-amine (**73**).*

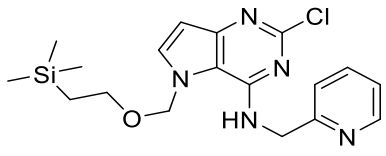

2,4-Dichloro-5-((2-(trimethylsilyl)ethoxy)methyl)-5*H*-pyrrolo[3,2-d]pyrimidine **70** (798 mg, 2.51 mmol) and pyridin-2-ylmethanamine (298 mg, 2.76 mmol) were reacted according to general procedure 1 in chloroform (10 mL) overnight at room temperature followed by 6 h at 50 °C to give 2-chloro-*N*-(pyridin-2-ylmethyl)-5-((2-(trimethylsilyl)ethoxy)methyl)-5*H*-pyrrolo[3,2-d]pyrimidin-4-amine **73** (910 mg, 2.33 mmol, 93%) as a white solid which was used without further purification. MS (ESI+) *m/z* calcd for $C_{18}H_{25}ClN_5OSi$ $[M + H]^+$ 390.2; found 390.1. UPLC (method B) t_R = 3.07 min, 78%.

*2-(2-Isopropylphenyl)-N-(pyridin-2-ylmethyl)-5-((2-(trimethylsilyl)ethoxy)methyl)-5H-pyrrolo[3,2-d]pyrimidin-4-amine (**74**).*

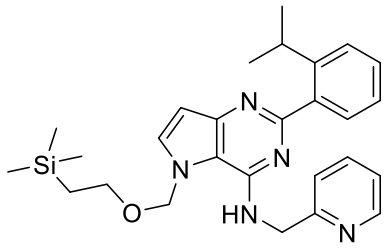

2-Chloro-*N*-(pyridin-2-ylmethyl)-5-((2-(trimethylsilyl)ethoxy)methyl)-5*H*-pyrrolo[3,2-d]pyrimidin-4-amine **73** (500 mg, 1.28 mmol) and (2-propan-2-ylphenyl)boronic acid (315 mg, 1.92 mmol) were reacted according to general procedure 2 for 60 min at 125 °C. Purification *via* silica gel chromatography (gradient elution 5 to 100% EtOAc in petroleum ether) yielded 2-(2-isopropylphenyl)-*N*-(pyridin-2-ylmethyl)-5-((2-(trimethylsilyl)ethoxy)methyl)-5*H*-pyrrolo[3,2-d]pyrimidin-4-amine **74** (563 mg, 1.19 mmol, 93%) as a white solid. MS (ESI+) *m/z* calcd for $C_{27}H_{36}N_5OSi$ $[M + H]^+$ 474.3; found 474.2. UPLC (method B) t_R = 2.97 min, 84%.

*2-(2-Isopropylphenyl)-N-(pyridin-2-ylmethyl)-5H-pyrrolo[3,2-d]pyrimidin-4-amine (**42**).*

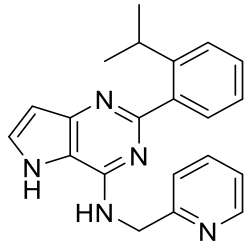

To a stirred solution of 2-(2-isopropylphenyl)-*N*-(pyridin-2-ylmethyl)-5-((2-(trimethylsilyl)ethoxy)methyl)-5*H*-pyrrolo[3,2-d]pyrimidin-4-amine **74** (150 mg, 0.320mmol) in DCM (5mL) was added trifluoroacetic acid (1 mL) and the reaction left to stir overnight at room temperature. The DCM was allowed to evaporate and the reaction allowed to stand for a further 18h. The reaction was concentrated under reduced pressure, dissolved in 7M methanolic ammonia, stirred for 3 h and concentrated under reduced pressure. Purification *via* preparatory HPLC (gradient elution 5 to 95% MeCN in H_2O with 0.1% NH_3) yielded 2-(2-isopropylphenyl)-N-(pyridin-2-ylmethyl)-5H-pyrrolo[3,2-d]pyrimidin-4-amine **42** (26 mg, 0.076 mmol, 24%) as a white solid. MS (ESI+) *m/z* calcd for $C_{21}H_{22}N_5$ $[M + H]^+$ 344.2; found 344.1. UPLC (method C) t_R = 4.53 min, >98%. ^{1}H NMR (300 MHz, Chloroform-d) δ 10.28 (s, 1H), 8.55 (ddd, J = 5.0, 1.8, 0.9 Hz, 1H), 7.71 (td, J = 7.7, 1.8 Hz, 1H), 7.59 – 7.53 (m, 1H), 7.41 – 7.35 (m, 2H), 7.35 – 7.30 (m, 1H), 7.28 – 7.17 (m, 3H), 6.66 (t, J = 5.3 Hz, 1H), 6.55 (d, J = 3.1 Hz, 1H), 4.91 (d, J = 5.4 Hz, 2H), 3.58 – 3.42 (m, 1H), 1.18 (d, J = 6.9 Hz, 6H).

NMR Spectra of compounds from Table 2:

Compound **1**:

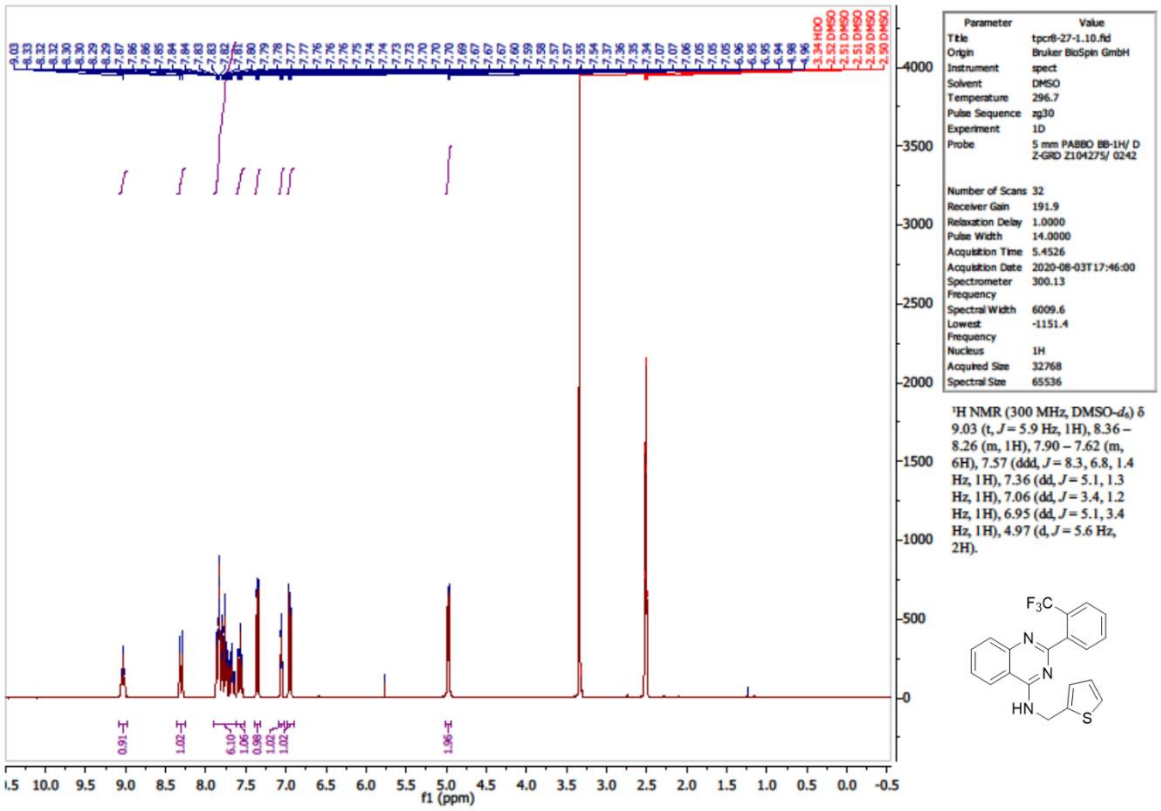

^{1}H NMR (300 MHz, DMSO-d_6) δ 9.03 (t, J = 5.9 Hz, 1H), 8.36 – 8.26 (m, 1H), 7.90 – 7.62 (m, 6H), 7.57 (ddd, J = 8.3, 6.8, 1.4 Hz, 1H), 7.36 (dd, J = 5.1, 1.3 Hz, 1H), 7.06 (dd, J = 3.4, 1.2 Hz, 1H), 6.95 (dd, J = 5.1, 3.4 Hz, 1H), 4.97 (d, J = 5.6 Hz, 2H).

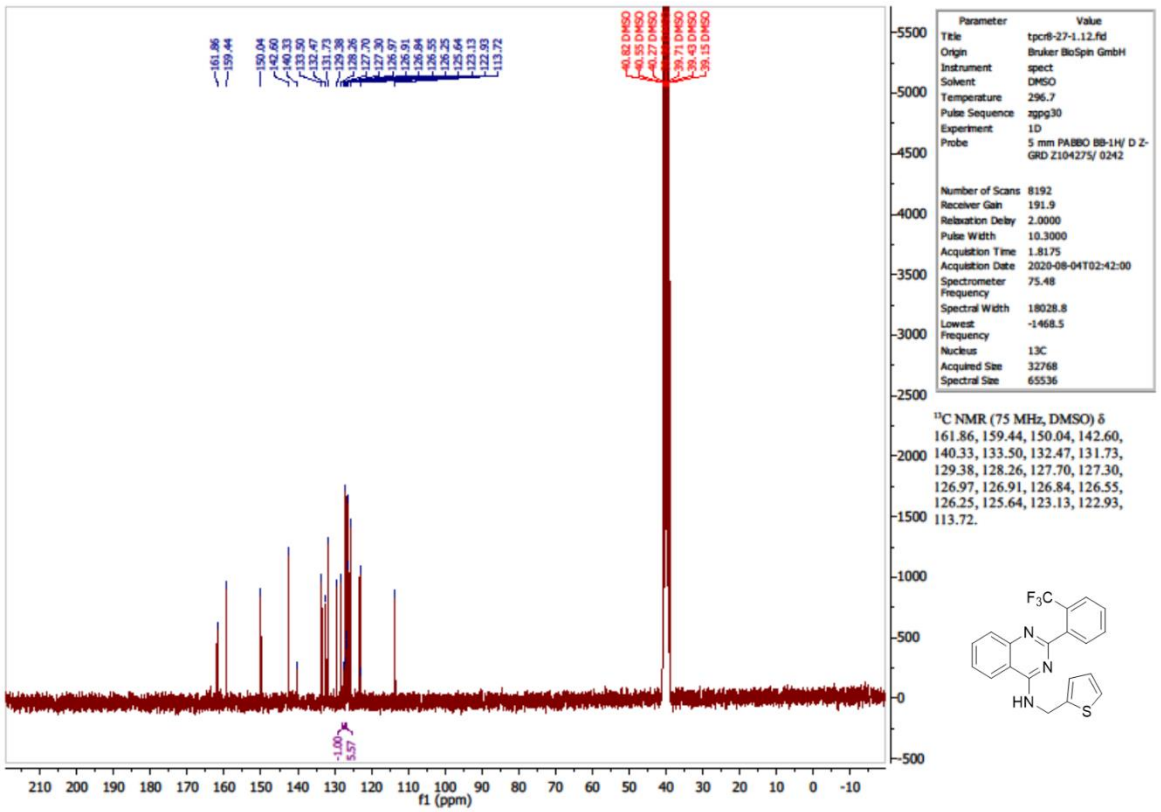

^{13}C NMR (75 MHz, DMSO) δ 161.86, 159.44, 150.04, 142.60, 140.33, 133.50, 132.47, 131.73, 129.38, 128.26, 127.70, 127.30, 126.97, 126.91, 126.84, 126.55, 126.25, 125.64, 123.13, 122.93, 113.72.

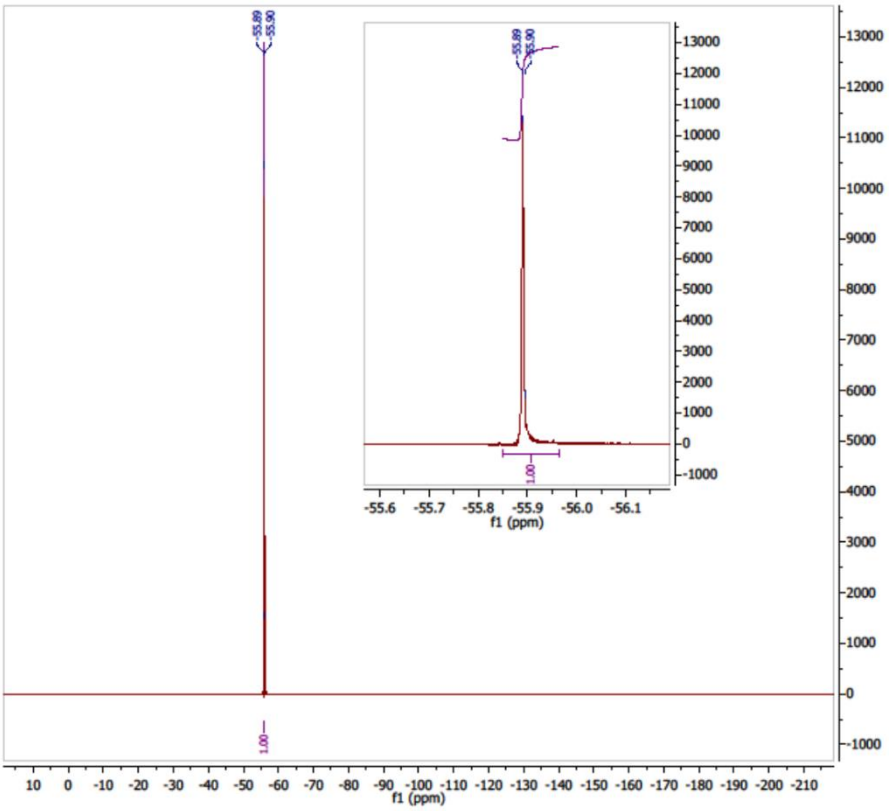

Parameter	Value
Title	tpcr8-27-1.11.fid
Origin	Bruker BioSpin GmbH
Instrument	spect
Solvent	DMSO
Temperature	296.9
Pulse Sequence	zgfhigqn.2
Experiment	1D
Probe	5 mm PABBO BB-1H/ D Z-GRD Z104275/ 0242
Number of Scans	32
Receiver Gain	191.9
Relaxation Delay	1.0000
Pulse Width	15.0000
Acquisition Time	0.9787
Acquisition Date	2020-08-03T17:50:00
Spectrometer Frequency	282.38
Spectral Width	66964.3
Lowest Frequency	-61722.4
Nucleus	19F
Acquired Size	65536
Spectral Size	131072

^{19}F NMR (282 MHz, DMSO-d_6) δ -55.89.

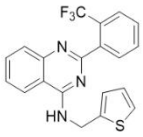

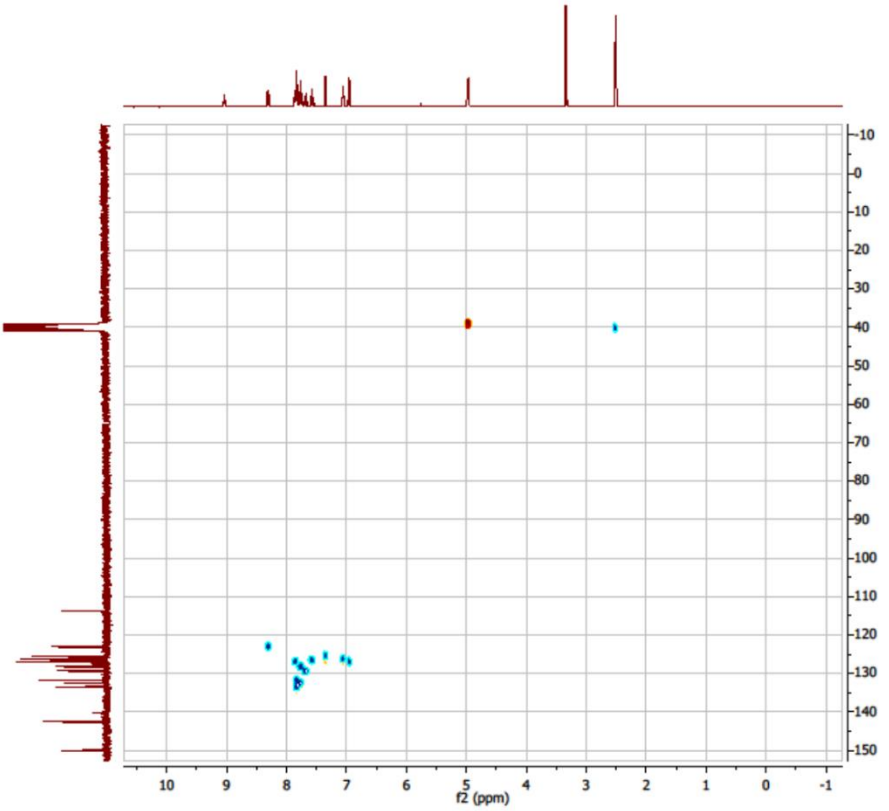

Parameter	Value
Title	tpcr8-27-1_2D.12.ser
Origin	Bruker BioSpin GmbH
Instrument	spect
Solvent	DMSO
Temperature	296.6
Pulse Sequence	hsqcedetgpsp.3
Experiment	HSQC-EDITED
Probe	5 mm PABBO BB-1H/ D Z-GRD Z104275/ 0242
Number of Scans	32
Receiver Gain	191.9
Relaxation Delay	1.0000
Pulse Width	14.0000
Acquisition Time	0.1420
Acquisition Date	2021-09-13T21:17:00
Spectrometer Frequency	(300.13, 75.47)
Spectral Width	(3605.8, 12500.0)
Lowest Frequency	(-388.5, -968.1)
Nucleus	(1H, 13C)
Acquired Size	(512, 256)
Spectral Size	(512, 512)

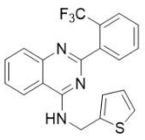

Compound **14**:

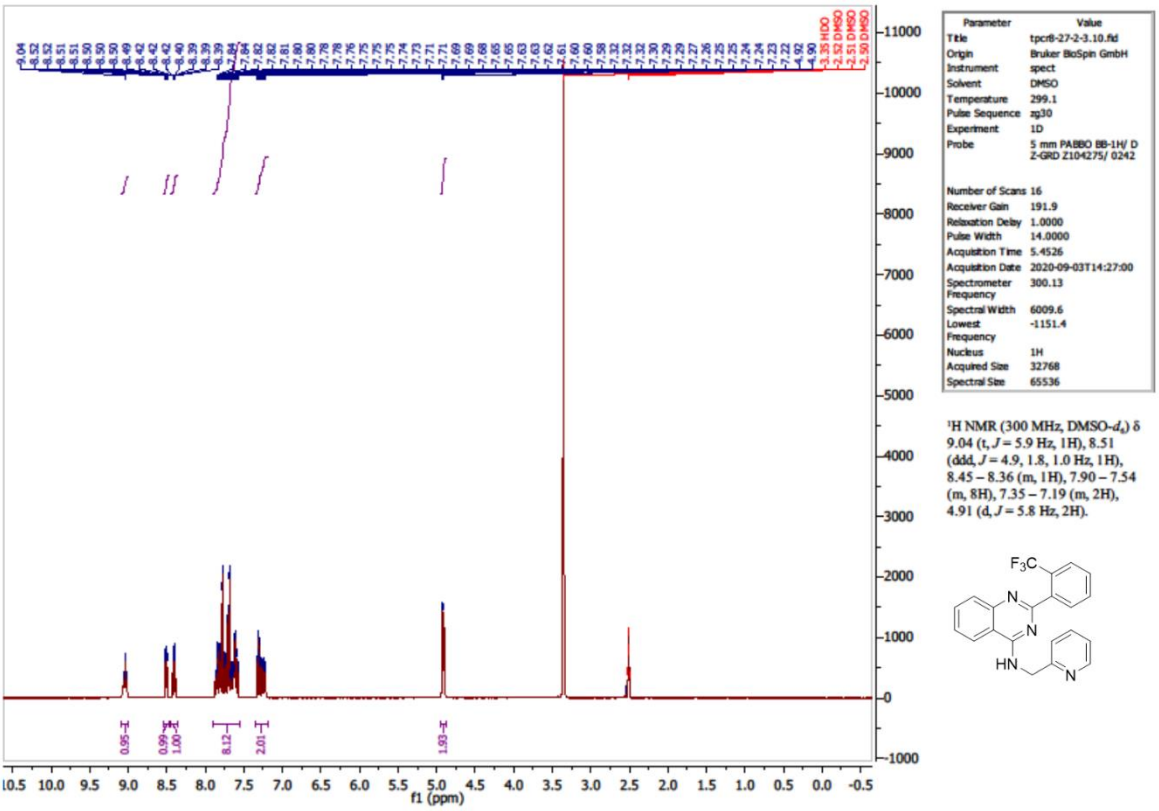

Parameter	Value
Title	tpcr8-27-2-3.10.fid
Origin	Bruker BioSpin GmbH
Instrument	spect
Solvent	DMSO
Temperature	299.1
Pulse Sequence	zg30
Experiment	1D
Probe	5 mm PABBO BB-1H/ D Z-GRD Z104275/ 0242
Number of Scans	16
Receiver Gain	191.9
Relaxation Delay	1.0000
Pulse Width	14.0000
Acquisition Time	5.4526
Acquisition Date	2020-09-03T14:27:00
Spectrometer Frequency	300.13
Spectral Width	6009.6
Lowest Frequency	-1151.4
Nucleus	1H
Acquired Size	32768
Spectral Size	65536

^{1}H NMR (300 MHz, DMSO-d_6) δ 9.04 (t, J = 5.9 Hz, 1H), 8.51 (ddd, J = 4.9, 1.8, 1.0 Hz, 1H), 8.45 – 8.36 (m, 1H), 7.90 – 7.54 (m, 8H), 7.35 – 7.19 (m, 2H), 4.91 (d, J = 5.8 Hz, 2H).

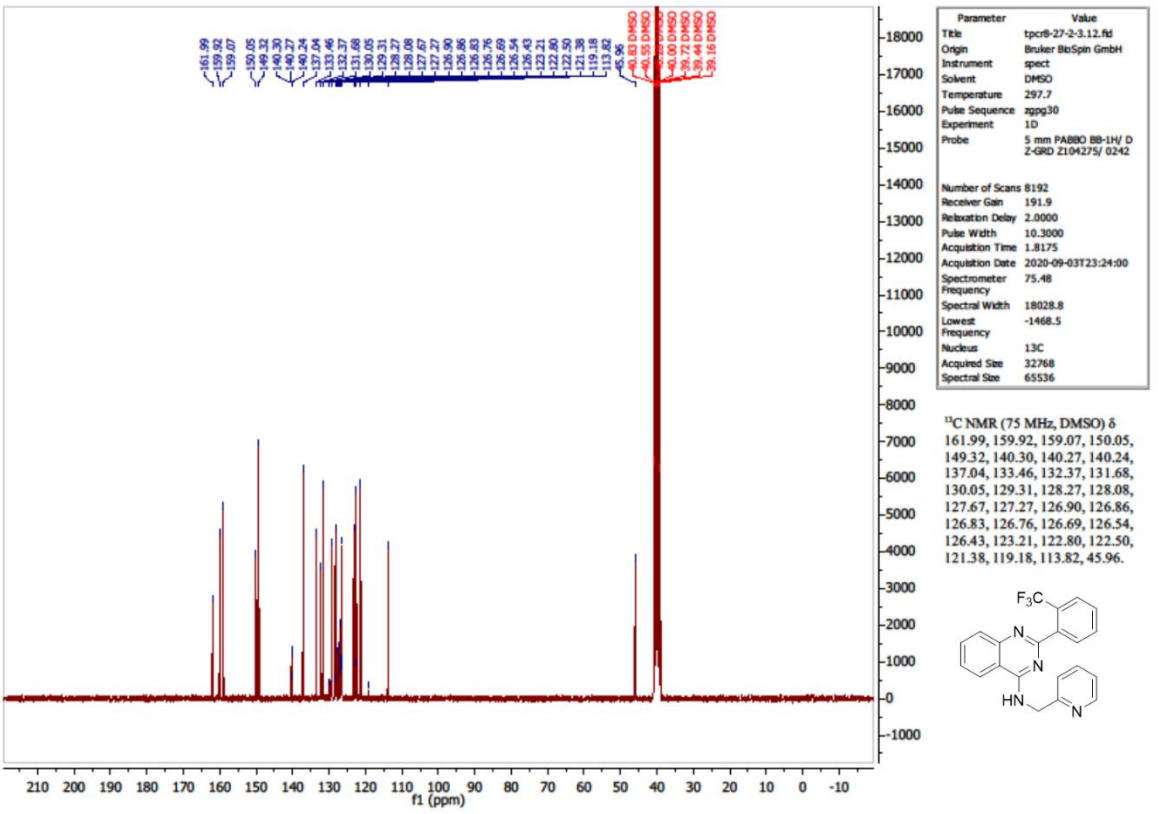

Parameter	Value
Title	tpcr8-27-2-3.12.fid
Origin	Bruker BioSpin GmbH
Instrument	spect
Solvent	DMSO
Temperature	297.7
Pulse Sequence	zgpg30
Experiment	1D
Probe	5 mm PABBO BB-1H/ D Z-GRD Z104275/ 0242
Number of Scans	8192
Receiver Gain	191.9
Relaxation Delay	2.0000
Pulse Width	10.3000
Acquisition Time	1.8175
Acquisition Date	2020-09-03T23:24:00
Spectrometer Frequency	75.48
Spectral Width	18028.8
Lowest Frequency	-1468.5
Nucleus	13C
Acquired Size	32768
Spectral Size	65536

^{13}C NMR (75 MHz, DMSO) δ 161.99, 159.92, 159.07, 150.05, 149.32, 140.30, 140.27, 140.24, 137.04, 133.46, 132.37, 131.68, 130.05, 129.31, 128.27, 128.08, 127.67, 127.27, 126.90, 126.86, 126.83, 126.76, 126.69, 126.54, 126.43, 123.21, 122.80, 122.50, 121.38, 119.18, 113.82, 45.96.

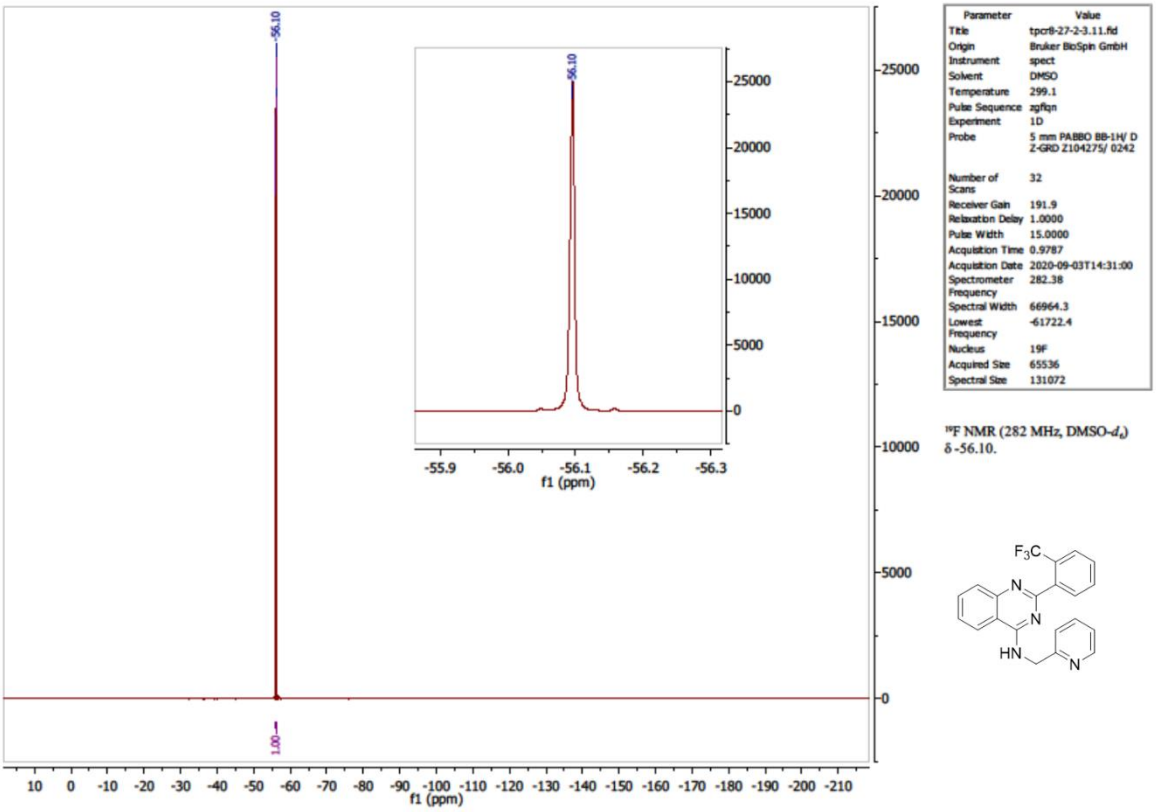

Parameter	Value
Title	tpcr8-27-2-3.11.fid
Origin	Bruker BioSpin GmbH
Instrument	spect
Solvent	DMSO
Temperature	299.1
Pulse Sequence	zgflqn
Experiment	1D
Probe	5 mm PABBO BB-1H/ D Z-GRD Z104275/ 0242
Number of Scans	32
Receiver Gain	191.9
Relaxation Delay	1.0000
Pulse Width	15.0000
Acquisition Time	0.9787
Acquisition Date	2020-09-03T14:31:00
Spectrometer Frequency	282.38
Spectral Width	66964.3
Lowest Frequency	-61722.4
Nucleus	19F
Acquired Size	65536
Spectral Size	131072

^{19}F NMR (282 MHz, DMSO-d_6) δ -56.10.

Compound **22**:

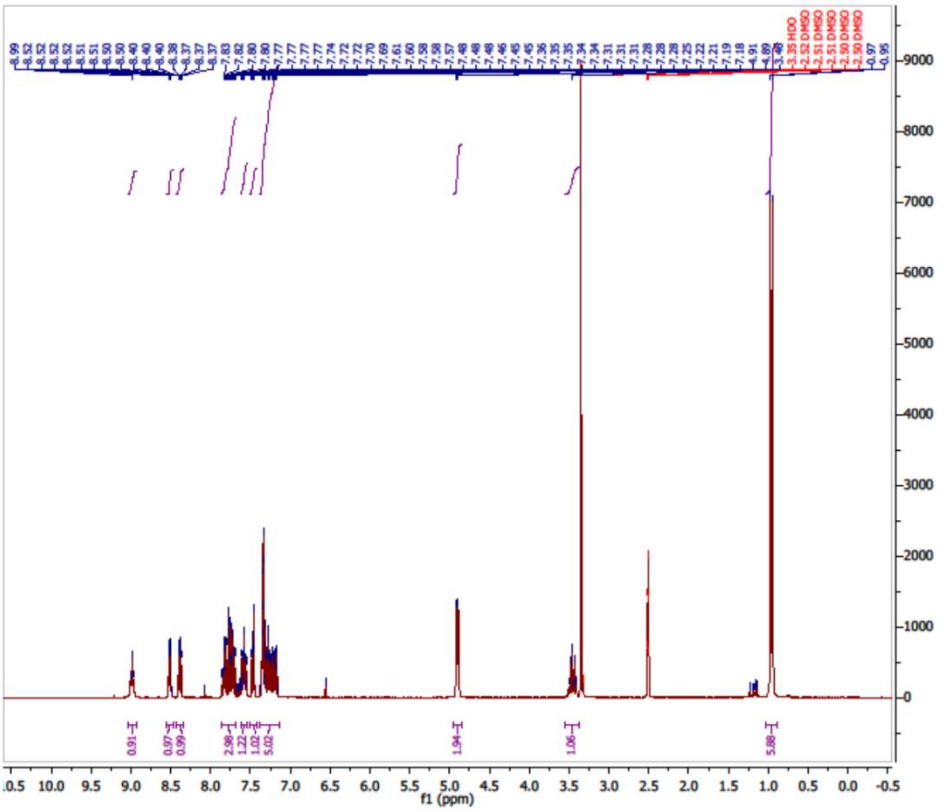

Parameter	Value
Title	tpcr8-27-3.30.fid
Origin	Bruker BioSpin GmbH
Instrument	spect
Solvent	DMSO
Temperature	295.8
Pulse Sequence	zg30
Experiment	1D
Probe	5 mm PABBO BB-1H/ D Z-GRD Z104275/ 0242
Number of Scans	32
Receiver Gain	191.9
Relaxation Delay	1.0000
Pulse Width	14.0000
Acquisition Time	5.4526
Acquisition Date	2020-08-04T07:25:00
Spectrometer Frequency	300.13
Spectral Width	6009.6
Lowest Frequency	-1151.4
Nucleus	1H
Acquired Size	32768
Spectral Size	65536

^{1}H NMR (300 MHz, DMSO-d_6) δ 8.99 (t, J = 6.0 Hz, 1H), 8.51 (ddd, J = 4.9, 1.9, 1.0 Hz, 1H), 8.43 – 8.34 (m, 1H), 7.86 – 7.68 (m, 3H), 7.61 – 7.54 (m, 1H), 7.47 (dt, J = 7.6, 1.1 Hz, 1H), 7.39 – 7.14 (m, 5H), 4.90 (d, J = 5.8 Hz, 2H), 3.46 (p, J = 6.9 Hz, 1H), 0.96 (d, J = 6.9 Hz, 6H).

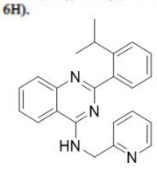

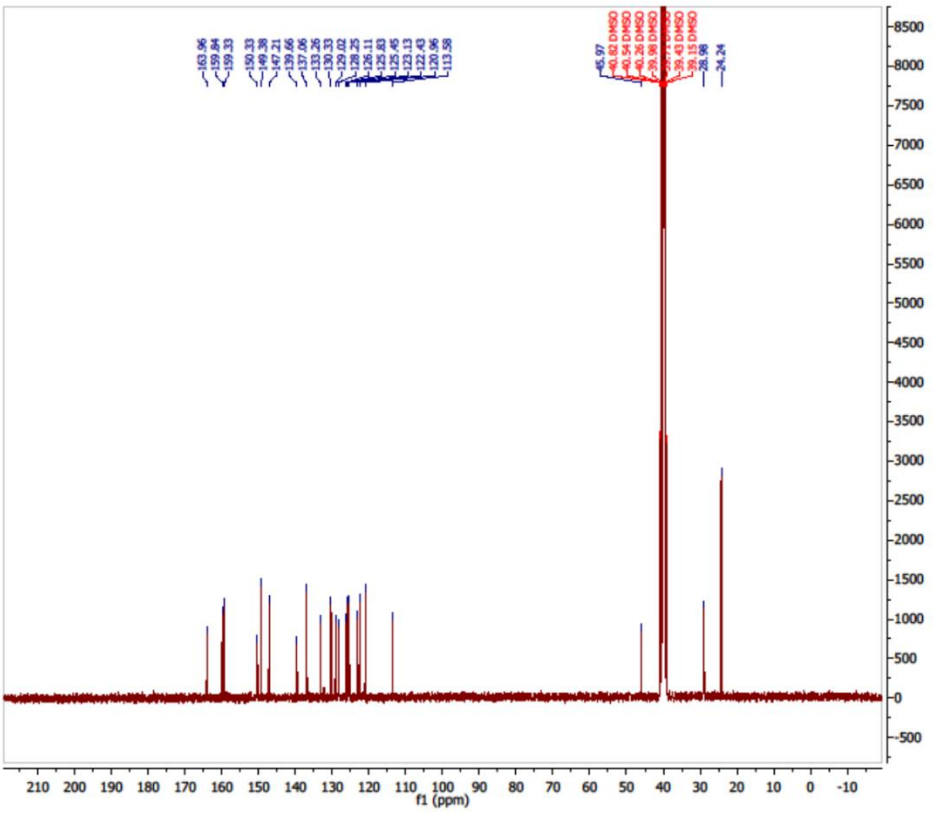

Parameter	Value
Title	tpcr8-27-3.33.fid
Origin	Bruker BioSpin GmbH
Instrument	spect
Solvent	DMSO
Temperature	297.1
Pulse Sequence	zgpg30
Experiment	1D
Probe	5 mm PABBO BB-1H/ D Z-GRD Z104275/ 0242
Number of Scans	4096
Receiver Gain	191.9
Relaxation Delay	2.0000
Pulse Width	10.3000
Acquisition Time	1.8175
Acquisition Date	2020-08-04T11:56:00
Spectrometer Frequency	75.48
Spectral Width	18028.8
Lowest Frequency	-1468.5
Nucleus	13C
Acquired Size	32768
Spectral Size	65536

^{13}C NMR (75 MHz, DMSO) δ 163.96, 159.84, 159.33, 150.33, 149.38, 147.21, 139.66, 137.06, 133.26, 130.33, 129.02, 128.25, 126.11, 125.83, 125.45, 123.13, 122.43, 120.96, 113.58, 45.97, 28.98, 24.24.

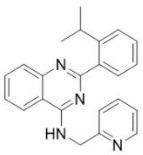

Compound **35**:

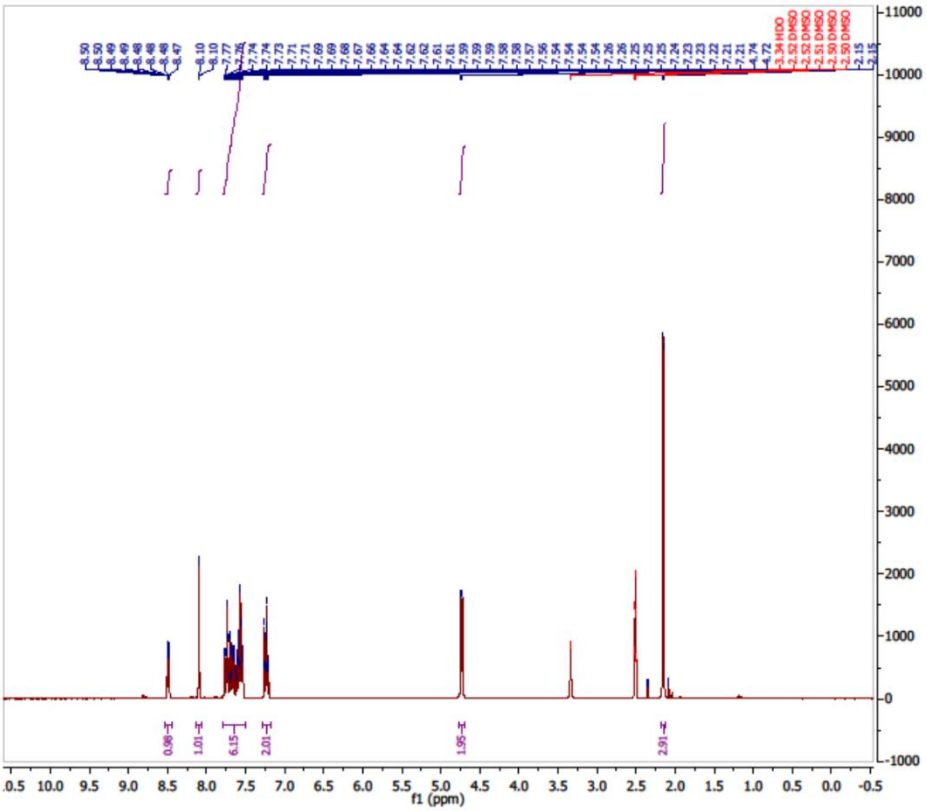

Parameter	Value
Title	tpcr8-027-6.50.fid
Origin	Bruker BioSpin GmbH
Instrument	spect
Solvent	DMSO
Temperature	297.7
Pulse Sequence	zg30
Experiment	1D
Probe	5 mm PABBO BB-1H/ D Z-GRD Z104275/ 0242
Number of Scans	32
Receiver Gain	191.9
Relaxation Delay	1.0000
Pulse Width	14.0000
Acquisition Time	5.4526
Acquisition Date	2020-08-05T22:05:00
Spectrometer Frequency	300.13
Spectral Width	6009.6
Lowest Frequency	-1151.4
Nucleus	1H
Acquired Size	32768
Spectral Size	65536

^{1}H NMR (300 MHz, DMSO-d_6) δ 8.49 (ddd, J = 4.8, 1.9, 1.0 Hz, 1H), 8.10 (d, J = 1.0 Hz, 1H), 7.80 – 7.51 (m, 6H), 7.29 – 7.18 (m, 2H), 4.73 (d, J = 5.8 Hz, 2H), 2.15 (d, J = 0.9 Hz, 3H).

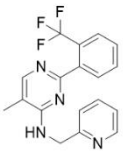

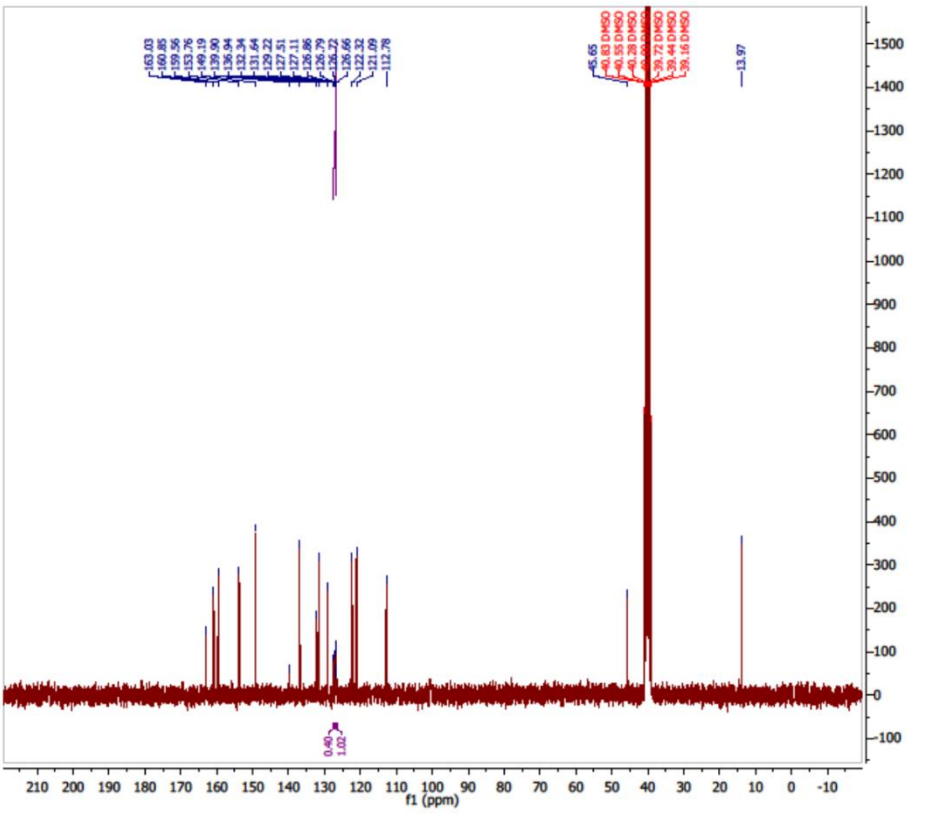

Parameter	Value
Title	tpcr8-027-6.53.fid
Origin	Bruker BioSpin GmbH
Instrument	spect
Solvent	DMSO
Temperature	298.3
Pulse Sequence	zgpg30
Experiment	1D
Probe	5 mm PABBO BB-1H/ D Z-GRD Z104275/ 0242
Number of Scans	4096
Receiver Gain	36.3
Relaxation Delay	2.0000
Pulse Width	10.3000
Acquisition Time	1.8175
Acquisition Date	2020-08-06T02:37:00
Spectrometer Frequency	75.48
Spectral Width	18028.8
Lowest Frequency	-1468.5
Nucleus	13C
Acquired Size	32768
Spectral Size	65536

^{13}C NMR (75 MHz, DMSO) δ 163.03, 160.85, 159.56, 153.76, 149.19, 139.90, 136.94, 132.34, 131.64, 129.22, 127.51, 127.11, 126.86, 126.79, 126.72, 126.66, 122.32, 121.09, 112.78, 45.65, 13.97.

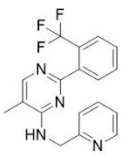

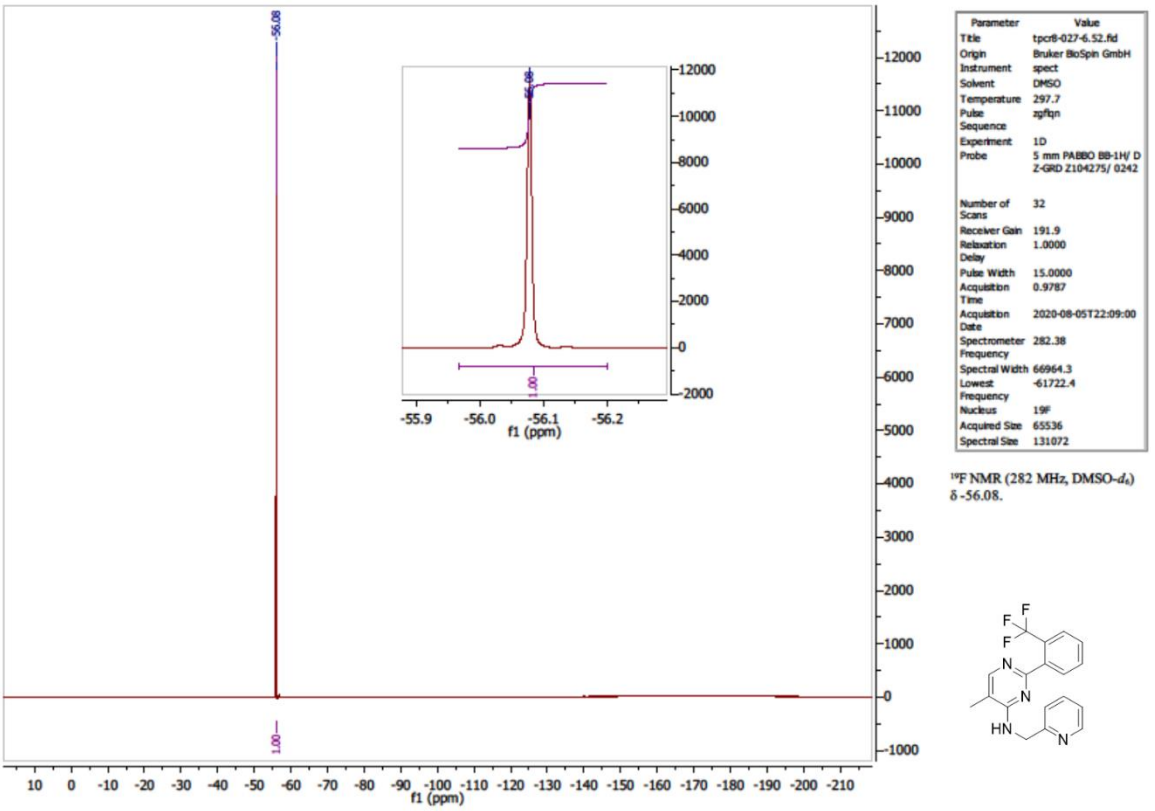

Parameter	Value
Title	tpcr8-027-6.52.fid
Origin	Bruker BioSpin GmbH
Instrument	spect
Solvent	DMSO
Temperature	297.7
Pulse Sequence	zgflqn
Experiment	1D
Probe	5 mm PABBO BB-1H/ D Z-GRD Z104275/ 0242
Number of Scans	32
Receiver Gain	191.9
Relaxation Delay	1.0000
Pulse Width	15.0000
Acquisition Time	0.9787
Acquisition Date	2020-08-05T22:09:00
Spectrometer Frequency	282.38
Spectral Width	66964.3
Lowest Frequency	-61722.4
Nucleus	19F
Acquired Size	65536
Spectral Size	131072

^{19}F NMR (282 MHz, DMSO-d_6) δ -56.08.

Compound **38**:

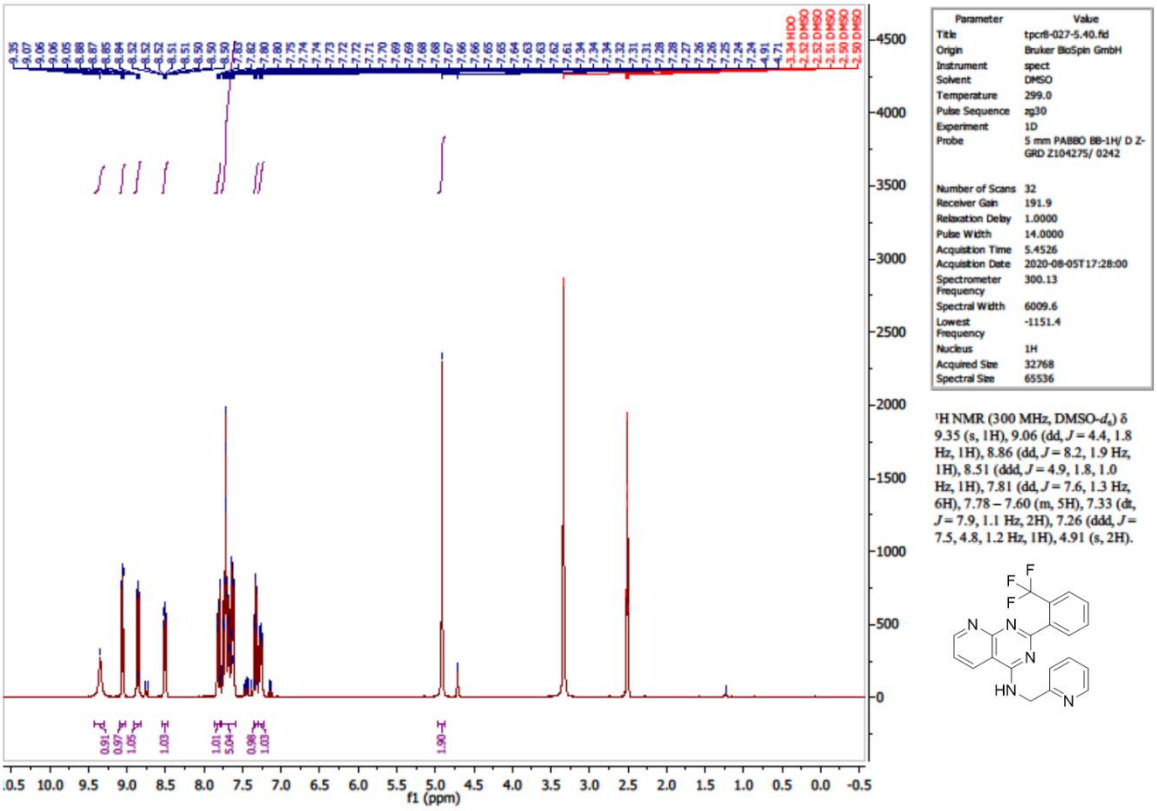

Parameter	Value
Title	tpcr8-027-5.40.fid
Origin	Bruker BioSpin GmbH
Instrument	spect
Solvent	DMSO
Temperature	299.0
Pulse Sequence	zg30
Experiment	1D
Probe	5 mm PABBO BB-1H/ D Z-GRD Z104275/ 0242
Number of Scans	32
Receiver Gain	191.9
Relaxation Delay	1.0000
Pulse Width	14.0000
Acquisition Time	5.4526
Acquisition Date	2020-08-05T17:28:00
Spectrometer Frequency	300.13
Spectral Width	6009.6
Lowest Frequency	-1151.4
Nucleus	1H
Acquired Size	32768
Spectral Size	65536

^{1}H NMR (300 MHz, DMSO-d_6) δ 9.35 (s, 1H), 9.06 (dd, J = 4.4, 1.8 Hz, 1H), 8.86 (dd, J = 8.2, 1.9 Hz, 1H), 8.51 (ddd, J = 4.9, 1.8, 1.0 Hz, 1H), 7.81 (dd, J = 7.6, 1.3 Hz, 6H), 7.78 – 7.60 (m, 5H), 7.33 (dt, J = 7.9, 1.1 Hz, 2H), 7.26 (ddd, J = 7.5, 4.8, 1.2 Hz, 1H), 4.91 (s, 2H).

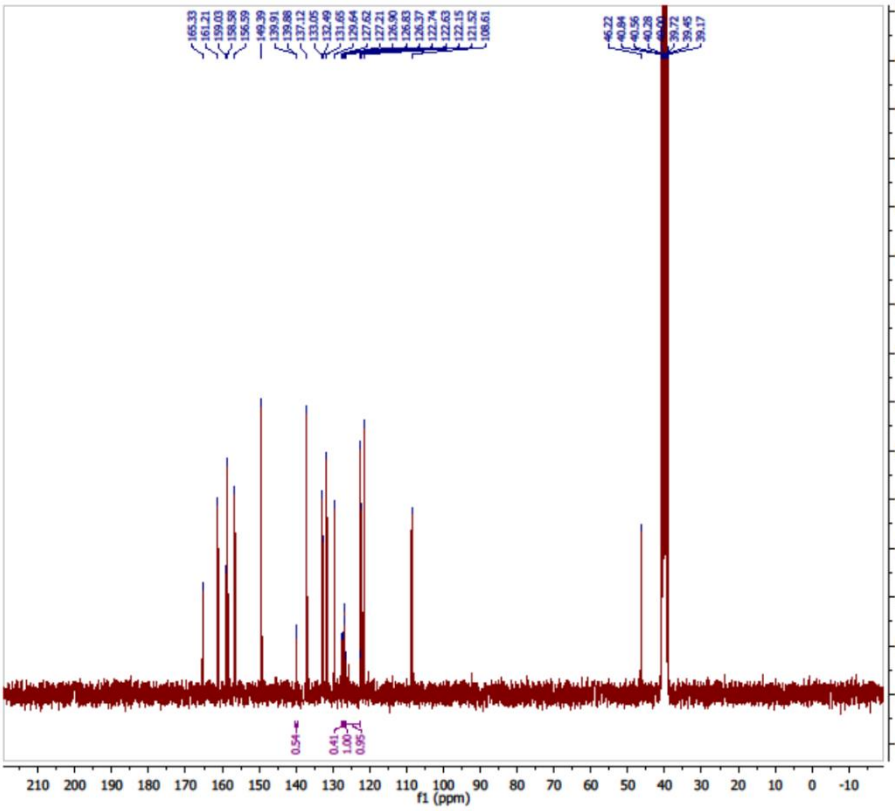

Parameter	Value
Title	tpcr8-027-5.43.fid
Origin	Bruker BioSpin GmbH
Instrument	spect
Solvent	DMSO
Temperature	298.3
Pulse Sequence	zgpg30
Experiment	1D
Probe	5 mm PABBO BB-1H/ D Z-GRD Z104275/ 0242
Number of Scans	4096
Receiver Gain	36.3
Relaxation Delay	2.0000
Pulse Width	10.3000
Acquisition Time	1.8175
Acquisition Date	2020-08-05T21:59:00
Spectrometer Frequency	75.48
Spectral Width	18028.8
Lowest Frequency	-1468.5
Nucleus	13C
Acquired Size	32768
Spectral Size	65536

^{13}C NMR (75 MHz, DMSO) δ 165.33, 161.21, 159.03, 158.58, 156.59, 149.39, 139.91, 139.88, 137.12, 133.05, 132.49, 131.65, 129.64, 127.62, 127.21, 126.90, 126.83, 126.37, 122.74, 122.63, 122.15, 121.52, 108.61, 46.22, 40.84, 40.56, 40.28, 40.00, 39.72, 39.45, 39.17.

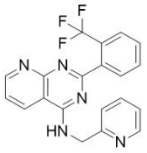

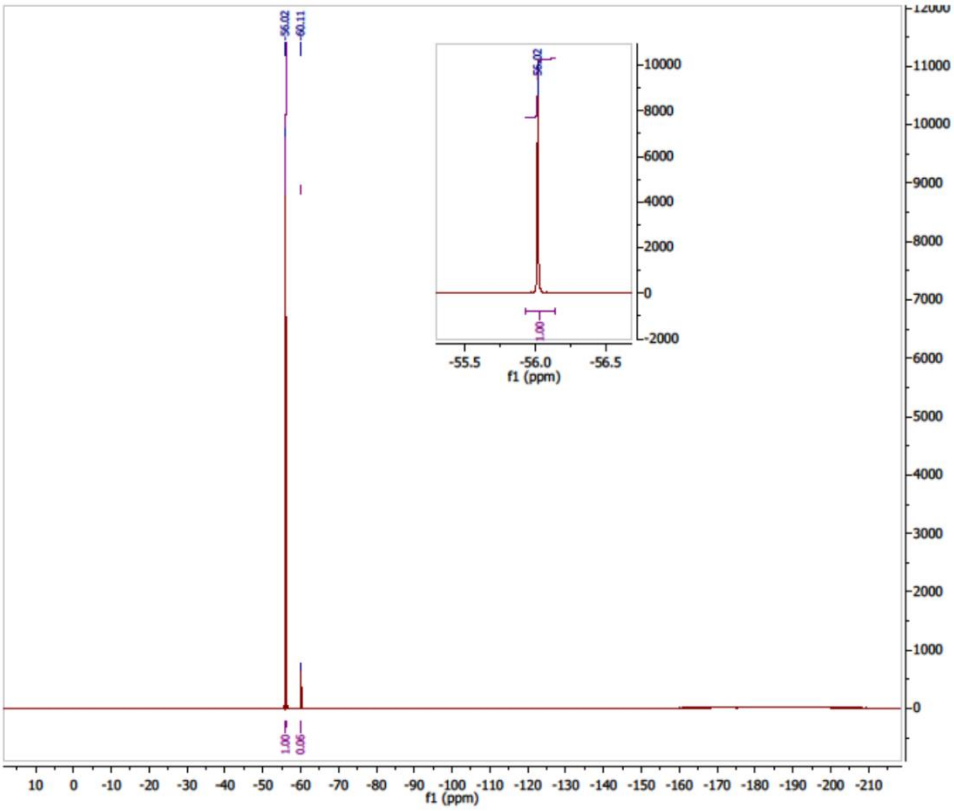

Parameter	Value
Title	tpcr8-027-5.42.fid
Origin	Bruker BioSpin GmbH
Instrument	spect
Solvent	DMSO
Temperature	298.9
Pulse Sequence	zgflqn
Experiment	1D
Probe	5 mm PABBO BB-1H/ D Z-GRD Z104275/ 0242
Number of Scans	32
Receiver Gain	191.9
Relaxation Delay	1.0000
Pulse Width	15.0000
Acquisition Time	0.9787
Acquisition Date	2020-08-05T17:32:00
Spectrometer Frequency	282.38
Spectral Width	66964.3
Lowest Frequency	-61722.4
Nucleus	19F
Acquired Size	65536
Spectral Size	131072

^{19}F NMR (282 MHz, DMSO-d_6) δ -56.02, -60.11.

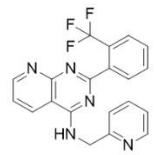

Compound **40**:

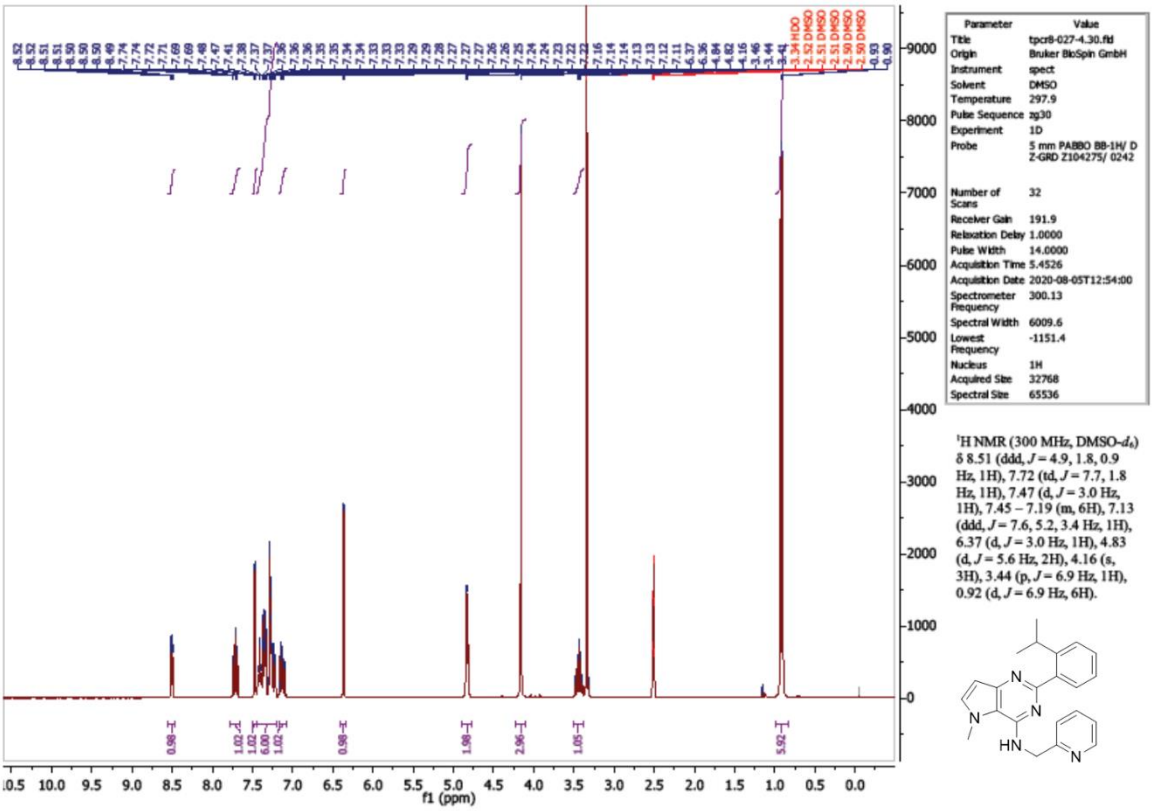

^{1}H NMR (300 MHz, DMSO-d_6) δ 8.51 (ddd, J = 4.9, 1.8, 0.9 Hz, 1H), 7.72 (td, J = 7.7, 1.8 Hz, 1H), 7.47 (d, J = 3.0 Hz, 1H), 7.45 – 7.19 (m, 6H), 7.13 (ddd, J = 7.6, 5.2, 3.4 Hz, 1H), 6.37 (d, J = 3.0 Hz, 1H), 4.83 (d, J = 5.6 Hz, 2H), 4.16 (s, 3H), 3.44 (p, J = 6.9 Hz, 1H), 0.92 (d, J = 6.9 Hz, 6H).

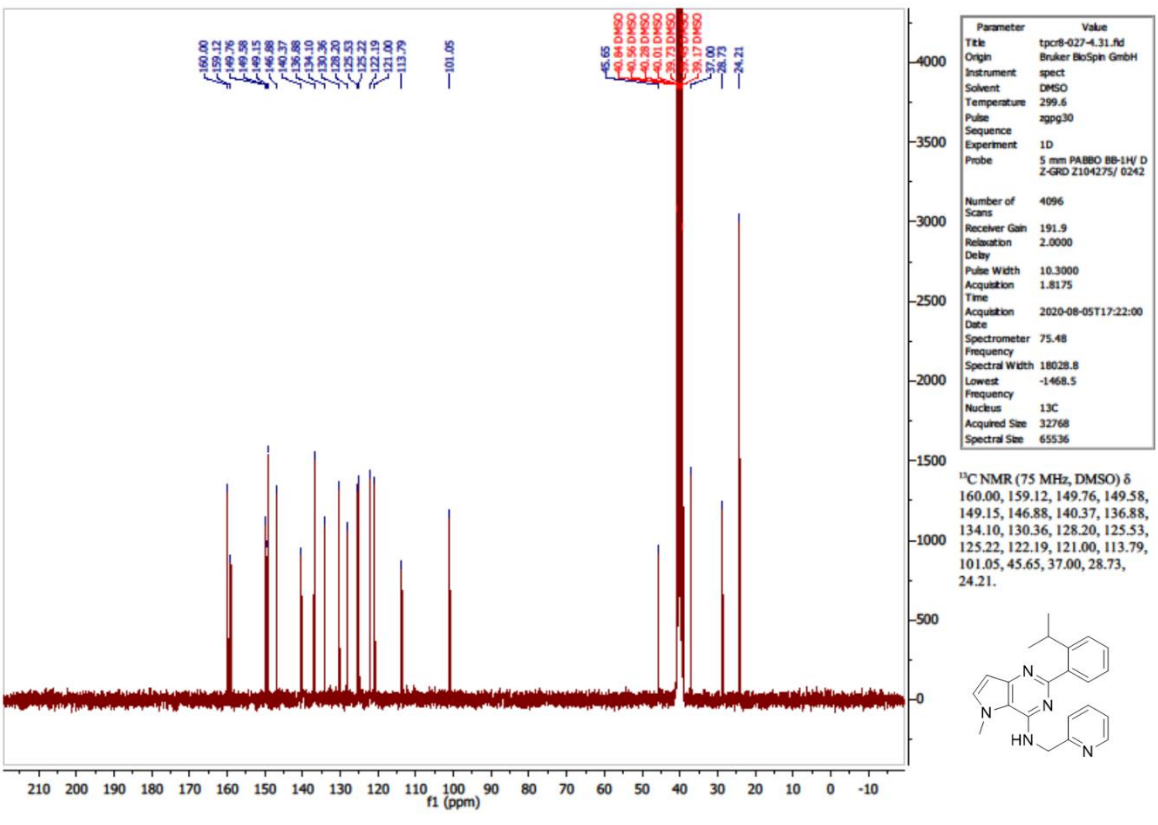

^{13}C NMR (75 MHz, DMSO) δ 160.00, 159.12, 149.76, 149.58, 149.15, 146.88, 140.37, 136.88, 134.10, 130.36, 128.20, 125.53, 125.22, 122.19, 121.00, 113.79, 101.05, 45.65, 37.00, 28.73, 24.21.

HPLC traces of compounds from Table 2:

Compound **1**:

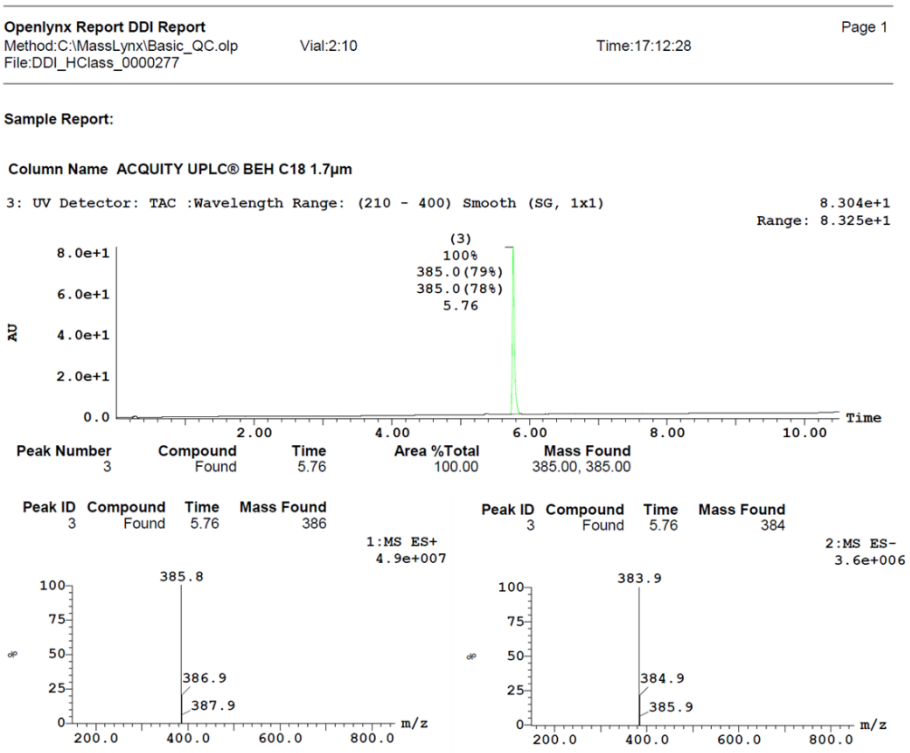

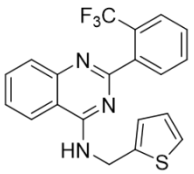

Exact Mass: 385.1

Compound **14**:

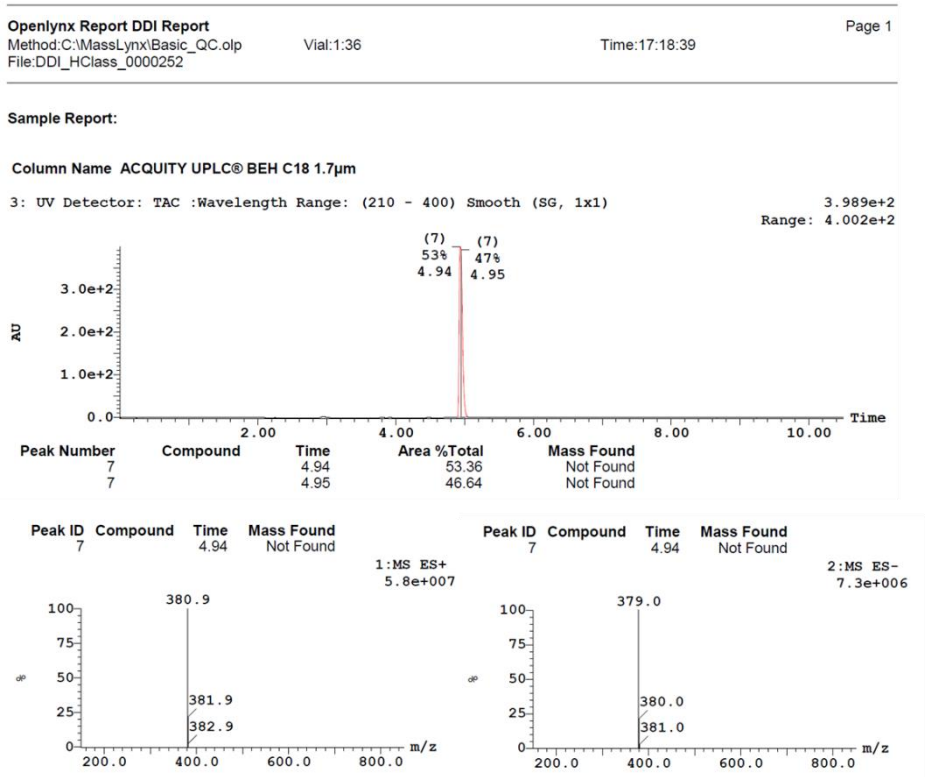

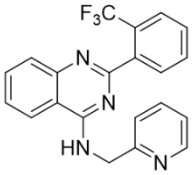

Exact Mass: 380.1

Compound **22**:

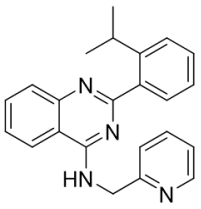

Exact Mass: 354.2

Openlynx Report DDI Report Page 1
Method:C:\MassLynx\b_basic_QC01.olp Vial:1:1 Time:17:47:14
File:DDI_HClass_0000789

Sample Report:

Column Name ACQUITY UPLC® BEH C18 1.7µm

3: UV Detector: TAC :Wavelength Range: (210 - 400) Smooth (SG, 1x1) 3.321e+2
Range: 3.333e+2

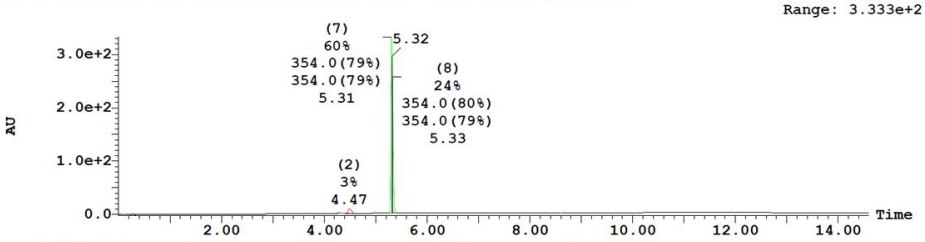

Peak Number	Compound	Time	Area %Total	Mass Found
2		4.47	3.47	Not Found
7	Found	5.31	59.63	354.00, 354.00
7	Found	5.32	13.30	354.00, 354.00
8	Found	5.33	23.61	354.00, 354.00

Peak ID	Compound	Time	Mass Found
7	Found	5.32	355

1:MS ES+
1.4e+007

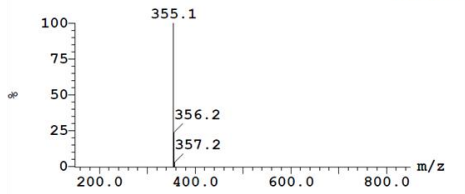

Peak ID	Compound	Time	Mass Found
8	Found	5.33	353

2:MS ES-
1.4e+006

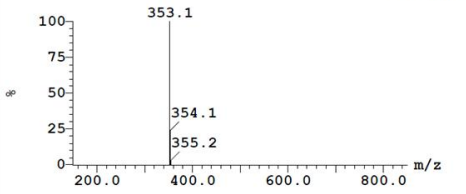

Compound **35**:

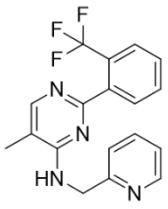

Exact Mass: 344.1

Openlynx Report DDI Report Page 1
Method:C:\MassLynx\b_basic_QC01.olp Vial:2:30 Time:09:31:26
File:DDI_HClass_0001661

Sample Report:

Column Name ACQUITY UPLC® BEH C18 1.7µm

3: UV Detector: TAC :Wavelength Range: (210 - 400) Smooth (SG, 1x1) 2.08e+2
Range: 2.115e+2

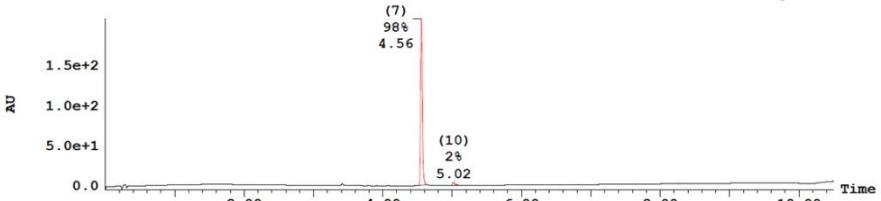

Peak Number	Compound	Time	Area %Total	Mass Found
7		4.56	97.51	Not Found
10		5.02	2.49	Not Found

Peak ID	Compound	Time	Mass Found
7		4.57	Not Found

1:MS ES+
2.3e+007

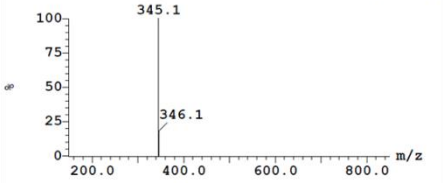

Peak ID	Compound	Time	Mass Found
7		4.57	Not Found

2:MS ES-
5.2e+005

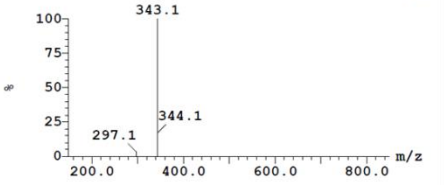

Compound **38**:

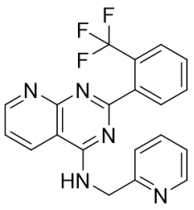

Exact Mass: 381.1

Openlynx Report DDI Report Page 1
Method:C:\MassLynx\b_acidic_QC03.olp Vial:1:9 Time:15:48:20
File:DDI_HClass_0024080

Sample Report:

Column Name ACQUITY UPLC® HSS C18 1.8µm

3: UV Detector: TAC :Wavelength Range: (230 - 400) Smooth (SG, 1x1) 1.088e+1
Range: 1.192e+1

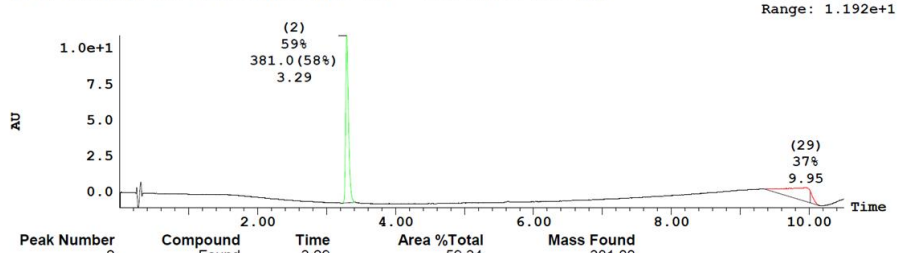

Peak Number	Compound	Time	Area %Total	Mass Found
2	Found	3.29	59.34	381.00
29		9.95	36.58	Not Found
30		10.02	4.08	Not Found

Peak ID	Compound	Time	Mass Found
3	Found	3.30	382

1:MS ES+
4.9e+006

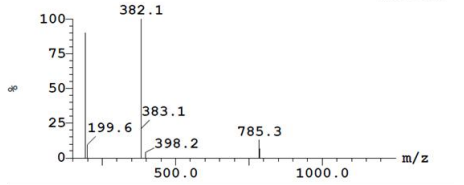

Peak ID	Compound	Time	Mass Found
2	Found	3.29	380

2:MS ES-
3.8e+004

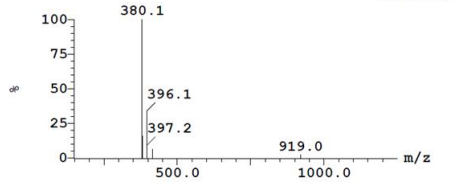

Compound **40**:

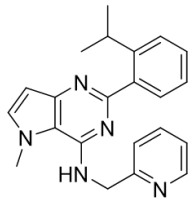

Exact Mass: 357.2

Openlynx Report DDI Report Page 1
Method:C:\MassLynx\b_basic_QC01.olp Vial:1:33 Time:09:08:46
File:DDI_HClass_0002138

Sample Report:

Column Name ACQUITY UPLC® BEH C18 1.7µm

3: UV Detector: TAC :Wavelength Range: (210 - 400) Smooth (SG, 1x1) 6.465e+1
Range: 6.526e+1

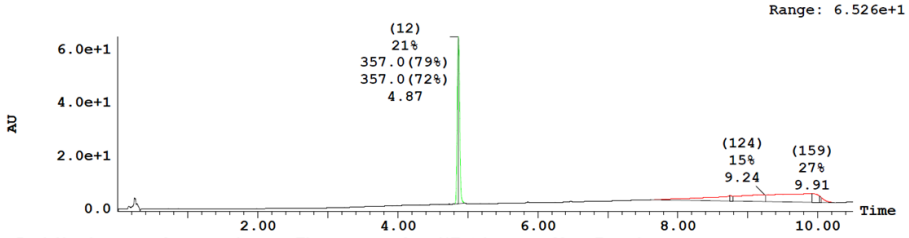

Peak Number	Compound	Time	Area %Total	Mass Found
12	Found	4.86	16.89	357.00, 357.00
12	Found	4.87	20.96	357.00, 357.00
99		8.74	12.69	Not Found
100		8.75	1.30	Not Found
124		9.24	14.52	Not Found
159		9.91	26.87	Not Found

Peak ID	Compound	Time	Mass Found
12	Found	4.86	358

1:MS ES+
8.6e+006

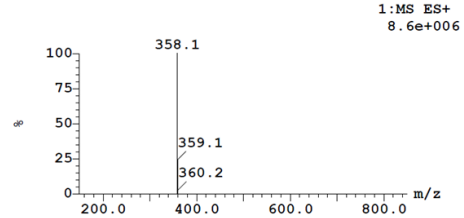

Peak ID	Compound	Time	Mass Found
12	Found	4.86	356

2:MS ES-
8.2e+004

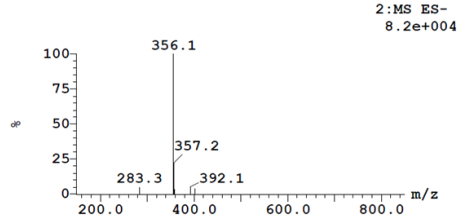

References

1) Clarke, J. H.; Giudici, M.-L.; Burke, J. E.; Williams, R. L.; Maloney, D. J.; Marugan, J.; Irvine, R. F. The Function of Phosphatidylinositol 5-Phosphate 4-Kinase γ (PI5P4Kγ) Explored Using a Specific Inhibitor That Targets the PI5P-Binding Site. Biochem. J. 2015, 466 (2), 359–367. https://doi.org/10.1042/BJ20141333.

2) Al-Ramahi, I.; Giridharan, S. S. P.; Chen, Y. C.; Patnaik, S.; Safren, N.; Hasegawa, J.; de Haro, M.; Gee, A. K. W.; Titus, S. A.; Jeong, H.; Clarke, J.; Krainc, D.; Zheng, W.; Irvine, R. F.; Barmada, S.; Ferrer, M.; Southall, N.; Weisman, L. S.; Botas, J.; Marugan, J. J. Inhibition of PIP4Kγ Ameliorates the Pathological Effects of Mutant Huntingtin Protein. Elife 2017, 6. https://doi.org/10.7554/eLife.29123.

3) Manz, T. D.; Sivakumaren, S. C.; Ferguson, F. M.; Zhang, T.; Yasgar, A.; Seo, H. S.; Ficarro, S. B.; Card, J. D.; Shim, H.; Miduturu, C. V.; Simeonov, A.; Shen, M.; Marto, J. A.; Dhe-Paganon, S.; Hall, M. D.; Cantley, L. C.; Gray, N. S. Discovery and Structure-Activity Relationship Study of (z)-5-Methylenethiazolidin-4-One Derivatives as Potent and Selective Pan-Phosphatidylinositol 5-Phosphate 4-Kinase Inhibitors. J. Med. Chem. 2020, 63 (9), 4880–4895. https://doi.org/10.1021/acs.jmedchem.0c00227.

4) Manz, T. D.; Sivakumaren, S. C.; Yasgar, A.; Hall, M. D.; Davis, M. I.; Seo, H. S.; Card, J. D.; Ficarro, S. B.; Shim, H.; Marto, J. A.; Dhe-Paganon, S.; Sasaki, A. T.; Boxer, M. B.; Simeonov, A.; Cantley, L. C.; Shen, M.; Zhang, T.; Ferguson, F. M.; Gray, N. S. Structure-Activity Relationship Study of Covalent Pan-Phosphatidylinositol 5-Phosphate 4-Kinase Inhibitors. ACS Med. Chem. Lett. 2020, 11 (3), 346–352. https://doi.org/10.1021/acsmedchemlett.9b00402.

5) Dexheimer, T. S.; Rosenthal, A. S.; Luci, D. K.; Liang, Q.; Villamil, M. A.; Chen, J.; Sun, H.; Kerns, E. H.; Simeonov, A.; Jadhav, A.; Zhuang, Z.; Maloney, D. J. Synthesis and Structure-Activity Relationship Studies of N -Benzyl-2-Phenylpyrimidin-4-Amine Derivatives as Potent Usp1/Uaf1 Deubiquitinase Inhibitors with Anticancer Activity against Nonsmall Cell Lung Cancer. J. Med. Chem. 2014, 57 (19), 8099–8110. https://doi.org/10.1021/jm5010495.

6) Young, R. J.; Green, D. V. S.; Luscombe, C. N.; Hill, A. P. Getting Physical in Drug Discovery II: The Impact of Chromatographic Hydrophobicity Measurements and Aromaticity. Drug Discov. Today 2011, 16 (17–18), 822–830. https://doi.org/10.1016/j.drudis.2011.06.001.

7) Valkó, K. Chromatographic Hydrophobicity Index by Fast-Gradient RP-HPLC: A High-Throughput Alternative to Log P/Log D. Anal. Chem. 1997, 69 (12), 2022–2029. https://doi.org/10.1021/ac961242d.